WSC

Harmful/Potentially Harmful Constituent (HPHC) Screening Part II (Smoke fractions P1) (SN: 167321)

Ignacio Gonzalez Suarez

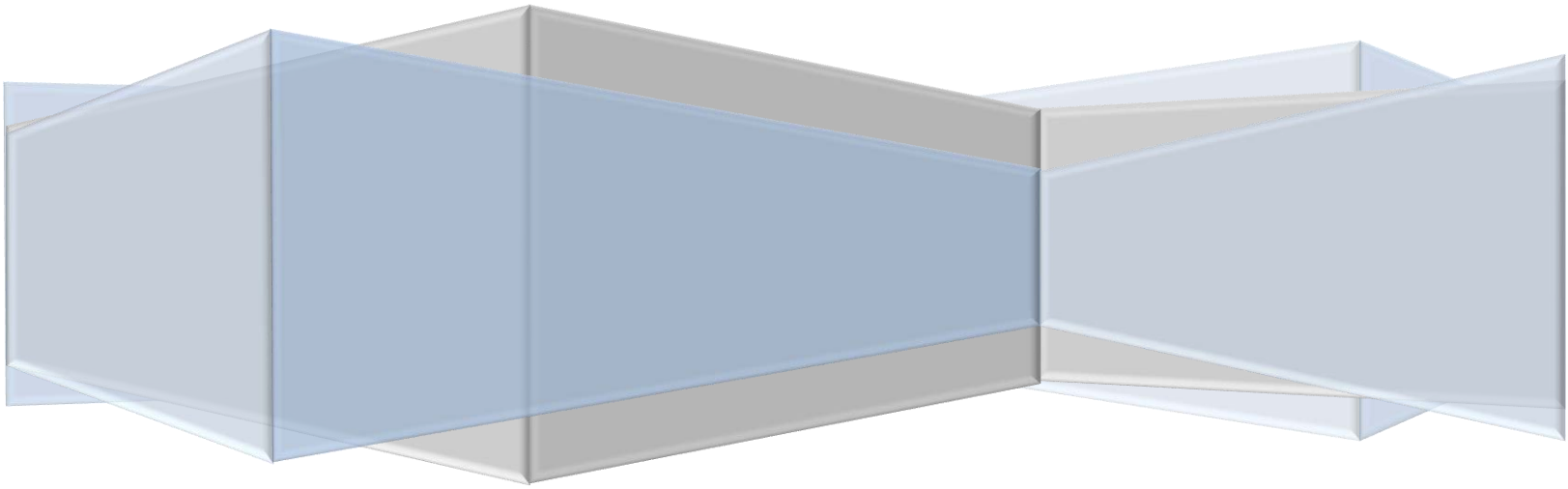

A report prepared for **Systems Toxicology** by

Philip Morris Products SA
Quai Jeanrenaud 5
2000 Neuchatel
Switzerland

Contents

1. Executive Summary

The harmful/potentially harmful constituent screening (Part II) study includes the testing of single smoke constituents, e-liquids, and aerosol fractions from reduced risk product candidates. The present study report is focused on the assessment of platform one (P1) aerosol fractions. The report is divided into three sections:

- *Comparison between 3R4F and P1 for each smoke/aerosol fraction*
- *Comparison of all three 3R4F smoke/P1 aerosol fractions*

2. Study Objective

The objective of the harmful/potentially harmful constituent (HPHC) screening (part II) was to generate robust transcriptomics data complemented by high content screening (HCS)-based toxicity assays to assess the *in vitro* biological impact of the different aerosol fractions (total particulate matter (TPM), gas vapor phase (GVP), and smoke-bubbled phosphate buffered saline (sbPBS)) of the reduced risk product (RRP) candidate P1 compared with the reference cigarette 3R4F.

This study provides valuable information about the potential of platform one (P1) to reduce the risk of smoke-related diseases. It is part of a staged approach described in the BSR strategy, which used systems biology to evaluate different exposure scenarios relevant to our business, including single HPHCs, HPHC mixtures, E-liquids, and RRP candidates.

3. Study Scope

This *in vitro* study exposed normal human bronchial epithelial (NHBE) cells to GVP, TPM, or sbPBS from P1 or the reference cigarette 3R4F. It forms part of the Project: "Cellular Systems Biology" and the WP "Biological impact assessment of MRTPs, aerosol constituents, mixtures, and E-liquids". All work was performed at PMI R&D Neuchâtel (Switzerland).

4. Study Design

Figure 1 summarizes the study design. Briefly, 24 h post-seeding, NHBE cells were exposed to different doses of GVP, TPM, or sbPBS from either P1 or the reference cigarette 3R4F. Initial toxicological assessment was performed by measuring cell viability and 13 HCS-based toxicity endpoints over multiple doses and two timepoints. Based on the results, three doses were selected for further transcriptomics evaluation at both timepoints.

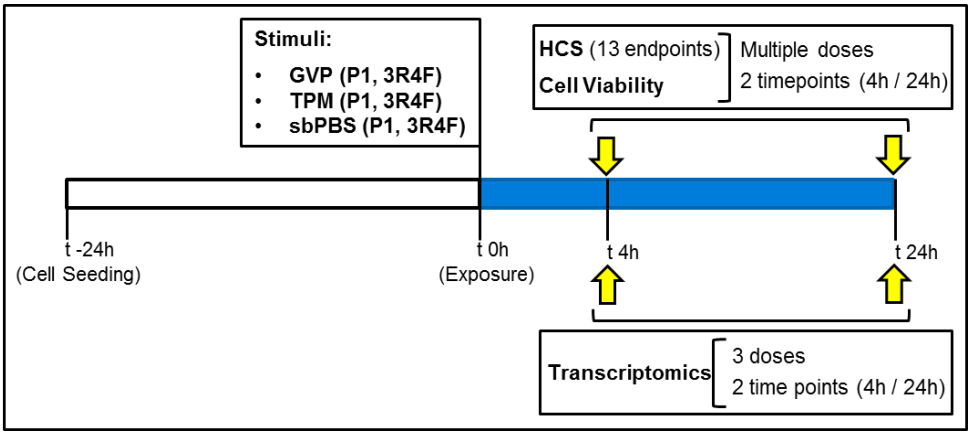

Figure 1: Study design. *NHBE cells were exposed for 4 h or 24 h to different doses of GVP, TPM, or sbPBS from P1 and 3R4F. Toxicological assessment was performed initially by HCS. Three doses were selected for further assessment via transcriptomics.*

5. Study Limitations

In terms of risk assessment, the use of whole smoke exposure is always recommended, as this results in an exposure closer to the real life situation. On the other hand, whole smoke exposure requires a very specific setup that was not compatible with the throughput and type of toxicity endpoints used in the study. Therefore, in the present study it was decided to use smoke fractions and not whole smoke.

As indicated in the SP, all smoke fractions were generated under the Health Canada Intense (HCI) smoke regimen, following the protocol established by the BSR smoke lab. To optimize trapping efficiency and minimize day-to-day variability, the BSR smoke lab modified the aerosol generation protocol for P1 fractions. Thus, the concentration of all P1 fractions was lower than that of previous studies. This may explain why we were not able to observe cytotoxicity in NHBE cells exposed to P1 even at the highest doses tested.

6. Main Conclusion

Exposure of NHBE cells to different P1 aerosol fractions resulted in lower toxicity compared with the respective 3R4F fraction.

When all three fractions were compared, TPM showed the highest level of toxicity, both for 3R4F and P1.

7. Background

Traditional toxicological risk assessment relies on the use of *in vivo* animal studies, which are often time-consuming and unable to provide high-throughput information or to efficiently identify global biological perturbations (Krewski et al, 2011). In recent years, therefore, a clear shift in the toxicological assessment of environmental agents has begun. Critical toxicity pathways perturbed upon exposure to such agents are now commonly identified and quantified using modern tools and technologies including medium and high-throughput *in vitro* screening assays, computational toxicology, systems biology, and pharmacokinetic modeling.

This new strategy also responds to the need of finding alternatives to animal testing. Although conducted *in vitro*, this approach is based on human cell lines and thus better represents human biology in certain aspects (especially when primary cell models are used).

In the present study, we compared the biological impact of different fractions (GVP, TPM, and sbPBS) of the RRP candidate P1 and the reference cigarette 3R4F. The biological impact was investigated using a HCS platform and 13 multi-parametric indicators of cellular toxicity, and complemented by microarray-based transcriptomics analysis followed by a computational approach leveraging mechanistic network models to identify and quantify perturbed molecular pathways.

We used NHBE cells because epithelial cells make up an efficient barrier against pathogens and aggressive molecules. These cells have been shown to release a variety of pro-inflammatory mediators including chemokines, cytokines, and growth factors through various signaling pathways following exposure to cigarette smoke and pathogens.

7.1 In vitro biological system: NHBE cells

NHBE cells are primary lung cells derived from a healthy adult non-smoking donor. Human primary cells are a better *in vitro* model to study human cell biology because of the absence of genetic modifications (always present in immortalized cell lines), which results in a closer phenotypic resemblance to healthy lung tissue. The choice of a healthy non-smoking donor is also justified to reduce the risk of capturing nonspecific cell responses associated with disease or smoke exposure and not to the tested compound. The *in vitro* model was selected based on the fact that the lung is the first organ exposed to cigarette smoke, as well as on the available in-house knowledge regarding culture conditions.

7.2 xCELLigence

The xCELLigence system is a real-time cellular analysis platform based on multi-electrode array technology. It uses tissue culture plates with sensor micro-electrodes covering approximately 70% of each well bottom. The presence of cells on top of the electrodes affects the local ionic environment at the electrode/solution interface, leading to an increase in electrode impedance. Therefore, the more cells attached to the electrodes, the greater the increase in electrode impedance. The impedance also depends on the quality of the cell interaction with the electrodes. For example, increased cell adhesion or spreading will lead to a greater change in electrode impedance. Thus, the electrode impedance can be used to monitor cell viability and cell number. The xCELLigence system uses a dimensionless parameter known as the "cell index" (CI), derived as the relative change in measured electrical impedance, to represent cell status. This is used as the output signal. The correlation between CI and cell viability is represented in ***Figure 2.*** CI is zero when cells are absent or poorly attached to the plate. Under the same physiological conditions, the more cells attached to the electrodes, the larger the CI value. Thus, CI is a quantitative measure of the cell number present in a well. Alternatively, a change in the cell status, such as cell morphology, cell adhesion, or cell viability will lead to a change in CI (adapted from Bucher Biotec, http://www.bucher.ch/en/products/acea/technology.html). The cellular lab at PMI Neuchâtel is equipped with an xCELLigence RTCA MP station (ACEA Biosciences, San Diego, CA, USA), which can analyze up to six different 96-well plates independently.

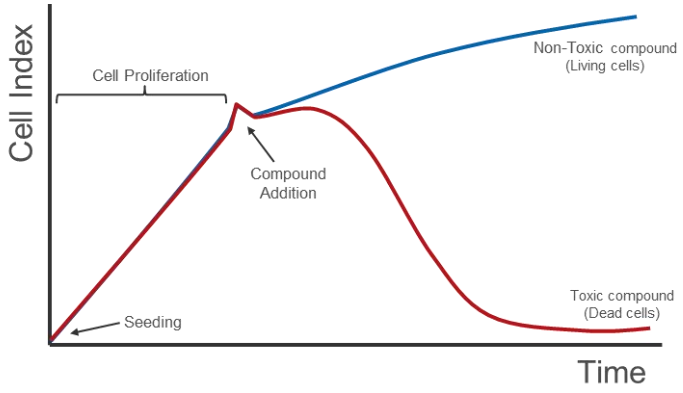

Figure 2. Correlation between cell index and cell viability in the xCELLigence system (adapted from ACEA Biosciences, http://www.aceabio.com/theory.aspx?cateid=281)

7.3 High Content Screening

HCS is an automated method used to identify substances that alter the phenotype of a cell in a particular manner. This technology is primarily used in biological research and involves a combination of fluorescence or confocal microscopy, a high-throughput image acquisition system, and a series of algorithms and software tools that enable image processing and analysis. By detecting antibody and fluorescent dye signals, the HCS technology can measure changes in target intensity and localization, and observe cellular morphology in live or fixed cells (Thermo_Scientific, 2012).

The cellular lab at PMI Neuchâtel is equipped with two *Cellomics* Array Scan VTI readers (Thermo Scientific, Waltham, MA, USA). Seven assays covering 13 different biological endpoints were established in NHBE cells in collaboration with Cyprotex (www.cyprotex.com; Macclesfield, UK) as part of the HPHC impact assessment study (https://disco.app.pmi/disco/drl/objectId/0901d 4ec8036b1cc). This technology is currently implemented in the Neuchâtel cellular laboratories.

The list of the endpoints is detailed in ***Table 1***:

Assay	#	Biological endpoint	Description
Included in all assays	**1**	**Cell count**	A decreasing number of cells per well indicates toxicity due to necrosis, apoptosis or a reduction in cellular proliferation
	2	**Nuclear area**	An increase in nuclear size can indicate necrosis or G2 cell cycle arrest and a decrease can indicate apoptosis
	3	**DNA structure**	An increase in DNA structure can indicate chromosomal instability and DNA damage
Cytotoxicity screening panel	**4**	**Mitochondrial mass**	A decrease in mitochondrial mass indicates loss of total mitochondria and an increase implies mitochondrial swelling or an adaptive response to cellular energy demands
	5	**Mitochondrial membrane potential**	A decrease indicates mitochondrial toxicity, as well as a potential role in apoptosis signaling, an increase in mitochondrial membrane potential indicates an adaptive response to cellular energy demands
	6	**Cell membrane permeability**	An increase in cell membrane permeability is a general indicator of cell death
	7	**Cytochrome C release**	An increase in cytochrome c release is one of the hallmarks of the apoptosis signaling cascade
DNA damage	**8**	**phospho-H2AX**	H2AX phosphorylation (detected by immunostaining) occurs following the induction of DNA double strand breaks (correlates with neutral comet assay – PMID: 17064697).
Oxidative stress	**9**	**DHE**	Dihydroethidium (DHE) is a non-fluorescent cell-permeable ROS-sensitive probe. It allows the detection of intracellular superoxide anion production by turning fluorescent upon oxidation.

Gluthatione content	**10**	**GSH**	Monochlorobimane added to the culture medium readily enters cells to form a fluorescent GSH-monochlorobimane adduct that can be measured fluorometrically. This reaction is catalyzed by glutathione S-transferase and allows the quantitative measurement of intracellular glutathione that is the principal intracellular low-molecular-weight thiol and plays a critical role in the cellular defense against agents that impose oxidative stress.
Apoptosis / necrosis	**11**	**Caspase 3/7**	An increase in caspase 3 / 7 activity indicates the onset of the cell signaling cascade leading to cell death by apoptosis.
	12	**Cell membrane permeability**	An increase in cell membrane permeability is a general indicator of cell death
Proliferation	**13**	**phospho-H3**	An increase in the mitotic marker phospho histone H3 (pH3) indicates an increase of cells in prophase due either to increase proliferation or to growth arrest. A decrease in pH3 indicates a decrease of cells undergoing mitosis.
Stress kinase	**14**	**Phospho-cJun**	An increase in phosphorylated-cJun indicates the upregulation of the stress kinase pathway, which includes downstream targets such as cell differentiation and apoptosis.

Table 1. List of HCS-based toxicity endpoints. *GSH (glutathione*)

7.4 Systems biology

The biological impact of 3R4F smoke and P1 aerosol fractions on NHBE cells was investigated by generating gene expression data and applying our in-house developed systems biology approach. This methodology uses the relationships between diverse elements in a biological system rather than analyzing them separately, and allows the elements to be investigated in response to perturbation. The toxicity of different fractions can then be evaluated in terms of network and pathway activation.

8. Experimental Protocol

8.1 Sample generation

TPM and GVP fractions were generated from the same smoke run, whereas sbPBS samples were generated separately. For each aerosol fraction, exposure to 3R4F and P1 samples was performed simultaneously and within the same plate.

8.1.1 TPM

TPM samples were generated from each test item in independent smoke runs, collected on glass fiber filters (44-mm diameter), and extracted by the syringe extraction method with 5 ml of ethanol in a glass vessel. For 3R4F, mainstream smoke from a total of six cigarettes, divided into two batches of three, was trapped on two separate glass fiber filters followed by ethanol extraction. The first filter was extracted with 5 ml of ethanol, while the second was extracted with the first crude extract. For P1, mainstream smoke from a total of 10 sticks, divided into two batches of five, was trapped on two separate glass fiber filters and extracted as described above.

8.1.2 GVP

GVP**,** defined as the substance that passes through the glass fiber filter, was collected by bubbling the smoke/aerosol through ice-cold PBS in a gas wash bottle. For 3R4F, mainstream smoke from a total of six cigarettes, divided into two batches of three, was trapped in 36 ml of PBS. For P1, mainstream smoke from a total of 10 cigarettes, divided into two batches of five, was trapped in 40 ml of PBS.

8.1.3 sbPBS

In a separate smoke run, sbPBS was generated by bubbling whole smoke through ice-cold PBS in a gas wash bottle. The number of sticks and volume of PBS for each item were the same as used for GVP. For additional details, please refer to the SP document: https://disco.app.pmi/ disco/ drl/ objectId /0901d4ec8044b45e.

8.1.4 Analytical determination of nicotine and carbonyls

Nicotine levels were determined in TPM samples by gas chromatography with flame ionization detector detection using isoquinoline as an internal standard.

Levels of carbonyls (formaldehyde, acetaldehyde, propionaldehyde, crotonaldehyde, methyl ethyl ketone, acetone, acrolein, and butyraldehyde) were determined in GVP and sbPBS samples. For this purpose, a 400 µl aliquot of bubbled PBS was derivatized with 600 µl of 2,4-dinitrophenylhydrazine for 30 min and then quenched with 50 µl of pyridine. The concentration of all eight carbonyls was then measured by liquid chromatography–electrospray ionization/multi-stage mass spectrometry using deuterated species as internal standards.

8.2 Toxicological assessment

8.2.1 PHASE 1: Exposure and cellular analysis

During the exposure phase, cell viability was initially evaluated using the xCELLigence system. A minimum of three independent experiments was performed for each test item and fraction. Dose ranges are described in ***Table 2***.

		DOSES (puff / l)																
3R4F TPM	Exp. 1-2	X	X	X	X	X	X	64	58	51	X	32	26	X	13	X	6	Vehicle
	Exp. 3-6	X	X	X	X	X	X	64	X	51	42	32	26	X	13	X	6	Vehicle
	Exp. 7-10	X	X	X	X	X	X	64	X	51	42	32	X	16	X	8	X	Vehicle
P1 TPM	Exp1-6	450	376	300	226	150	X	75	X	X	X	38	X	X	X	X	X	Vehicle
	Exp1-7	450	376	300	226	150	X	75	X	X	X	X	X	X	X	X	X	Vehicle
3R4F GVP	Exp. 1-5	X	X	X	200	X	100	X	X	50	X	X	25	X	13	X	6	Vehicle
P1 GVP	Exp. 1-3	X	350	300	200	X	100	X	X	50	X	X	25	X	X	X	X	Vehicle
3R4F sbPBS	Exp. 1-6	X	X	X	200	X	100	X	X	50	X	X	25	X	13	X	6	Vehicle
P1 sbPBS	Exp. 1-3	X	350	300	200	140	X	70	X	X	X	35	X	X	X	X	X	Vehicle

Table 2. Dose ranges tested in NHBE cells by xCELLigence.

NHBE cells were seeded into E-Plate View 96-well tissue culture plates (ACEA Biosciences) at a density of 4.8 × 10^3 cells per well in 100 µl of culture medium and incubated for 24 h at 37C and 5%

CO_2. Cells were then exposed to seven different doses of the aerosol fractions for an additional 24 h. Appropriate positive (carbonyl cyanide m-chlorophenyl hydrazine) and negative controls (culture medium, ethanol/PBS) were included in each experiment. Cell viability, measured as change in CI, was monitored and recorded throughout the duration of the experiment. Experiments were performed in triplicate.

Based on the cell viability results, we selected six doses for each test item and aerosol fraction to be tested via HCS analysis. A minimum of three independent experiments was performed for each test item and fraction. Dose ranges are described in **Table 3**.

	DOSES (puff / l)															
3R4F TPM	Exp. 1	X	X	X	X	X	64	51	42	32	26	X	13	X	6	Vehicle
	Exp. 2-6	X	X	X	X	X	64	51	42	32	X	16	X	8	X	Vehicle
P1 TPM	Exp. 1	450	380	300	226	150	75	X	X	38	X	X	X	X	X	Vehicle
	Exp. 2-4	450	380	300	226	150	75	X	X	X	X	X	X	X	X	Vehicle
3R4F GVP	Exp. 1-5	X	X	200	100	50	25	13	X	6	Vehicle					
P1 GVP	Exp. 1-3	350	300	200	100	50	25	X	X	X	Vehicle					
3R4F sbPBS	Exp. 1-6	X	X	200	X	100	X	50	X	25	13	6	Vehicle			
P1 sbPBS	Exp. 1-3	350	300	200	140	X	70	X	35	X	X	X	Vehicle			

Table 3. Dose ranges tested in NHBE cells by HCS.

NHBE cells were plated in 96-well tissue culture treated black walled clear bottomed polystyrene plates at a density of 8 × 10^3 cells/well (except for the mitosis endpoint, where 3× 10^3 cells/well were seeded) for 24 h prior to dosing. They were then dosed (in triplicate) with vehicle (ethanol or PBS) or increasing concentrations of the different test items and aerosol fractions and incubated for 4 h or 24 h. Appropriate positive controls for each HCS endpoint were included in all experiments. For further details, please see the SP. At the end of the incubation period, the cells were loaded with the specific dye or antibody and the plate was then scanned using an automated fluorescent cellular imager (ArrayScan® VTI, Thermo Scientific).

PHASE 2: Exposure and RNA extraction

Based on the *Phase 1* results, we selected doses from each test item and smoke fraction for gene expression analysis (***Table 4***). Two exposure times (4 h and 24 h) were selected. The highest dose was then selected for each test item and fraction so that at least 60% viability was observed by xCELLigence. For 3R4F, the highest doses of TPM (32 cig/L), GVP (100 cig/L), and sbPBS (100 cig/L) were only selected for the 4 h timepoint because of the excessive cell death levels observed at the 24 h timepoint. For P1, the highest dose was that which could be tested without interference from the vehicle. Additional lower doses were selected to compare the biological effects across fractions and against 3R4F.

	DOSES (puff/l)					
3R4F TPM	X	X	X	32*	25	13
P1 TPM	X	X	38	32	25	X
3R4F GVP	X	100*	X	X	25	13
P1 GVP	350	100	X	X	25	13
3R4F sbPBS	X	100*	X	X	25	13
3R4F sbPBS	350	100	X	X	25	13

Table 4. Doses of TPM, GVP, and sbPBS for Phase 2 (transcriptomics). *NHBE cells were exposed for 4 h or 24 h.* *doses used only for the 4 h timepoint.

NHBE cells were plated on 96 well tissue culture treated transparent polystyrene plates at 8 x 10^3 cells / well in 100µl of medium for 24 h prior dosing. They were then dosed and incubated for a further 4 h or 24 h. Three biological replicates were used per concentration. Three independent experiments (three independent aerosol generations) were performed. Cell viability was tested in parallel via xCELLigence (***Figure 3***). Cell viability was maintained above 60% in all cases, the only exception was 3R4F sbPBS at the 24h time point where one of the samples was below 60%.

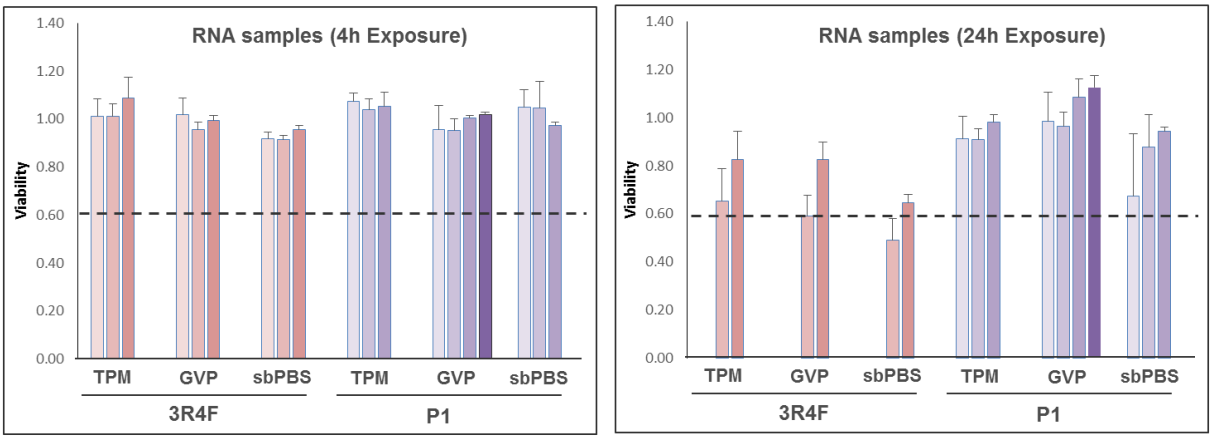

Figure 3. Cell viability in RNA extraction experiments*. Values were normalized to vehicle control in each case. Dotted line indicates 60% cell viability. Color gradients indicate increasing concentrations (lighter shades being the highest doses). Note that the highest dose for all 3R4F fractions was only selected for the 4 h timepoint.*

RNA was extracted following supplier instructions and using a randomization plan. Briefly:

- RNA extraction was performed using the RNeasy micro kit (Qiagen, Venlo, Netherlands).
- In order to have enough material for next step, 4 wells were pooled for all doses and vehicles. 3R4F and P1 were always tested in the same plate. Due to the high number of samples, the aerosol fractions were tested in separate plates. All doses and time points for a given experiment were processed for RNA extraction on the same day according to the randomization plan.
- A total of 120 RNA samples were extracted. The elution volume was the same (22ul) for the samples generated from 2 wells or from 4 wells.
- RNA concentration was measured using a Nanodrop (Thermo Scientific, Wilmington, USA).

- RNA integrity was checked using an Agilent 2100 Bioanalyzer (Agilent Technologies, Sta Clara, USA).
- RNa was hybridized onto Affymetrix GeneChip® Human Genome U133 Plus 2.0 Array chips (Affymetrix, Sta. Clara, USA)

8.3 Generation of transcriptomic samples

Sample randomization protocol

According to the experimental design, a block randomization was performed using the exposure plates as a blocking factor.

8.4 Computational Methods

8.4.1 Raw data quality control

Chip images were initially evaluated for scan artifacts and the data were then processed through the standard QC pipeline. Briefly, raw data files were read by the ReadAffy function of the Affymetrix package (Gautier et al, 2004) from the Bioconductor suite of microarray analysis tools (Gentleman et al, 2004) available for the R statistical environment (R Development Core Team, 2007). The quality was controlled by generating and examining RNA degradation plots (AffyRNAdeg function of the affy package), Normalized Unscaled Standard Error, and Relative Log Expression (RLE) plots (affyPLM package (Brettschneider et al, 2008)), and calculating the MA(RLE) values. Additionally an eye-check of the pseudo-images was done to ensure that no spatial effect was present.

8.4.2 Microarray data processing

Data processing and scoring methods were implemented in the R statistical environment(Smyth, 2005). Raw RNA expression data were analyzed using the affy and limma packages of the Bioconductor suite of microarray analysis tools available in the R statistical environment (Bolstad et al, 2003; Gentleman et al, 2004; Nielsen et al, 2005). Robust Multichip Average (GCRMA) background correction and quantile normalization were used to generate probe set expression values. For each data set, an overall linear model was fitted to the data for all groups of replicates, and specific contrasts of interest were evaluated to generate raw *p*-values for each probe set on the expression array, which in turn were adjusted by the Benjamini–Hochberg procedure.

8.4.3 Network-based analysis

Leveraging the "cause-and-effect" network models together with Network Perturbation Amplitude algorithms (Martin et al, 2014; Martin et al, 2012), gene expression fold-changes were translated into differential values for each network node (denoted by *f*). The node differential values were in turn summarized into a quantitative measure of network perturbation amplitude (NPA). This was computed as a Sobolev norm on the signed directed graph underlying the network (*N*), which could be expressed as a quadratic form, $1/\#edges \cdot f^T Q_N f$. Thus, to summarize, the NPA algorithm

considers two main input components, the "cause-and-effect" network model describing the mechanism and a gene expression data set from a well-designed experiment.

In addition to the confidence intervals of the NPA scores, which accounted for experimental error (e.g., biological variation between samples in an experimental group), companion statistics were derived to inform on the specificity of the NPA score with respect to the biology described in the network. Two permutation tests were implemented (Martin et al, 2014); the first assessed if the results were specific to the underlying evidence (i.e., gene fold-changes) in the model, leading to a permutation *P*-value (denoted by *O in the figures when <0.05). The second test assessed whether the "cause-and-effect" layer of the network significantly contributed to the amplitude of network perturbation (denoted by K* in the figures when <0.05). The network was considered to be specifically perturbed if both *P*-values were low (typically <0.05), and the perturbation was significant if, in addition, the confidence interval was above zero.

8.4.3.1 Biological impact factor (BIF) scoring

The network models represent functionally distinct biological processes characterizing the systems under consideration. To objectively evaluate the overall biological impact relative to a reference within the experiment (typically a standardized CS exposure), the sum of the significant network perturbations for the contrast *i* were normalized with respect to the corresponding sum for the reference. Hence, the relative BIF (RBIF) for the contrast *i* is defined as follows:

$$RBIF(i) = \frac{\sum_{Net}\ w_i^{Net}\, f_i^{Net^T} Q_{Net}\, f_i^{Net}}{\sum_{Net}\ w_{REF}^{Net}\, f_{REF}^{Net^T}\, Q_{Net}\, f_{REF}^{Net}} = \frac{\sum_{Net}\ w_i^{Net} NPA_{Net}(i)}{\sum_{Net}\ w_{REF}^{Net} NPA_{Net}(REF)},$$

where the weights account for three statistics associated with the above outlined NPA algorithm.

The contribution of a given subset, S, of network models (e.g., cell stress sub-networks), for a contrast *i*, is given as follows:

$$Contrib_S(i) = \frac{\sum_S w_i^S NPA_s(i)}{\sum_{Net} w_i^{Net} NPA_{Net}(i)}$$

(because Net is a disjointed union of subsets of networks, the contributions sum to one).

The relative BIF is therefore decomposed into network components (cell stress, pulmonary inflammation, cell proliferation, apoptosis, necroptosis, senescence, DNA damage, and autophagy) by considering the quantities $Contrib_S(i)\ RBIF(i)$, which are represented as starplots.

Finally, because RBIF is an aggregated quantity, two contrasts can have the same relative biological effect while arising from different network models. To identify those situations, a comparability coefficient can be computed as follows:

$$\delta = \frac{\sum_{Net}\ w_i^{Net} w_{REF}^{Net}\, f_i^{Net^T}\, Q_{Net}\, f_{REF}^{Net}}{\sqrt{\sum_{Net}\ w_i^{Net} NPA_{Net}(i)}\sqrt{\sum_{Net}\ w_{REF}^{Net} NPA_{Net}(REF)}}.$$

This coefficient is essentially the *cos* angle between *i* and REF for the scalar product defined in the NPA algorithm.

9. Results

9.1 Cell viability

Cell viability was continuously monitored during the first 24 h after cell exposure to the different fractions and test items. A minimum of three independent experiments with freshly generated samples was performed, and three technical replicates per dose were used in each experiment. The effect on cell viability of the different items after 4 h and 24 h of exposure (same timepoints selected for HCS and transcriptomics analysis) is detailed below.

9.1.1 GVP

Exposure to GVP from the reference cigarette 3R4F resulted in a dose-dependent decrease in NHBE cell viability (***Figure 4***). This was already observed after 4 h of exposure, although a stronger effect was observed after 24 h. After plotting all experiments and fitting the data to a nonlinear dose-response inhibitory curve using GraphPad Prism (V. 5.00 for Windows, GraphPad Software, San Diego, CA, USA), an EC50 value of **61 puffs/L** (R^2:0.952) was obtained. By contrast, no effects on cell viability were observed upon exposure to GVP from P1.

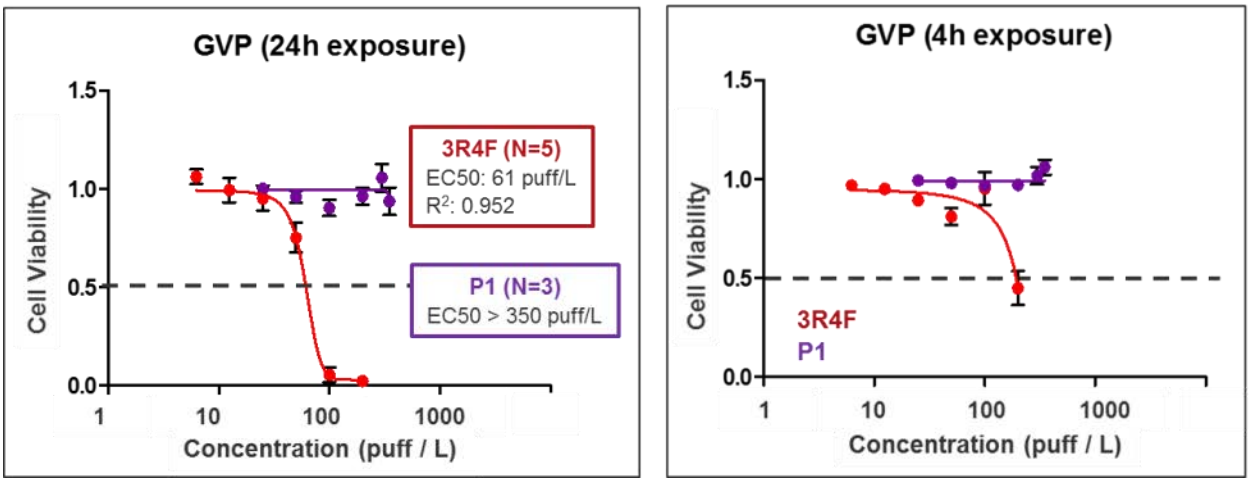

Figure 4. Cell viability in NHBE cells exposed to GVP from 3R4F and P1 for 4 h (right) or 24 h (left). *Values are normalized to vehicle (PBS). Dotted line indicates 50% cell viability. Values represent mean ± SEM from all experiments. N: number of independent experiments (identical for 4 h and 24 h timepoints).*

9.1.2 sbPBS

Exposure to sbPBS from the reference cigarette 3R4F also resulted in a dose-dependent decrease in NHBE cell viability (***Figure 5***). This was already observed after 4 h of exposure, but a stronger effect was observed after 24 h. When all experiments were plotted together and data were fitted to a nonlinear dose-response inhibitory curve (GraphPad), an EC50 value of **42 puffs/L** (R^2:0.753) was obtained. In the case of P1, no effects were observed at the 4 h timepoint. No effect on cell viability was observed after exposure of NHBE cells to GVP from P1, although a 30% decrease in cell viability was observed after 24 h exposure at high doses (>300 puffs/l).

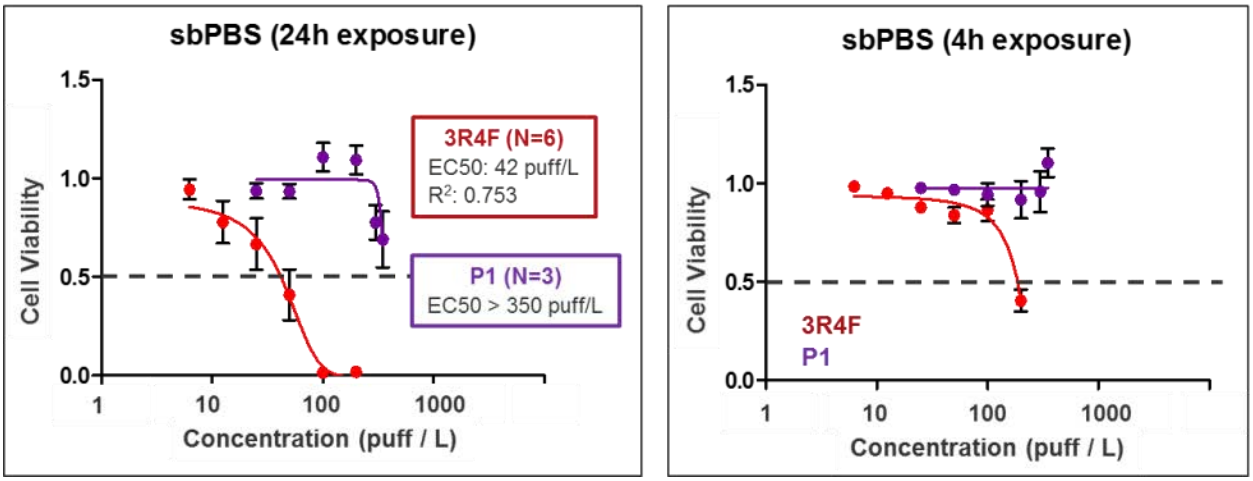

Figure 5. Cell viability in NHBE cells exposed to sbPBS from 3R4F and P1 for 4 h (right) or 24 h (left). *Values are normalized to vehicle (PBS). Dotted line indicates 50% cell viability. Values represent mean ± SEM from all experiments. N: number of independent experiments (identical for 4 h and 24 h timepoints).*

9.1.3 TPM

Exposure to TPM from the reference cigarette 3R4F again resulted in a dose-dependent decrease in NHBE cell viability (***Figure 6***). This was already observed after 4 h of exposure, although a stronger effect was observed after 24 h. Plotting all experiments together and fitting data to a nonlinear dose-response inhibitory curve (GraphPad), resulted in an EC50 value of **30 puffs/L** (R^2:0.810). No effects on cell viability were observed upon exposure to TPM from P1.

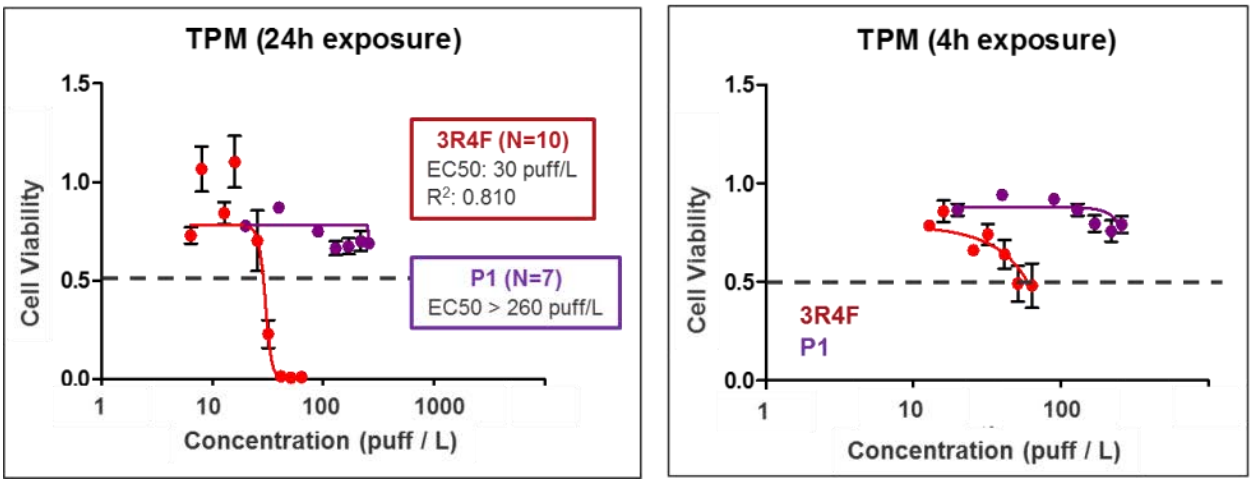

Figure 6: Cell viability in NHBE cells exposed to TPM from 3R4F and P1 for 4 h (right) or 24 h (left). *Values are normalized to vehicle (PBS). Dotted line indicates 50% cell viability. Values represent mean ± SEM from all experiments. N: number of independent experiments (identical for 4 h and 24 h timepoints).*

9.2 HCS

In parallel with cell viability, 13 additional indicators of toxicity were measured by HCS after exposure for either 4 h or 24 h to the 3R4F GVP fraction or the synthetic mixture. Freshly generated P1 and 3R4F samples were tested in parallel in three independent experiments, and three technical replicates per dose were used in each experiment. In the case of 3R4F, the graphs below include historical data for three additional experiments in which P1 was not tested. These data were incorporated into the HCS graphs to increase the number of datapoints per dose and exposure time. No major differences between the two sets of 3R4F data (historical and the current study) were observed.

9.2.1 GVP

Cell count, nuclear size, and DNA structure

These three parameters were measured by default in all HCS assays. Within each independent experiment, the values of each parameter were calculated as the average of five out of the seven assays (DNA damage, oxidative stress, stress kinase, apoptosis, and cytotoxicity panel). Values were normalized to those of the vehicle control. Data from the mitosis and GSH content assays were not included in the calculation because of technical differences in assay setup (different nuclear dye)

Cell count measures the average number of cells per microscope field in a total of 20 fields (Figure 7). No change in cell count was observed at the 4 h timepoint. However, at 24 h, a dose-dependent decrease in cell count was observed for 3R4F, but no major effect was observed for P1 despite the use of higher doses.

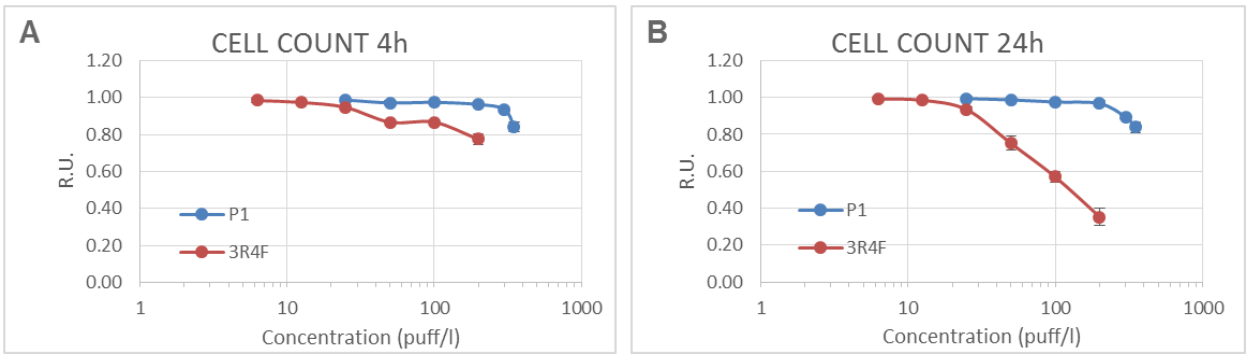

Figure 7. Changes in NHBE cell count in cells exposed to the GVP fraction from 3R4F and P1 for 4 h (A) or 24 h (B). *Values are normalized to the vehicle control and represent mean ± SEM.*

Changes in **nuclear size** could suggest either G2 cell cycle arrest (if increased) or apoptosis (if decreased). Notably, the extent of these alterations dramatically depends on the cell type so toxicity may occur with no detectable changes in nuclear size. Indeed, no changes in nuclear size were detected for 3R4F or P1 at any timepoint (***Figure 8***).

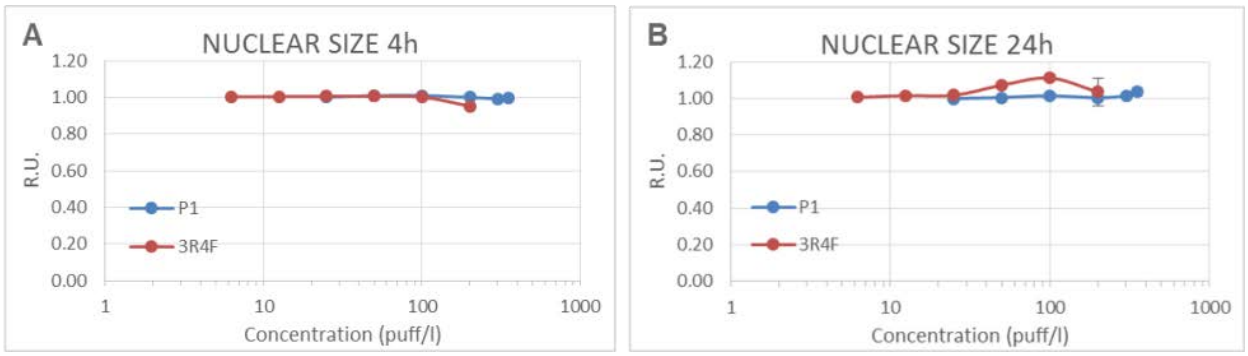

Figure 8. Changes in nuclear size in NHBE cells exposed to the GVP fraction from 3R4F or P1 for 4 h (A) or 24 h (B). *Values are normalized to the vehicle control and represent mean ± SEM.*

DNA structure measures changes in the nuclear distribution of chromatin (the complex formed by DNA and proteins that makes up the content of the nucleus). In normal human cells, chromatin is evenly distributed throughout the nucleus. However, in the presence of genomic instability or DNA fragmentation, the nuclear distribution of chromatin is altered and this can be detected as an increase in the DNA structure parameter. As shown in ***Figure 9***, no major changes in DNA structure were observed at the 4 h timepoint. At 24 h, a moderate increase in DNA structure was observed for 3R4F. This increase only occurred at doses that caused a significant decrease in cell count. No changes were observed for P1 at 24 h.

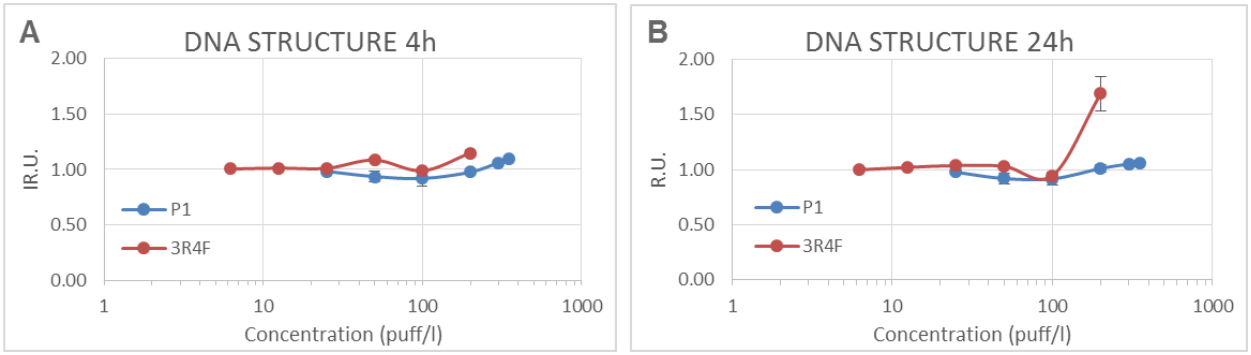

Figure 9. Changes in DNA structure in NHBE cells exposed to the GVP fraction from 3R4F or P1 for 4 h (A) or 24 h (B). *Values are normalized to the vehicle control and represent mean ± SEM.*

DNA damage

The genotoxic potential of 3R4F and P1 was measured as the number of cells that stained positive for phosphorylated histone H2A.X (p-H2AX) a well-established marker of DNA double strand breaks (DSBs). DSBs are considered the most deleterious form of DNA damage, because if not repaired correctly they can lead to the loss of genetic material, mutations, and cancer. Histone H2A.X is an H2A variant histone required for checkpoint-mediated cell cycle arrest and DNA repair following DSBs (Lowndes & Toh, 2005). Within minutes after the generation of a DSB, H2A.X is phosphorylated at Ser139 at sites of DNA damage (Lowndes & Toh, 2005). This event is critical for the development of an appropriate DNA damage response.

Exposure to 3R4F resulted in an increase in DNA damage at both the 4 h and 24 h timepoints, but only at the highest dose. The increase observed for 3R4F at 4 h occurred in the absence of cell death and thus corresponds to true genotoxicity. By contrast, the effect observed at the 24 h timepoint was accompanied by a significant decrease in cell death and is likely the result of cytotoxicity-induced genotoxicity. With respect to P1, no effects were observed at any timepoint (***Figure 10***). Taken together, these results indicate that the GVP fraction from 3R4F, but not from P1, has the potential to induce genotoxicity.

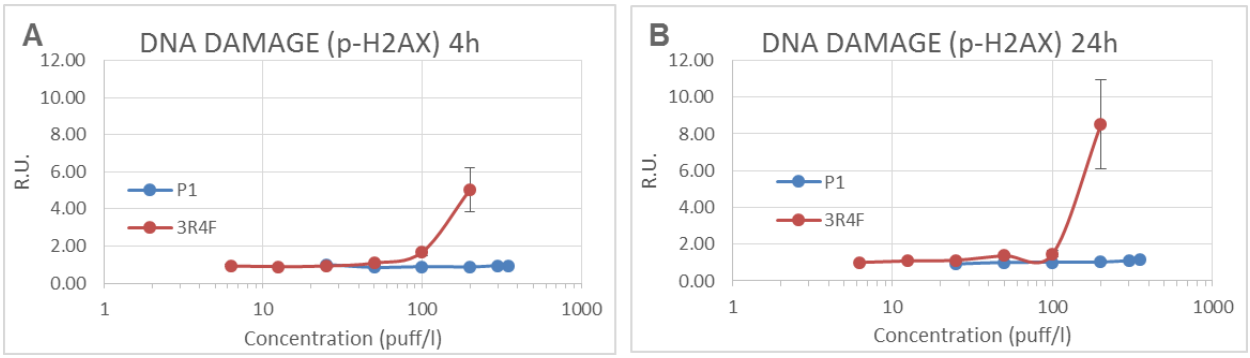

Figure 10. DNA damage in NHBE cells exposed to the GVP fraction from 3R4F or P1 for 4 h (A) or 24 h (B). *DNA damage was measured as pH2AX. Values are normalized to the vehicle control and represent mean ± SEM.*

Stress kinase (phospho c-Jun)

c-Jun N-terminal kinases are a group of proteins that belong to the mitogen-activated protein kinase family and are activated in response to a variety of stress stimuli (e.g., reactive oxygen species (ROS), radiation, or inflammatory signals). c-Jun kinases regulate many important cellular processes, including cell growth and differentiation, and several cell survival and apoptosis pathways (Wisdom et al, 1999).

No effects were observed with respect to the stress kinase pathway at 4 h. However, at 24 h, exposure to the GVP fraction of 3R4F resulted in a dose-dependent increase in c-Jun phosphorylation (***Figure 11***). No effect was observed for P1. These results indicate that the GVP fraction from 3R4F, but not from P1, induces cellular stress in NHBE cells.

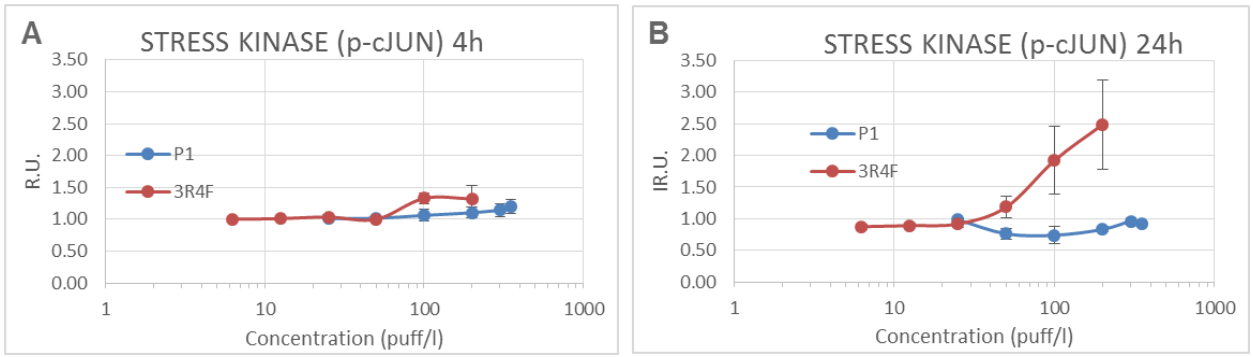

Figure 11. Activation of the stress kinase pathway in NHBE cells exposed to the GVP fraction from 3R4F or P1 for 4 h (A) or 24 h (B). *Stress kinase activation was measured as p-cJun. Values are normalized to the vehicle control and represent mean ± SEM.*

Oxidative stress and GSH content

Oxidative stress is the result of either the increased production of ROS or a significant decrease of cellular antioxidant defenses, such as GSH. Under normal circumstances, a cell can overcome small perturbations and maintain redox homeostasis. However, if oxidative stress is severe or prolonged, it can damage cellular components (e.g. proteins, lipids, or DNA) and eventually cause cell death. The presence of ROS in NHBE cells was detected with a specific dye (dihydroethidium, DHE). The levels of cellular antioxidants were investigated by measuring the GSH content. GSH is a small peptide synthesized by most mammalian cells, which acts as a natural antioxidant and prevents ROS-induced damage. GSH also contributes to the maintenance of the cellular redox potential, so a decrease in its levels is indicative of oxidative stress (Armstrong et al, 2002).

No effects were observed for either test item after 4 h of exposure. However, after 24 h, exposure to the GVP fraction of 3R4F resulted in an increase in ROS formation. This effect was only observed at doses causing significant cell loss, so could reflect the presence of dead cells rather than being directly caused by 3R4F GVP. No response was observed for P1 at 24 h (***Figure 12***).

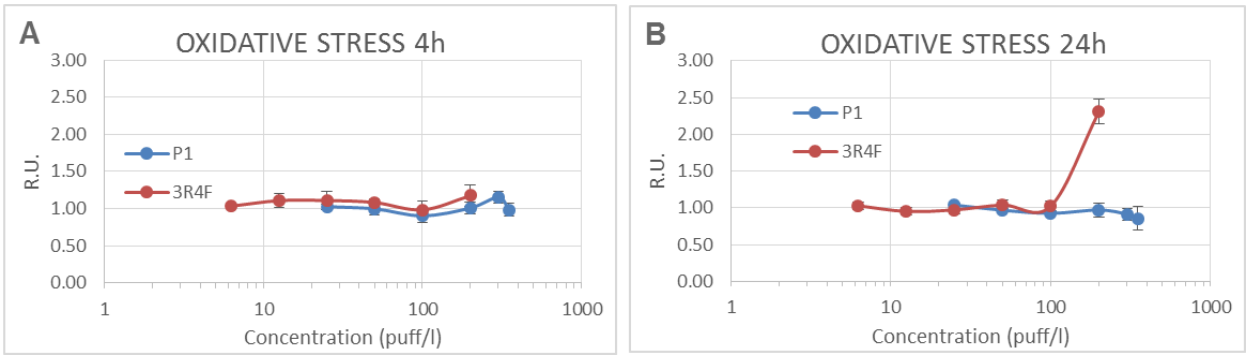

Figure 12. Oxidative stress in NHBE cells exposed to the GVP fraction from 3R4F or P1 for 4 h (A) or 24 h (B). Oxidative stress was measured by staining with dihydroethidium (DHE). *Values are normalized to the vehicle control and represent mean ± SEM.*

Exposure to 3R4F caused a dose-dependent decrease in the GSH content that was observed at both 4 h and 24 h. This effect occurred at exposure times and doses at which no significant cell loss was observed, so should be considered a true indication of oxidative stress. In the case of P1, a dose-dependent decrease in GSH was also observed at 4 h, although the response was lower than that of 3R4F (***Figure 13***). The fact that GSH levels were not decreased at the 24 h timepoint suggests that the effects of P1 GVP were only transient and did not saturate the cell's defense mechanisms, thus allowing the restoration of cellular GSH stores.

Taken together, these results indicate that GVP from 3R4F has a much higher potential to induce oxidative stress in NHBE cells than P1.

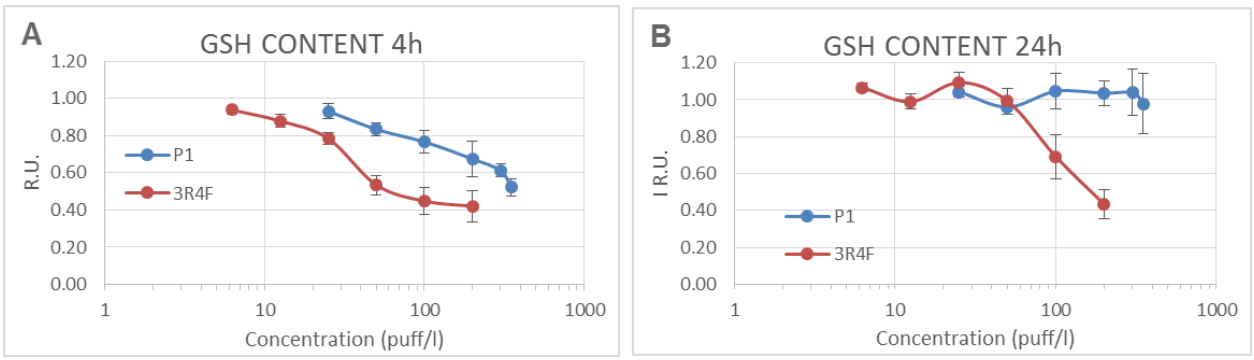

Figure 13. Changes in GSH content in NHBE cells exposed to the GVP fraction from 3R4F or P1 for 4 h (A) or 24 h (B). *Values are normalized to the vehicle control and represent mean ± SEM.*

Mitosis

Histone H3 is specifically phosphorylated during chromosome condensation in mitosis and rapidly becomes dephosphorylated when mitosis is completed. These phosphorylation and de-phosphorylation events are well characterized, so p-H3 has been used as a readout in cell cycle inhibitor profiling studies. Increased p-H3 levels could reflect a G2/M cell cycle arrest if no other indicators of proliferation (e.g. cell number) are also increased.

No changes in p-H3 levels were observed after 4 h of exposure to either 3R4F or P1 (***Figure 14A***). At 24 h, an increase in p-H3 was observed for 3R4F, but not for P1 (***Figure 14B***).

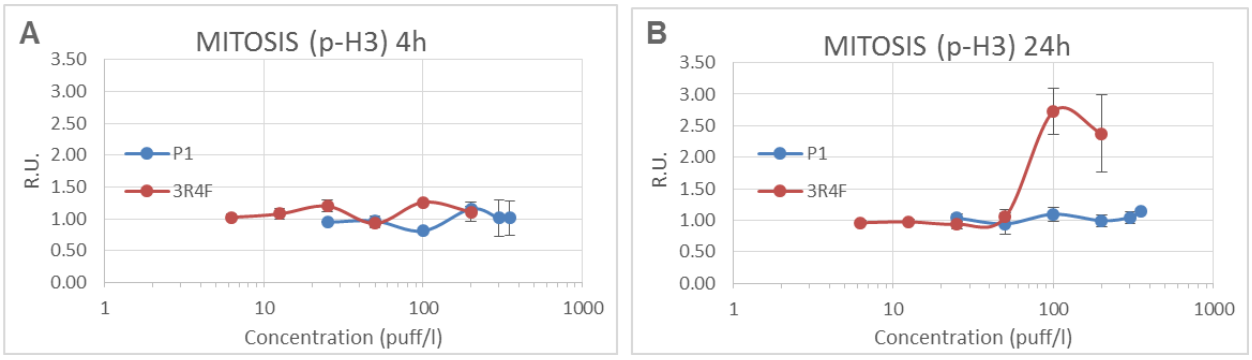

Figure 14. Changes in p-H3 levels in NHBE cells exposed to the GVP fraction from 3R4F or P1 for 4 h (A) or 24 h (B). *Values are normalized to the vehicle control and represent mean ± SEM.*

Apoptosis and necrosis

Apoptosis is the process of programed cellular death involving a series of highly regulated biochemical events that eventually lead to cell destruction. Some of these changes include membrane blebbing, cell shrinkage, chromatin condensation, and DNA fragmentation. This is a naturally occurring process that plays an essential role in organism development (e.g. embryogenesis) and survival (e.g. preventing tumor formation) (Edinger & Thompson, 2004). Additionally, apoptosis can be exogenously induced through exposure to chemotherapeutic drugs or cigarette smoke. The presence of apoptosis in NHBE cells was initially detected by measuring the activity of caspase 3 and caspase 7, two essential mediators of the signaling cascade leading to cell death. Cytochrome c is a small heme protein associated with the inner mitochondrial membrane, and is an essential

component of the electron transport chain. Its release from the mitochondrion is a key step of the apoptotic process (Ott et al, 2002), so was also detected in this study as a second marker of apoptosis.

Necrosis is a non-regulated process usually caused by external factors such as infections, toxins, or trauma. It results in inflammation, which can become chronic and lead to tissue damage. The main cellular changes associated with necrosis include ATP depletion and increased membrane permeability and disruption, leading to cellular swelling and rupture (Edinger & Thompson, 2004). Some of these events can also be observed at very late stages of apoptosis. The presence of necrosis in NHBE cells was detected using a dead cell dye (TO-PRO®-3, Life Technologies, Grand Island, NY, USA) that only stains cells when the integrity of the cellular membrane is compromised.

No effects in caspase activity were observed at 4 h (***Figure 15A***). After 24 h, a dose-dependent increase in caspase activity was observed for both 3R4F and P1 (***Figure 15B***). At any given dose, the effect of P1 GVP was lower than that of 3R4F.

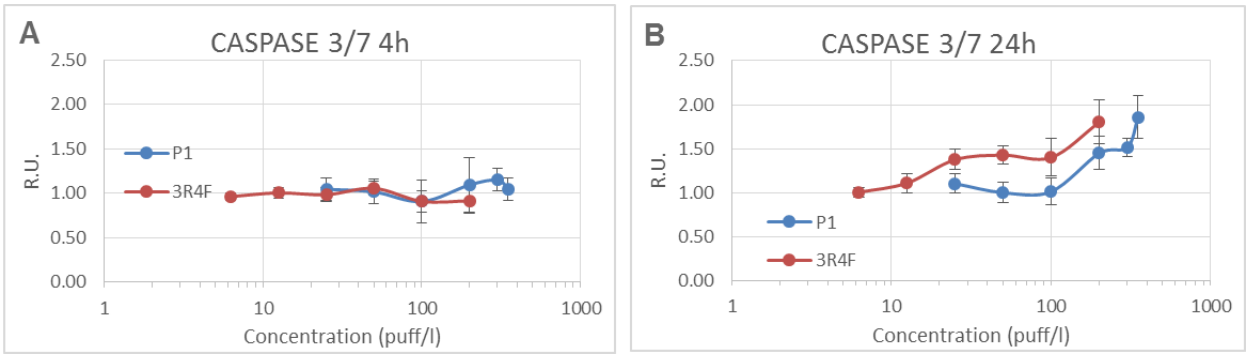

Figure 15. Apoptosis in NHBE cells exposed to the GVP fraction from 3R4F or P1 for 4 h (A) or 24 h (B)*. Values are normalized to the vehicle control and represent mean ± SEM.*

No significant increase in the cytochrome c release was observed after 4 h exposure to either 3R4F or P1 GVP (***Figure 16A***). At 24 h, an increase in cytochrome c release was observed for 3R4F GVP, but only at the highest dose (***Figure 16B***). This effect occurred in the presence of significant cell loss (>50%, ***Figure 7B***) so should be interpreted carefully, because it may be secondary to cytotoxicity. No effects were observed at 24 h for P1 GVP.

In the case of 3R4F, the results observed for cell membrane permeability mirrored those of caspase 3/7 activity and cytochrome c. No effects were observed at 4 h (***Figure 17A***), but a dose-dependent increase occurred at 24 h (***Figure 17B***). The results for cell membrane permeability should be interpreted carefully because some cellular effects of necrosis are also observed in the last stages of apoptosis. By contrast, exposure to P1 GVP showed no changes in cell membrane permeability at any timepoint.

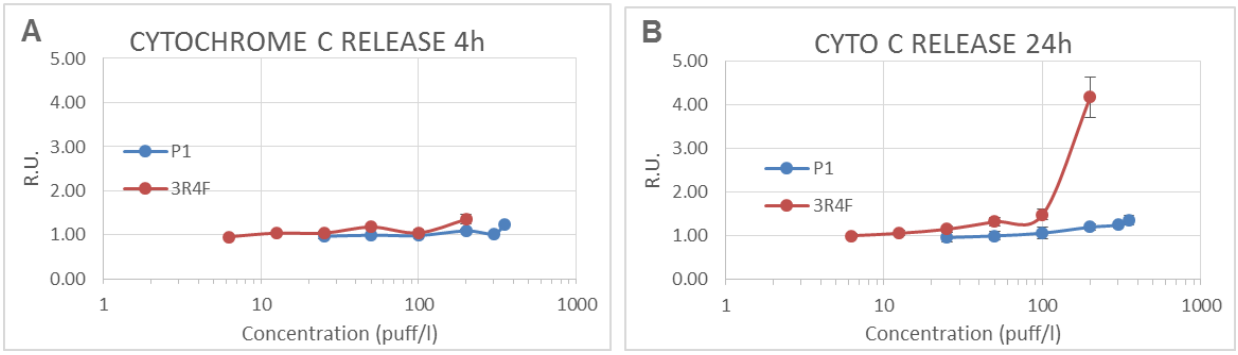

Figure 16. Cytochrome c release in NHBE cells exposed to the GVP fraction from 3R4F or P1 for 4 h (A) or 24 h (B)*. Values are normalized to the vehicle control and represent mean ± SEM.*

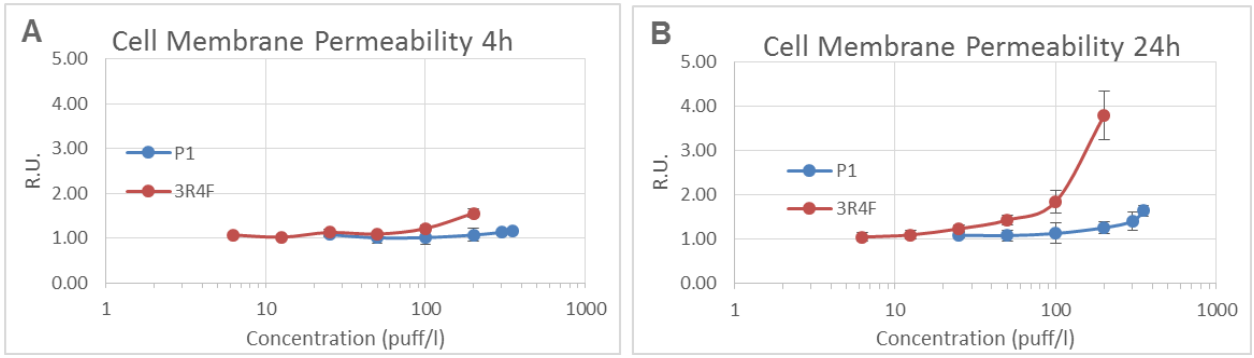

Figure 17. Necrosis in NHBE cells exposed to the GVP fraction from 3R4F or P1 for 4 h (A) or 24 h (B)*. Values are normalized to the vehicle control and represent mean ± SEM.*

Taken together, these results indicate that the GVP fraction of 3R4F has a greater potential to induce cell death via apoptosis or necrosis than P1 GVP. Moreover, the P1 GVP fraction increases caspase activity at high doses, but this is not accompanied by cell death or changes in cytochrome c release or membrane permeability. This again suggests that the apoptotic potential of P1 GVP is lower, and that longer exposures are required to observe cytotoxic effects.

Mitochondrial membrane potential and mitochondrial mass

Mitochondria are the cellular organelles responsible for energy generation *via* a series of redox chemical reactions collectively known as phosphorylative oxidation. While there are other energy sources in the cell (e.g. glycolysis), induction of mitochondrial toxicity can have a serious impact on cellular viability. The induction of mitochondrial toxicity was determined here with a specific dye (MitoTracker®, Life Technologies) that allowed us to measure two mitochondrial parameters: mitochondrial membrane potential and mitochondrial mass.

No effects were observed at 4 h for 3R4F or P1 GVP with respect to the mitochondrial membrane potential (***Figure 18A***) or mitochondrial mass (***Figure 19A)***. At 24 h, 3R4F GVP caused an increase in mitochondrial membrane potential (hyperpolarization) (***Figure 18B***), and a decrease in mitochondrial mass (***Figure 19B)***, but only at the highest dose at which significant cell loss was observed. These changes should therefore be interpreted with care because they could also be

secondary to the presence of cytotoxicity. By contrast, no changes in mitochondrial membrane potential or mitochondrial mass were observed at 24 h for P1 GVP.

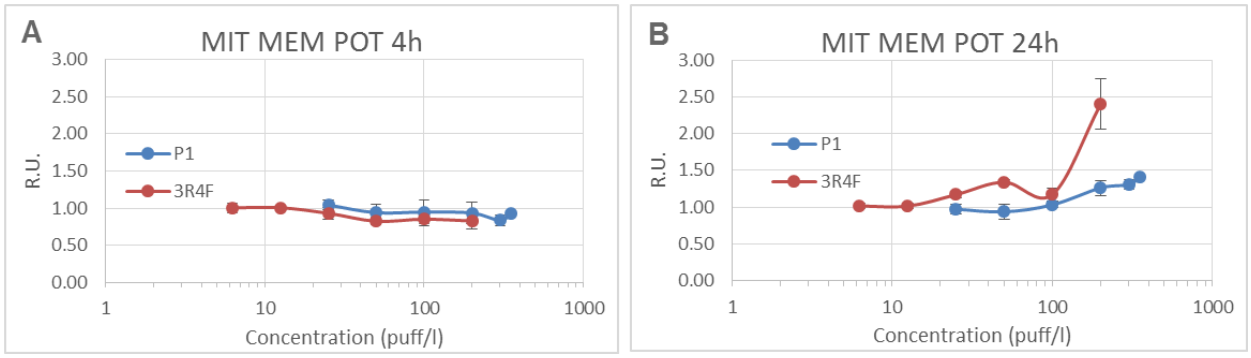

Figure 18. Mitochondrial membrane potential in NHBE cells exposed to the GVP fraction from 3R4F or P1 for 4 h (A) or 24 h (B). *Values are normalized to the vehicle control and represent mean ± SEM.*

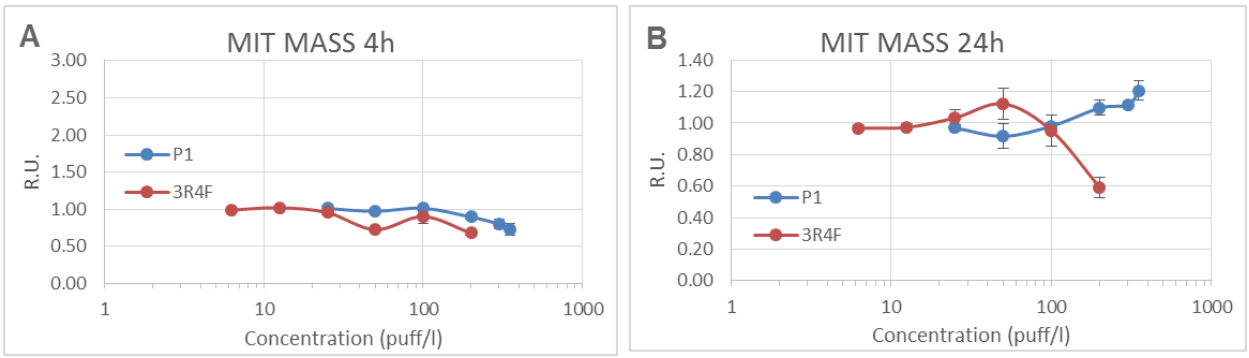

Figure 19. Mitochondrial mass in NHBE cells exposed to the GVP fraction from 3R4F or P1 for 4 h (A) or 24 h (B). *Values are normalized to the vehicle control and represent mean ± SEM.*

Taken together, these results suggest that 3R4F GVP may impact mitochondrial function, whereas P1 had no apparent effect on mitochondrial health, at least at the experimental conditions tested.

9.2.2 TPM

Cell count, nuclear size, and DNA structure

No change in cell count was observed at the 4 h timepoint (***Figure 20***). At 24 h, a dose-dependent decrease in cell count was observed for 3R4F. More than 50% cell loss was observed at doses above 40 puffs/L. A dose-dependent response was also observed for P1, although the effect was much lower than that of 3R4F. Even at the highest tested dose (260 puffs/L), the cell loss was below 50%.

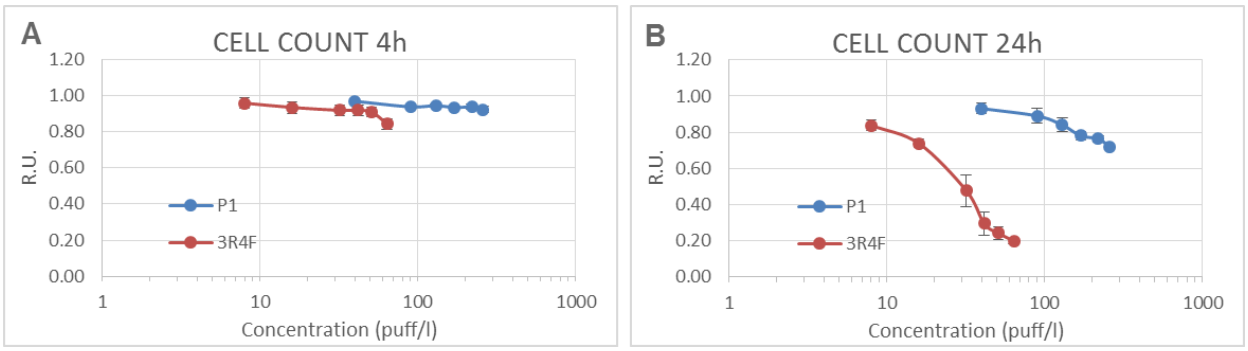

Figure 20. Changes in cell count in NHBE cells exposed to the TPM fraction from 3R4F and P1 for 4 h (A) or 24 h (B). *Values are normalized to the vehicle control and represent mean ± SEM.*

No changes in nuclear size were detected for 3R4F or P1 TPM at any timepoint (***Figure 21***).

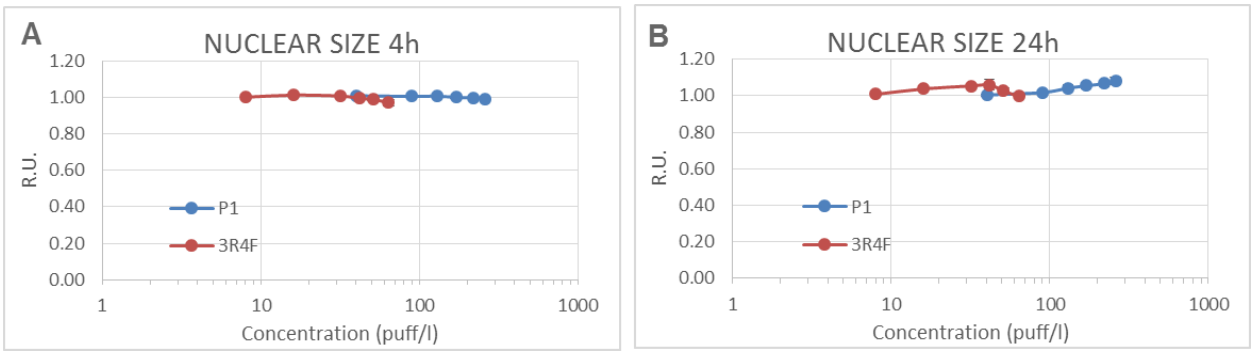

Figure 21. Changes in nuclear size in NHBE cells exposed to the TPM fraction from 3R4F or P1 for 4 h (A) or 24 h (B . *Values are normalized to the vehicle control and represent mean ± SEM.*

As shown in ***Figure 22*****,** no major changes in DNA structure were observed at the 4 h timepoint. At 24 h, a moderate dose-dependent increase in DNA structure was observed for 3R4F. This increase only occurred at doses at which significant cell loss was observed. No changes were observed for P1 at 24 h.

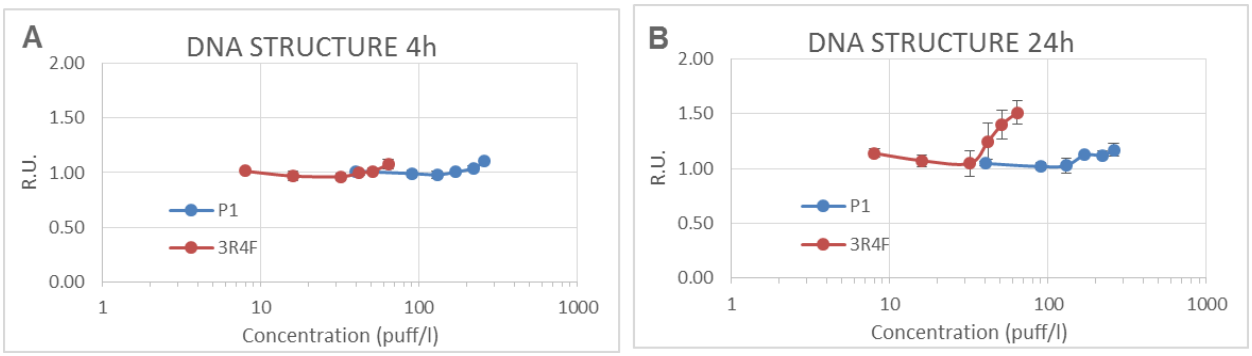

Figure 22. Changes in DNA structure in NHBE cells exposed to the TPM fraction from 3R4F or P1 for 4 h (A) or 24 h (B). *Values are normalized to the vehicle control and represent mean ± SEM.*

DNA damage

Exposure to 3R4F TPM resulted in a dose-dependent increase in DNA damage at both 4 h and 24 h. In most cases, the increase in DNA damage occurred in the absence of significant cell loss and thus corresponds to true genotoxicity. The effect observed at the highest doses at the 24 h timepoint was accompanied by >50% cell loss and is likely the result of cytotoxicity-induced genotoxicity. Exposure to P1 TPM also caused a dose-dependent increase in DNA damage, observed both at 4 h and 24 h. However, these effects occurred at much higher doses than those of 3R4F (***Figure 23C***).

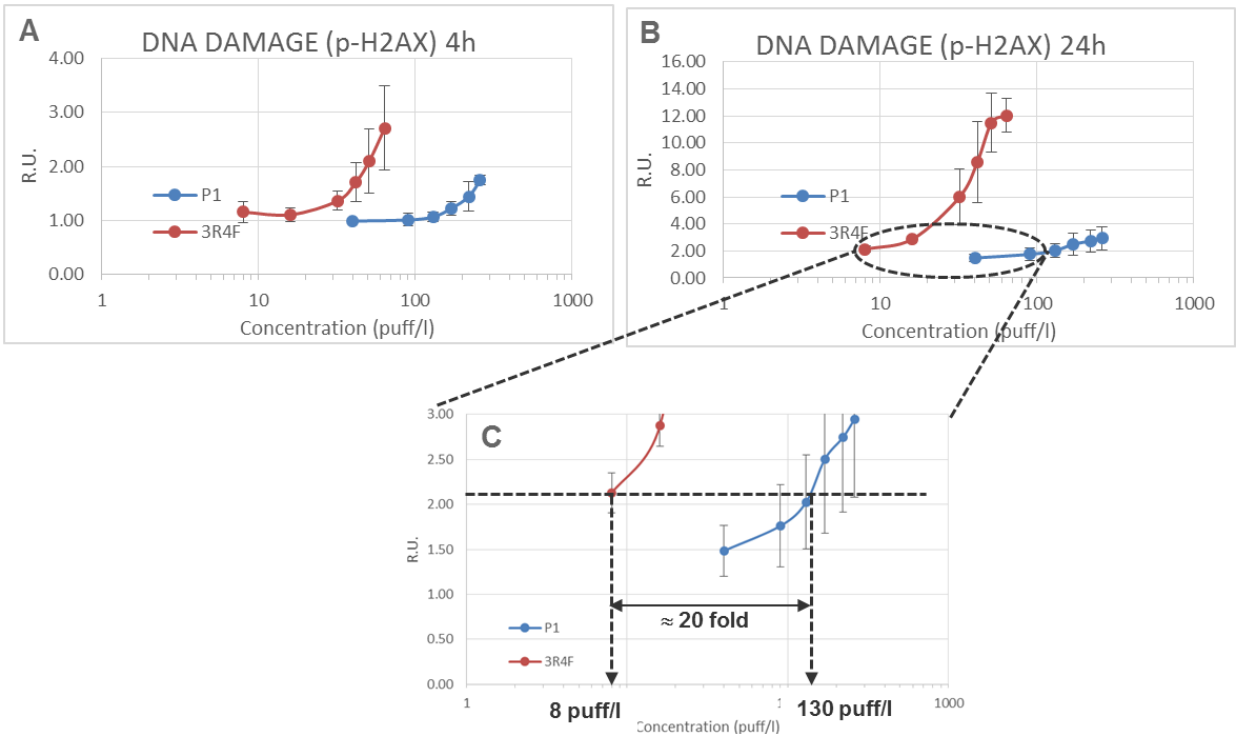

Figure 23. DNA damage in NHBE cells exposed to the TPM fraction from 3R4F or P1 for 4 h (A) or 24 h (B). *(C) is a magnification of the area highlighted in (B). DNA damage was measured as pH2AX. Values are normalized to the vehicle control and represent mean ± SEM.*

Taken together, these results indicate that the TPM fraction from 3R4F has a higher potential to induce genotoxicity than P1.

Stress kinase (phospho c-Jun)

No effects were observed at 4 h for either 3R4F or P1 TPM. However, at 24 h, exposure to 3R4F TPM resulted in a dose-dependent increase in c-Jun phosphorylation (***Figure 24***). No effect was observed for P1. These results indicate that the TPM fraction from 3R4F, but not from P1, induces cellular stress in NHBE cells

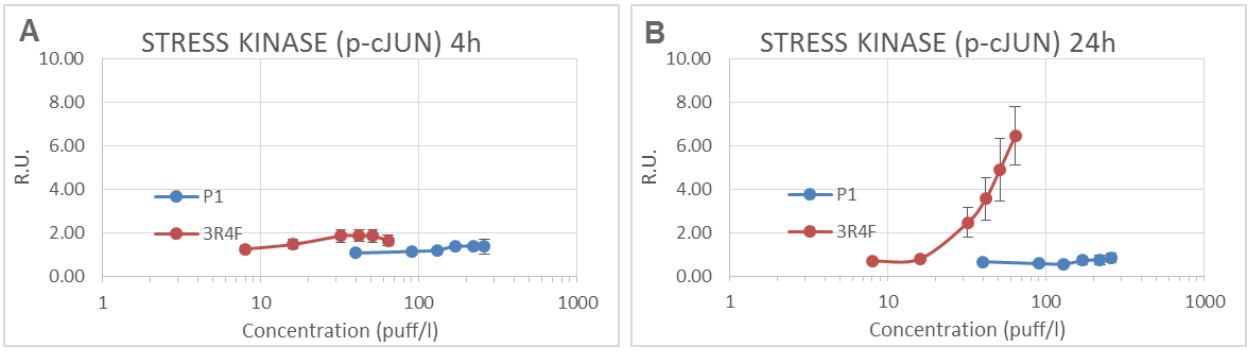

Figure 24. Activation of the stress kinase pathway in NHBE cells exposed to the TPM fraction from 3R4F or P1 for 4 h (A) or 24 h (B). *Stress kinase activation was measured as p-cJun. Values are normalized to the vehicle control and represent mean ± SEM.*

Oxidative stress and GSH content

Because of interference with the DHE signal, it was not possible to measure the impact of 3R4F TPM in oxidative stress.

Exposure to 3R4F caused a dose-dependent decrease in GSH content, observed at both 4 h and 24 h. This effect occurred at exposure times and doses at which no significant cell loss was observed, so should be considered a true indication of oxidative stress. In the case of P1, a minor decrease in GSH content was observed at 4 h and a moderate dose-dependent decrease was also observed at 4 h. The response to P1 TPM was lower than that of 3R4F (***Figure 25***).

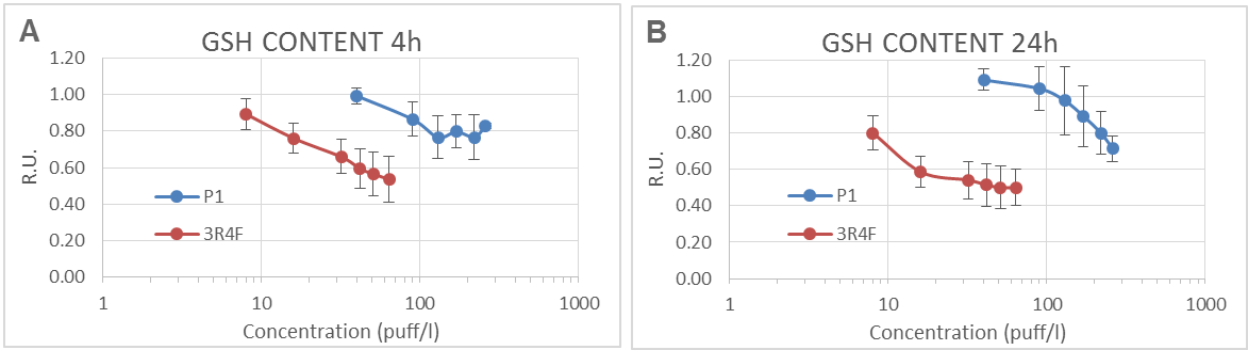

Figure 25. Changes in GSH content in NHBE cells exposed to the TPM fraction from 3R4F or P1 for 4 h (A) or 24 h (B). *Values are normalized to the vehicle control and represent mean ± SEM.*

Taken together, these results indicate that TPM from 3R4F has a much higher potential to induce oxidative stress in NHBE cells than P1.

Mitosis

No changes in p-H3 levels were observed after 4 h of exposure to either 3R4F or P1 TPM (***Figure 26A***). At 24 h, a dose-dependent increase in p-H3 was observed for 3R4F. This is indicative of a cell growth arrest because it was not accompanied by an increase in cell count. In the case of P1 TPM, a moderate increase in p-H3 was observed at high doses, although the response was lower than that of 3R4F (***Figure 26B***).

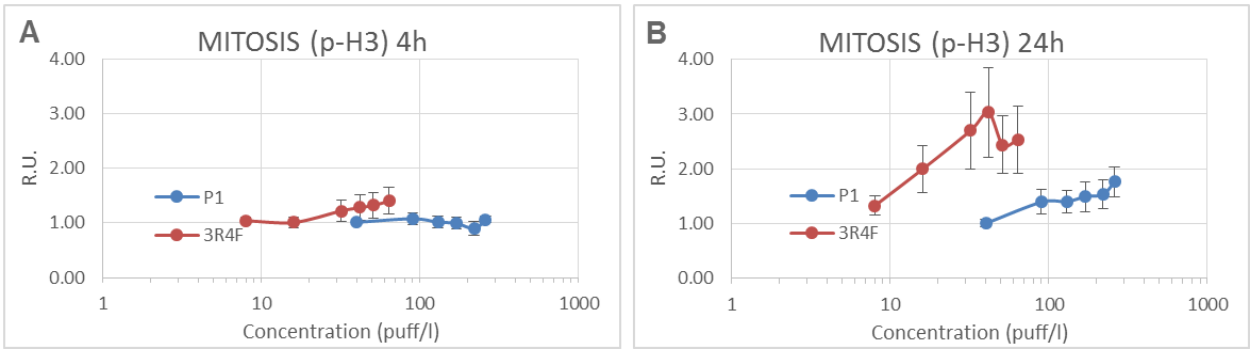

Figure 26. Changes in p-H3 levels in NHBE cells exposed to the TPM fraction from 3R4F or P1 for 4 h (A) or 24 h (B)*. Values are normalized to the vehicle control and represent mean ± SEM.*

Apoptosis and necrosis

Because of interference with the caspase 3/7 assay, it was not possible to measure the impact of 3R4F TPM for this particular endpoint.

No significant increase in the release of cytochrome c was observed after 4 h exposure to either 3R4F or P1 TPM (***Figure 27A***). At 24 h, a dose-dependent increase in cytochrome c release was observed for 3R4F TPM (***Figure 27B***). Only a moderate increase was observed for P1 TPM at 24 h. In the case of 3R4F, the results observed for cell membrane permeability mirrored those of caspase 3/7 activity and cytochrome c.

A dose-dependent increase in cell membrane permeability was observed for 3R4F TPM at 4h but not for P1 (***Figure 28A***). At 24 h, both 3R4F and P1 caused a dose-dependent increase in cell membrane permeability (***Figure 28B***). Nevertheless, at any given dose, the effect of P1 was much lower than that of 3R4F (***Figure 28C***).

Taken together, these results indicate that the TMP fraction of 3R4F has a higher potential to induce apoptosis or necrosis than P1 TPM.

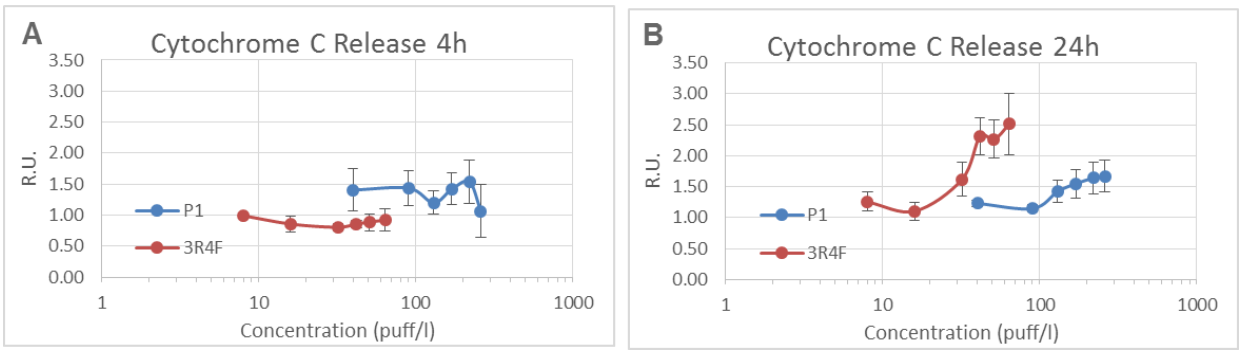

Figure 27. Cytochrome c release in NHBE cells exposed to the TPM fraction from 3R4F or P1 for 4 h (A) or 24 h (B)*. Values are normalized to the vehicle control and represent mean ± SEM.*

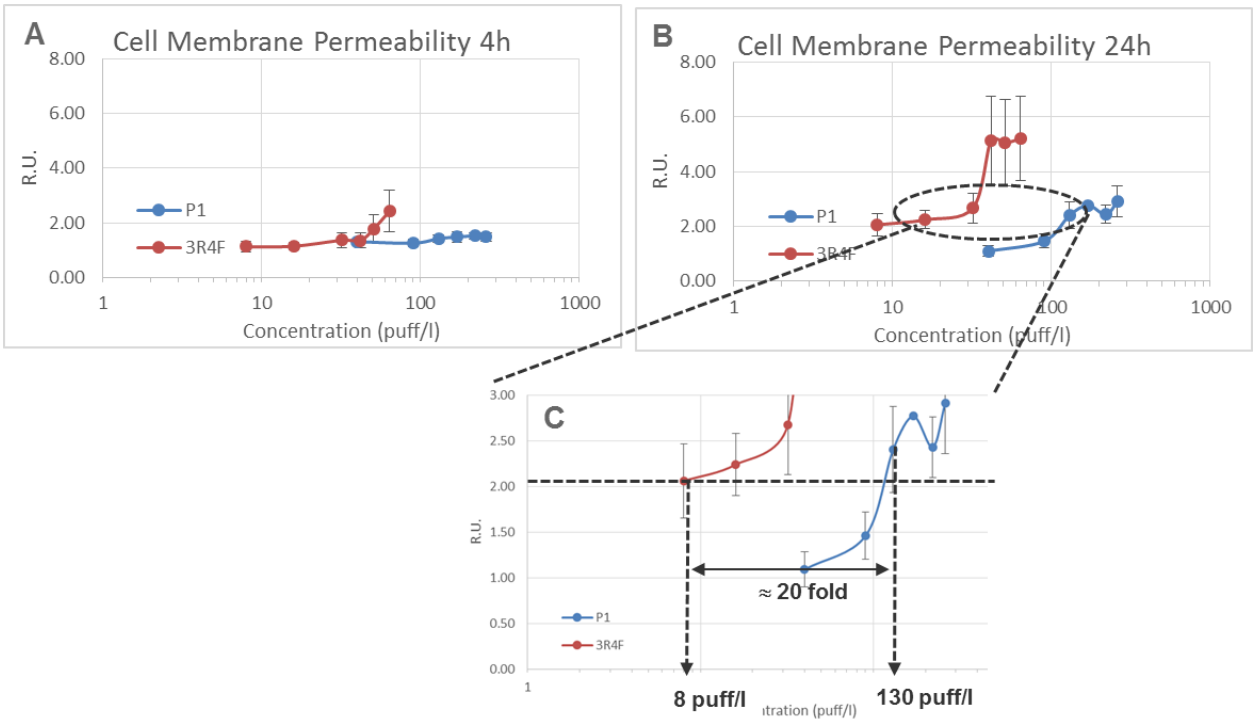

Figure 28. Necrosis in NHBE cells exposed to the TPM fraction from 3R4F or P1 for 4 h (A) or 24 h (B)*.* (C) is a magnification of the area highlighted in (B). *Values are normalized to the vehicle control and represent mean ± SEM.*

Mitochondrial membrane potential and mitochondrial mass

At 4 h, both 3R4F and P1 caused a dose-dependent decrease in the mitochondrial membrane potential (depolarization), although the effect was lower in P1 (***Figure 29A***). This effect, however, was not accompanied by a decrease in the mitochondrial mass (***Figure 30A).*** Together, these results suggest the presence of mitochondrial stress, an often reversible step that precedes mitochondrial destruction.

At 24 h, exposure to 3R4F showed a tendency to decrease the mitochondrial membrane potential as the dose increased (except for the sudden increase in signal at the 42 puffs/L endpoint, for which we do not have a clear explanation) (***Figure 29B)***. This effect also occurred without significant changes in mitochondrial mass (***Figure 30B)***. Although these results suggest the existence

of mitochondrial stress, additional experiments are necessary to confirm the presence of mitochondrial toxicity.

In the case of P1, 24 h exposure resulted in a dose-dependent increase in both the mitochondrial membrane potential and mitochondrial mass. Although the doses at which these effects were observed were comparatively higher than those tested for 3R4F, the data suggest that, at higher doses, P1 TPM induces mitochondrial toxicity.

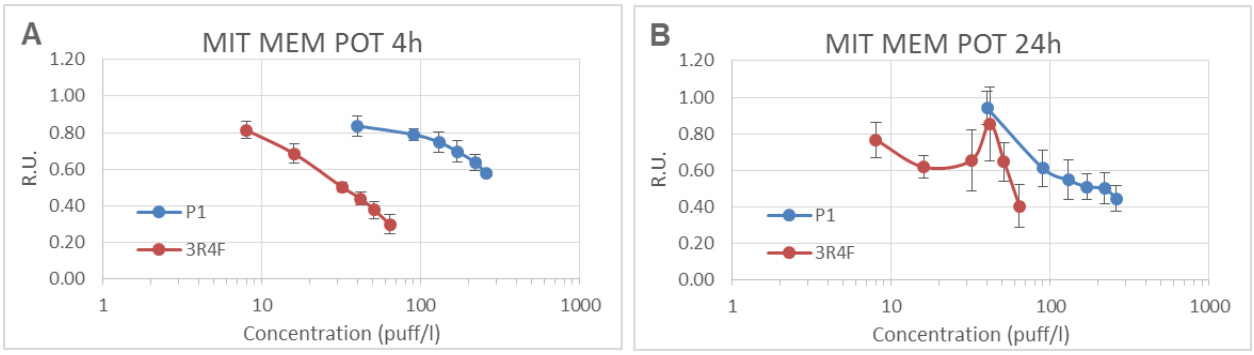

Figure 29. Mitochondrial membrane potential in NHBE cells exposed to the TPM fraction from 3R4F or P1 for 4 h (A) or 24 h (B). *Values are normalized to the vehicle control and represent mean ± SEM.*

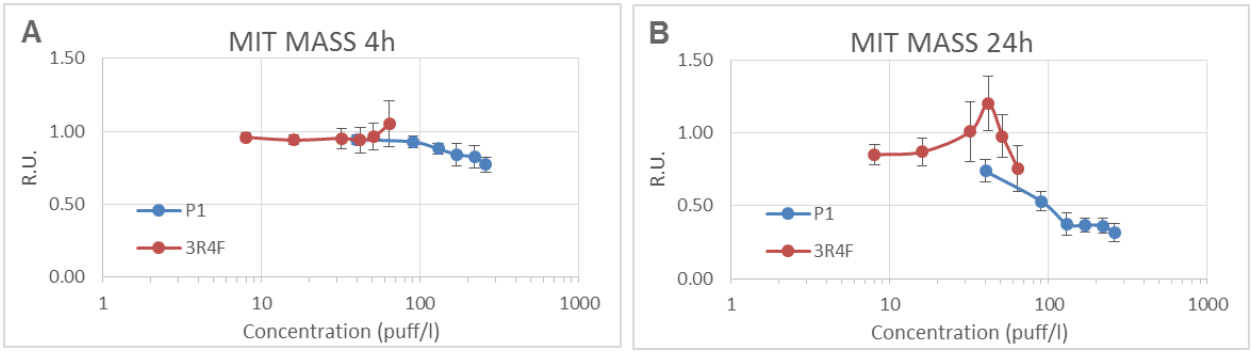

Figure 30. Mitochondrial mass in NHBE cells exposed to the TPM fraction from 3R4F or P1 for 4 h (A) or 24 h (B). *Values are normalized to the vehicle control and represent mean ± SEM.*

Taken together, these results suggest that both 3R4F and P1 TPM can impact on mitochondrial function, although higher doses are required to observe an effect from P1.

9.2.3 sbPBS

Cell count, nuclear size, and DNA structure

The results are shown in ***Figure 31.*** No change in cell count was observed at the 4 h timepoint. At 24 h, a dose-dependent decrease in cell count was observed for 3R4F, and a >50% cell loss was observed at doses above 100 puffs/L. A dose-dependent response was also observed for P1, although the effect was much lower than that of 3R4F. Even at the highest tested dose (350 puffs/L) cell loss was below 50%.

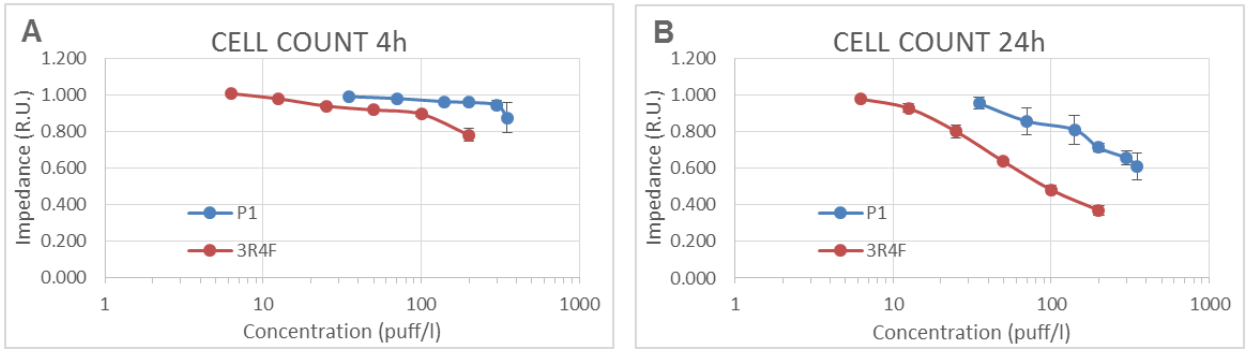

Figure 31. Changes in cell count in NHBE cells exposed to the sbPBS fraction from 3R4F and P1 for 4 h (A) or 24 h (B). *Values are normalized to the vehicle control and represent mean ± SEM.*

No changes in nuclear size were detected for 3R4F or P1 TPM at any timepoint (***Figure 32***).

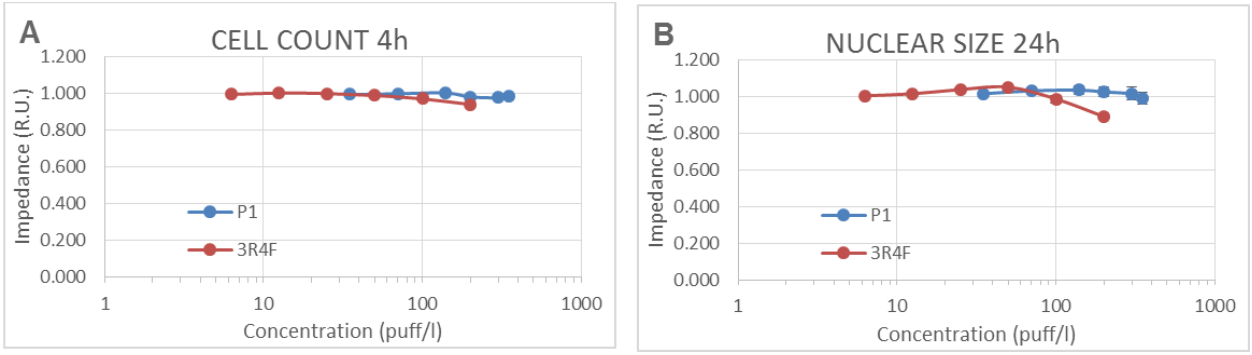

Figure 32. Changes in nuclear size in NHBE cells exposed to the sbPBS fraction from 3R4F or P1 for 4 h (A) or 24 h (B). *Values are normalized to the vehicle control and represent mean ± SEM.*

As shown in ***Figure 33,*** no major changes in DNA structure were observed at the 4 h timepoint. At 24 h, a moderate dose-dependent increase in DNA structure was observed for 3R4F. This increase only occurred at doses at which significant cell loss was observed. No changes were observed for P1 at 24 h.

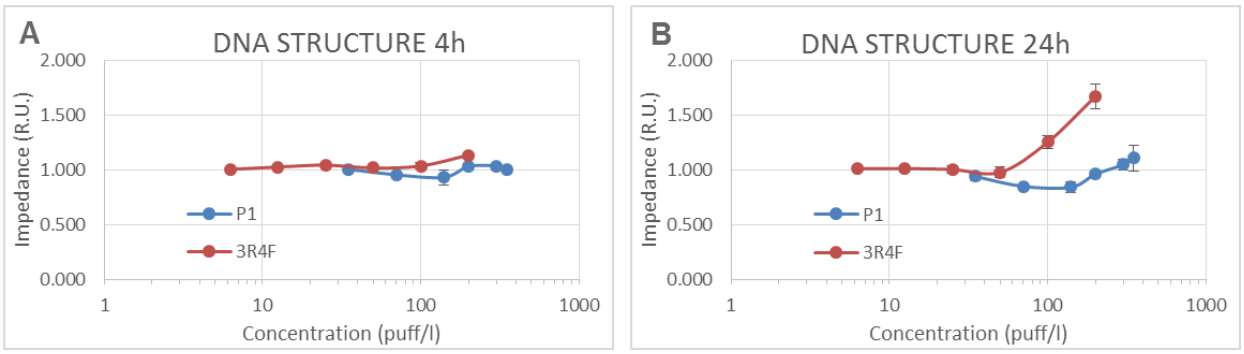

Figure 33. Changes in DNA structure in NHBE cells exposed to the sbPBS fraction from 3R4F or P1 for 4 h (A) 4 or 24 h (B). *Values are normalized to the vehicle control and represent mean ± SEM.*

DNA damage

Exposure to 3R4F resulted in an increase in DNA damage at both 4 h and 24 h, but only at the two highest doses. The increase observed for 3R4F at 4 h occurred in the absence of cell death and thus corresponds to true genotoxicity. The effect observed at the 24 h timepoint was accompanied by >50% cell loss, so is likely to reflect cytotoxicity-induced genotoxicity. With respect to P1, no effects were observed at any timepoint (***Figure 34***).

Taken together, these results indicate that sbPBS from 3R4F, but not from P1, has the potential to induce genotoxicity.

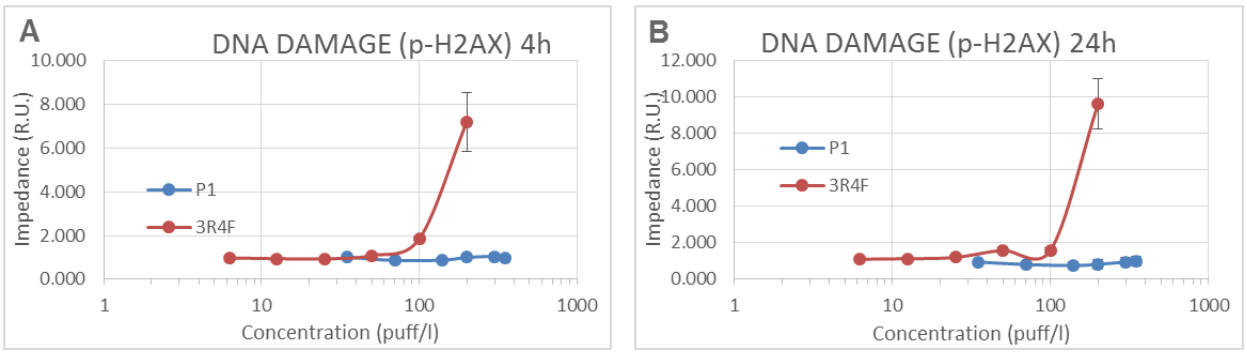

Figure 34. DNA damage in NHBE cells exposed to the sbPBS fraction from 3R4F or P1 for 4 h (A) or 24 h (B). *DNA damage was measured as pH2AX. Values are normalized to the vehicle control and represent mean ± SEM.*

Stress kinase (phospho c-Jun)

No effects were observed at 4 h for either 3R4F or P1 TPM (***Figure 35A***). However, at 24 h, exposure to 3R4F sbPBS resulted in a dose-dependent increase in c-Jun phosphorylation (***Figure 35B***). The decrease in signal observed at the highest 3R4F dose is likely to reflect the high cellular loss. In the case of P1, a moderate increase in p-cJun was observed at high doses, although the magnitude of the response was lower than that of 3R4F. These results indicate that sbPBS from 3R4F is able to induce a much higher level of cellular stress in NHBE cells than P1

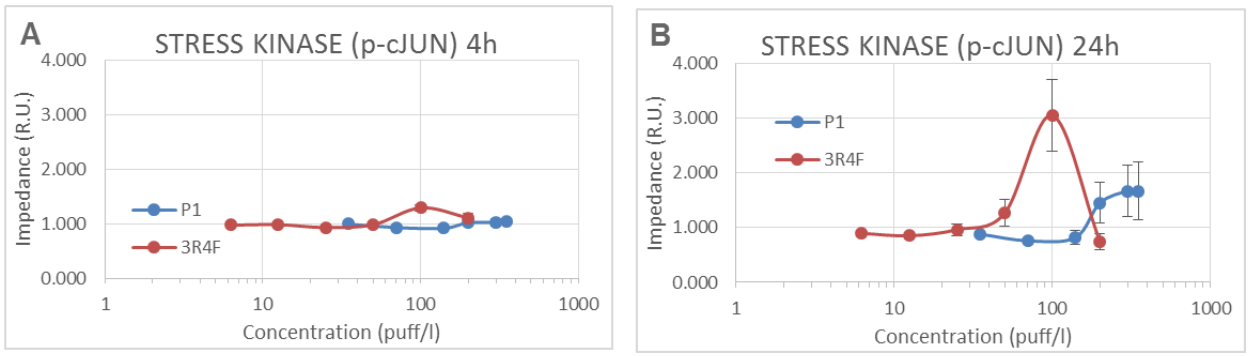

Figure 35. Activation of the stress kinase pathway in NHBE cells exposed to the sbPBS fraction from 3R4F or P1 for 4 h (A) or 24 h (B). *Stress kinase activation was measured as p-cJun. Values are normalized to the vehicle control and represent mean ± SEM.*

Oxidative stress and GSH content

No effects were observed for either test item at 4 h. After 24 h, exposure to 3R4F sbPBS caused an increase in ROS formation. However, this effect was only observed at high doses that also caused significant cell loss, so could reflect the presence of dead cells. No response was observed for P1 at 24 h (***Figure 36***).

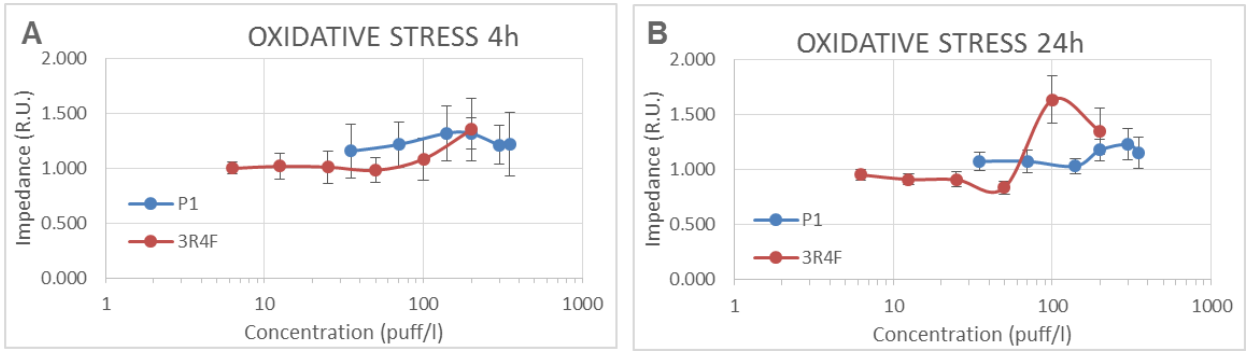

Figure 36. Oxidative stress in NHBE cells exposed to the sbPBS from 3R4F or P1 for 4 h (A) or 24 h (B). Oxidative stress was measured by staining with dihydroethidium (DHE). *Values are normalized to the vehicle control and represent mean ± SEM.*

Exposure to 3R4F caused a dose-dependent decrease in GSH content that was observed at both 4 h and 24 h. This effect occurred at exposure times and doses at which no significant cell loss was observed, so should be considered a true indication of oxidative stress. In the case of P1, a dose-dependent decrease in GSH was also observed at 4 h and 24 h, although the response was lower than that of 3R4F (***Figure 37***).

Taken together, these results indicate that 3R4F sbPBS has a much higher potential to induce oxidative stress in NHBE cells than P1.

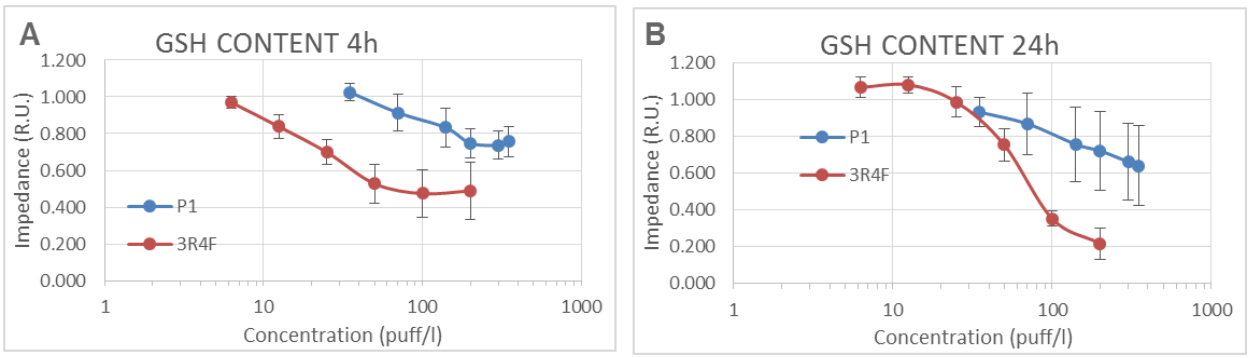

Figure 37. Changes in GSH content in NHBE cells exposed to the sbPBS from 3R4F or P1 for 4 h (A) or 24 h (B). *Values are normalized to the vehicle control and represent mean ± SEM.*

Mitosis

No changes in p-H3 levels were observed after 4 h of exposure to either 3R4F or P1 (***Figure 38A***). At 24 h, an increase in p-H3 was observed for both 3R4F and P1, although much higher concentrations of P1 were required to achieve the same response as in 3R4F (***Figure 38B***).

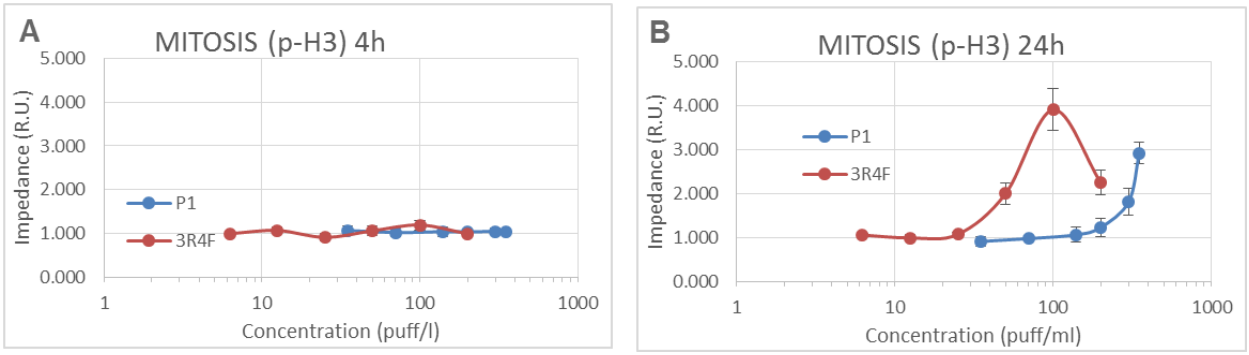

Figure 38. Changes in p-H3 levels in NHBE cells exposed to the sbPBS from 3R4F or P1 for4 h (A) or 24 h (B). *Values are normalized to the vehicle control and represent mean ± SEM.*

Apoptosis and necrosis

No major changes in caspase 3/7 activity were observed for 3R4F or P1 at 4 h or 24 h (***Figure 39A and B***).

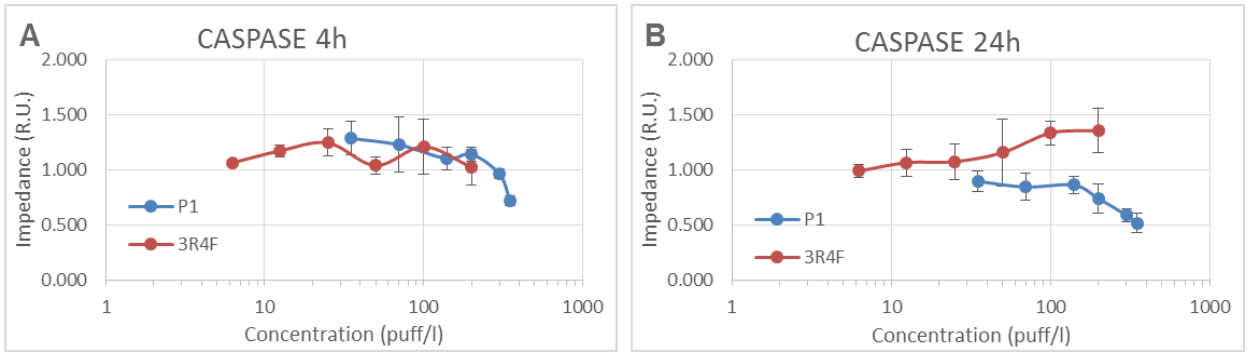

Figure 39. Apoptosis in NHBE cells exposed to the sbPBS from 3R4F or P1 for 4 h (A) or 24 h (B). *Values are normalized to the vehicle control and represent mean ± SEM.*

No significant increase in cytochrome c release was observed after 4 h exposure to either 3R4F or P1 sbPBS (***Figure 40A***). At 24 h, an increase in cytochrome c release was observed for 3R4F, but only at the two highest doses (***Figure 40B***). This effect occurred in the presence of >50% cell loss and thus should be interpreted with caution because it may be secondary to cytotoxicity. A dose-dependent increase in cytochrome c release was observed in P1 at 24 h. This effect occurred at doses resulting in <50% cell loss, so appeared to be indicative of apoptosis.

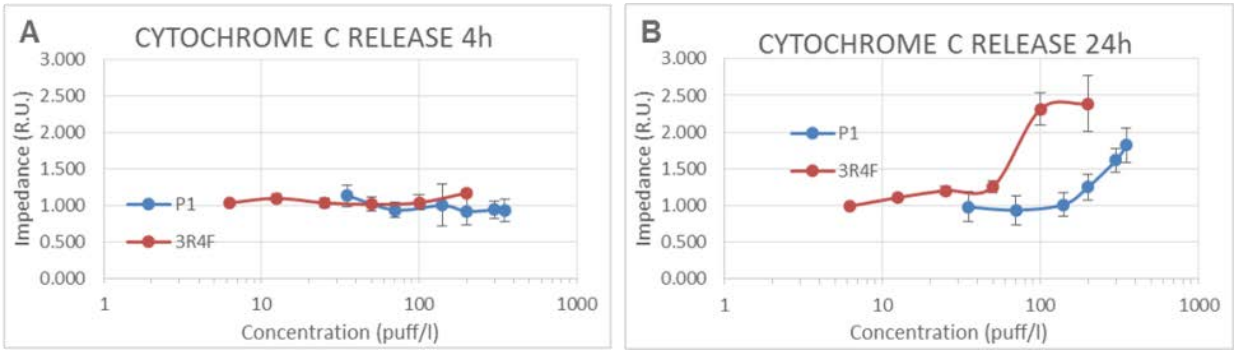

Figure 40. Cytochrome c release in NHBE cells exposed to the sbPBS from 3R4F or P1 for 4 h (A) or 24 h (B). *Values are normalized to the vehicle control and represent mean ± SEM.*

In the case of 3R4F, a dose-dependent increase in cell membrane permeability was observed at 4 h and 24 h (***Figure 41 A and B***). No effects were observed for P1 at any timepoint.

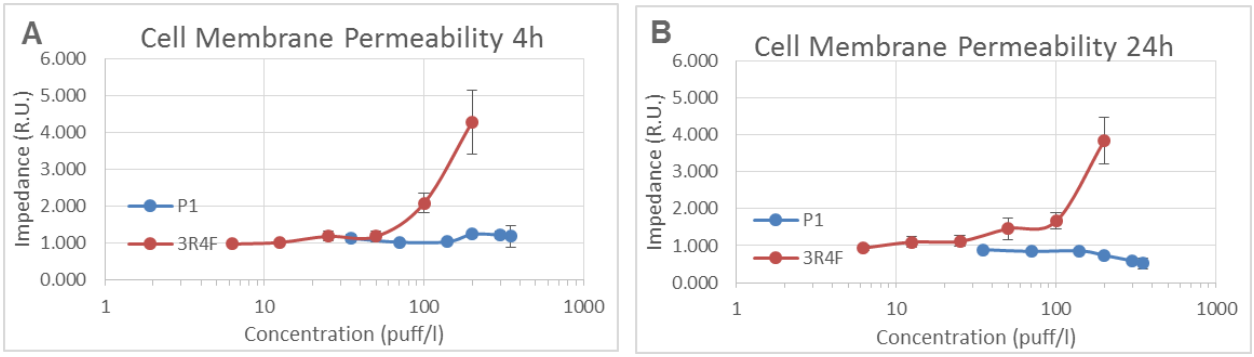

Figure 41. Necrosis in NHBE cells exposed to the sbPBS from 3R4F or P1 for 4 h (A) or 24 h (B). *Values are normalized to the vehicle control and represent mean ± SEM.*

Taken together, these results indicate that sbPBS from 3R4F has the potential to induce cell death via apoptosis and necrosis. In the case of P1, the results suggest a low potential to induce apoptosis, and only at high doses (>100 puffs/L).

Mitochondrial membrane potential and mitochondrial mass

No effects were observed at 4 h for 3R4F or P1 with respect to mitochondrial membrane potential (***Figure 42A***) and only a moderate effect was observed in mitochondrial mass (***Figure 43A)***.

At 24 h, 100 puffs/L 3R4F sbPBS caused an increase in mitochondrial membrane potential (hyperpolarization) (***Figure 42B***) with no changes in mitochondrial mass. This suggested an adaptive mitochondrial response to protect the cell from oxidative or cellular stress. At higher doses, the effects on mitochondrial potential and mass are likely to be nonspecific and a consequence of the elevated cell loss. In the case of P1, a dose-dependent increase in the mitochondrial membrane potential was observed at doses above 120 puffs/L. This occurred with no change in mitochondrial mass, so could reflect a true adaptive response.

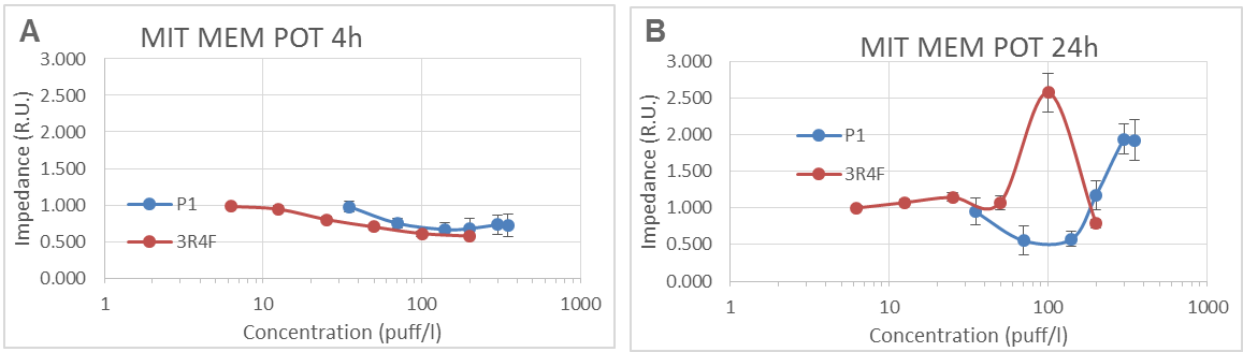

Figure 42. Mitochondrial membrane potential in NHBE cells exposed to the sbPBS from 3R4F or P1 for 4 h (A) or 24 h (B). *Values are normalized to the vehicle control and represent mean ± SEM.*

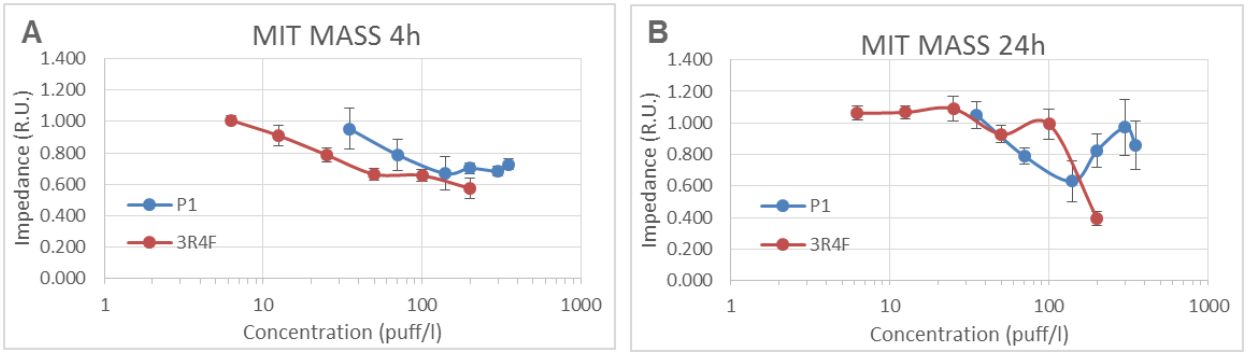

Figure 43. Mitochondrial mass in NHBE cells exposed to the sbPBS from 3R4F or P1 for 4 h (A) or 24 h (B). *Values are normalized to the vehicle control and represent mean ± SEM.*

Overall, the results are not conclusive; while they suggest that both 3R4F and P1 induce mitochondrial stress, additional experiments are required to confirm this.

10. TRANSCRIPTOMIC ANALYSIS

10.1 GVP

10.1.1 Differentially Expressed Genes

Figure 44 shows the volcano plots for NHBE cells exposed to the GVP fraction from 3R4F and P1 after 4 h of exposure compared with a control exposure (PBS). Cells were exposed to three different doses of 3R4F and four doses of P1. The volcano plot is a representation of the signal-to-noise in the gene expression data. The x-axis represents the log2-fold changes, while the y-axis shows the associated –log10 (fdr). The wider the volcano, the greater the fold-changes; similarly, the higher the volcano, the more significant the fold-changes.

Exposure to 3R4F GVP increased the number of differentially expressed genes (DEG), with the highest number observed at the 100 puffs/L dose (236 up-regulated and 81 down-regulated). At the 25 puffs/L dose, only two DEG were identified, possibly because of a loss of statistical power from greater variability within the replicate samples. Exposure to P1 GVP resulted in fewer DEG than 3R4F at all comparable doses. The maximum number of DEG was observed at 13 puffs/L (17 up-regulated and 159 down-regulated).

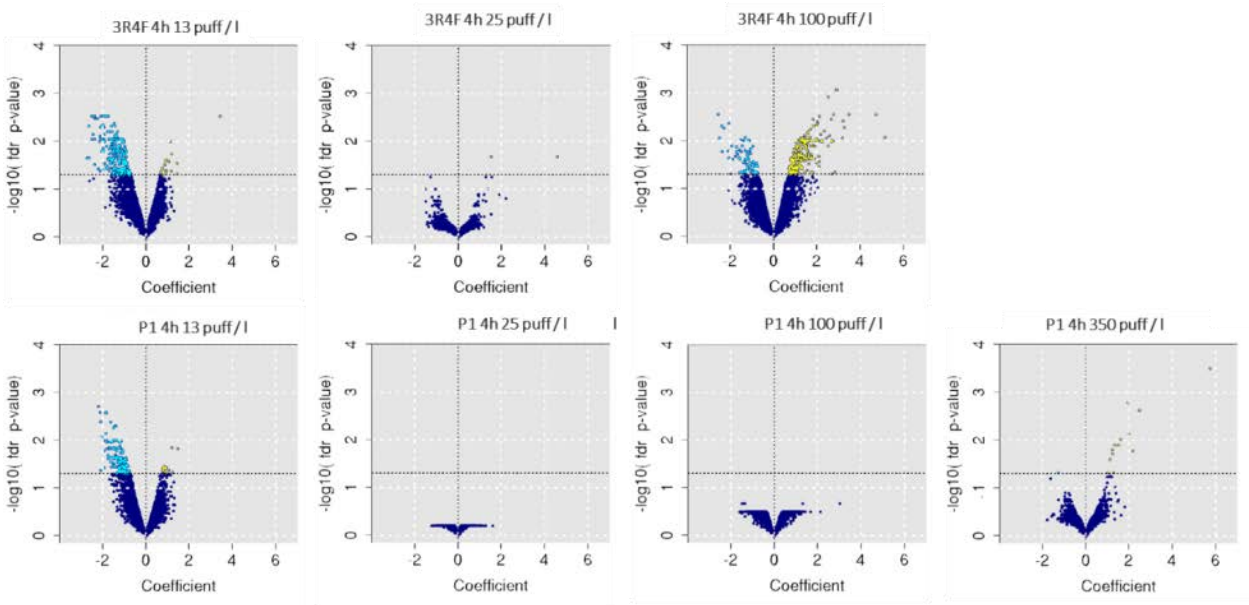

Figure 44. Volcano plots for NHBE cells exposed to the GVP from 3R4F or P1 at the 4-h timepoint. *The gene expression change, calculated as the log2 fold-change, is plotted on the x-axis and the statistical significance, proportional to the negative log10-adjusted p-value, is plotted on the y-axis. Yellow and cyan dots highlight genes that are significantly up- and down-regulated, respectively. Dark blue dots are not statistically significant.*

Figure 45 shows the volcano plots for NHBE cells exposed to the GVP fraction from 3R4F and P1 after 24 h of exposure compared with a control exposure (PBS). The 100 puffs/L dose of 3R4F could not be analyzed at 24 h because of the high cell death. No DEG were found in 3R4F-exposed cells. With the exception of the 13 puffs/L dose, no DEG were observed for P1-exposed cells either.

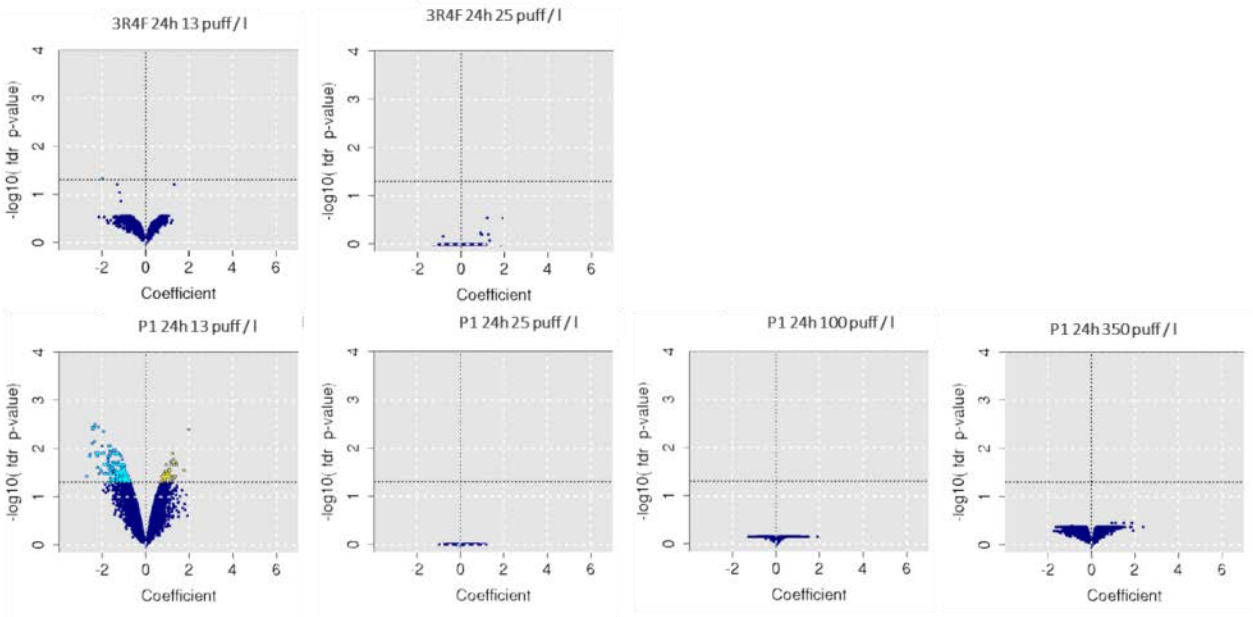

Figure 45. Volcano plots for NHBE cells exposed to the GVP from 3R4F or P1 at the 24-h timepoint. *The gene expression change, calculated as the log2 fold-change, is plotted on the x-axis and the statistical significance, proportional to the negative log10-adjusted p-value, is plotted on the y-axis. Yellow and cyan dots highlight genes that are significantly up- and down-regulated, respectively. Dark blue dots are not statistically significant.*

10.1.2 Analysis of transcriptomic data using a network approach

The use of computational network models to interpret transcriptomic data provides a more detailed molecular understanding of biological network perturbations because the models extract mechanistic information from systems biology datasets. A three-step model building process has been described previously (Gebel et al, 2013; Schlage et al, 2011; Westra et al, 2011), from which we developed a computational approach that enabled the perturbation of biological processes to be quantitatively measured (Hoeng et al, 2012; Martin et al, 2012). The new network perturbation amplitude (NPA2) algorithms overcame some limitations and assumptions of our previously published algorithms (Martin et al, 2014; Martin et al, 2012), with NPA2 integrating network topology with the directionality and sign of the edges. BIF is an aggregated quantity for the biological impact that results from the exposure of a biological system to one or more stimuli. It provides a systems-wide score for all processes that are captured in the network models and their associated NPA scores.

10.1.2.1 Network selection

Network pre-selection was carried out because not all networks are applicable to NHBE cells. The networks are shown in **Table 5**. A selection criterion was that the included subnetworks must have been built in the context of (lung) epithelial cells. Only included subnetworks were used for NPA2 and BIF calculations.

	INCLUDED in BIF Calculation	EXCLUDED in BIF Calculation
Cell Proliferation network	Cell Proliferation/Calcium	
	Cell Proliferation/Cell Cycle	
	Cell Proliferation/Cell Interaction	
	Cell Proliferation/Clock	
	Cell Proliferation/Epigenetics	
	Cell Proliferation/Growth Factor	
	Cell Proliferation/Hedgehog	
	Cell Proliferation/Jak Stat	
	Cell Proliferation/Mapk	
	Cell Proliferation/Notch	
	Cell Proliferation/Nuclear Receptors	
	Cell Proliferation/PGE2	
	Cell Proliferation/Wnt	
Cell Stres network	Cell Stress/Drug Metabolism Response	Cell Stress/Endothelial Shear Stress
	Cell Stress/Endoplasmic Reticulum Stress	
	Cell Stress/Hypoxic Stress	
	Cell Stress/NFE2L2 Signaling	
	Cell Stress/Osmotic Stress	
	Cell Stress/Oxidative Stress	
DACS network	DACS/Apoptosis/-Caspase cascade	DACS/Apoptosis-Agglomerated
	DACS/Apoptosis/-ER stress-induced apoptosis	DACS/DNA Damage-Agglomerated
	DACS/Apoptosis/-MAPK signaling	DACS/Necroptosis-Agglomerated
	DACS/Apoptosis/-NFkB signaling	DACS/Senescence-Agglomerated
	DACS/Apoptosis/-PKC signaling	
	DACS/Apoptosis/-Prosurvival mitochondrial signaling	
	DACS/Apoptosis/-TNFR1Fas signaling	
	DACS/Autophagy/-ATG induction of autophagy	
	DACS/Autophagy/-mTOR signaling	
	DACS/Autophagy/-Nutrient transporter signature	
	DACS/DNA Damage/-Components affecting TP53 activity	
	DACS/DNA Damage/-Components affecting TP63 activity	
	DACS/DNA Damage/-Components affecting TP73 activity	
	DACS/DNA Damage/-DNA damage to G1S checkpoint	
	DACS/DNA Damage/-DNA damage to G2M checkpoint	
	DACS/DNA Damage/-Double-Strand Break Response	
	DACS/DNA Damage/-Inhibition of DNA Repair	
	DACS/DNA Damage/-TP53 TS	
	DACS/Necroptosis/-Fas activation	
	DACS/Necroptosis/-Gene Signature	
	DACS/Senescence/-Oncogene induced senescence	
	DACS/Senescence/-Regulation by tumor suppressors	
	DACS/Senescence/-Regulation of p16INK expression	
	DACS/Senescence/-Replicative senescence	
	DACS/Senescence/-Stress induced premature senescence	
	DACS/Senescence/-Transcriptional regulation of the SASP	
Pulmonary Inflammatory Processes network	IPN/Epithelial cell barrier defense	IPN/Dendritic cell activation
	IPN/Epithelial proinflammatory signaling	IPN/Dendritic cell migration to lymph noc
	IPN/Mucus hypersecretion	IPN/Dendritic cell migration to tissue
	IPN/Tissue damage	IPN/Macrophage activation
		IPN/Macrophage differentiation
		IPN/Macrophage mediated recruitment
		IPN/Mast cell activation
		IPN/Megakaryocyte differentiation
		IPN/Neutrophil chemotaxis
		IPN/Neutrophil response
		IPN/NK cell activation
		IPN/Tc response
		IPN/Th17 differentiation
		IPN/Th1 differentiation
		IPN/Th2 differentiation
		IPN/Treg response

Table 5 : List of included and excluded networks for transcriptomic data analysis.

10.1.2.2 Relative BIF

Figure 46 shows the relative BIF values for NHBE cells exposed to 3R4F and P1 GVP at each timepoint. The highest BIF value corresponded to 100 puffs/L 3R4F at 4 h and was used as a reference (100% response). The BIF values in the other groups are expressed as % of the maximum response.

At the 4 h timepoint, exposure to 3R4F caused an increase in relative BIF. A dose-dependent increase in BIF values was also observed for P1, although the biological impact was lower than that of 3R4F at all comparable doses. Even the highest P1 dose tested (350 puffs/L) had a lower biological impact than the highest 3R4F dose (100 puffs/L). At 24 h, the biological impact was typically lower than at 4 h.

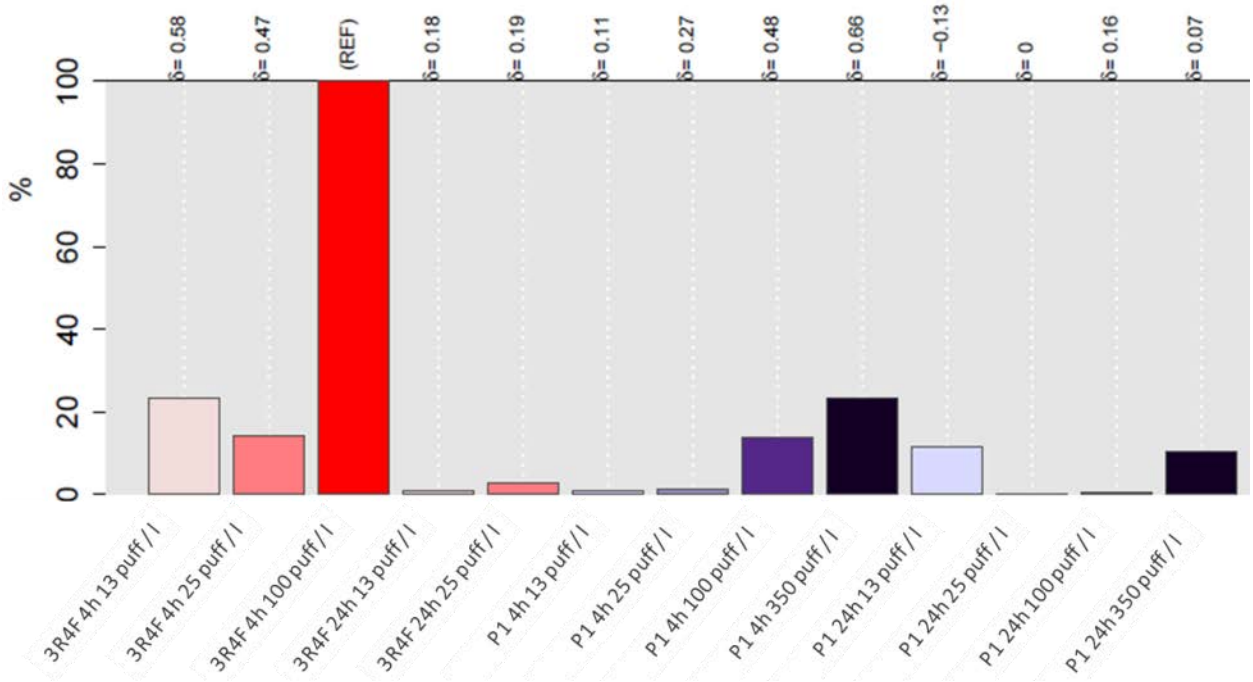

Figure 46: Overall BIF for NHBE cells exposed to 3R4F and P1 GVP using the selected networks (see Table 5). *Biological Impact Factor (BIF) analysis. The percentages show the relative biological impact derived from the cumulated network perturbations caused by the treatment relative to the reference (defined as the treatment comparison showing the highest perturbation). For each treatment comparison, the value (–1 to 1) indicates how similar the underlying network perturbations are with respect to the reference (REF). A value of 1 indicates that all networks are perturbed by the same mechanisms.*

10.1.2.3 Individual network contribution

The biological processes that contributed most to the overall BIF at each timepoint are detailed in the star plots in ***Figure 47***. After 4 h exposure, the most perturbed networks (those that contributed most to the BIF value) were cell stress, proliferation, and senescence. Necroptosis and autophagy were the least involved processes. At comparable doses, the biological impact of P1 GVP was much lower than that of 3R4F.

After 24 h of exposure, the most perturbed networks were still cell stress and proliferation.

Nevertheless, the level of perturbation was considerably lower than at the 4 h timepoint. This effect could be explained, at least in part, by the fact that the GVP phase of 3R4F smoke is enriched in carbonyls and other volatile compounds. Therefore, it is reasonable to assume that after 24 h in culture, most of the constituents of the GVP phase have evaporated from the culture medium, and that only the acute effects of GVP (4 h) can be observed. This observation also suggests the existence of a toxicity threshold for 3R4F GVP exposure. At doses of 13–25 puffs/L, the cells would tolerate the toxic effects of 3R4F. However, at higher doses (100 puffs/L), the acute effects of 3R4F exposure would likely overcome the cell's defense mechanisms, leading to the activation of cellular death programs. This hypothesis would explain the high cellular death observed after exposure to 100 puffs/L 3R4F for 24 h, which prevented the transcriptomic analysis of this sample.

Each network can be decomposed into several subnetworks representing one or more specific biological processes. Heat maps were generated to gain more insights into the similarities and differences of the perturbed subnetworks at the 4h timepoint (***Figure 48***). For clarity purposes, and because of the low biological impact observed at 24 h, this timepoint was not considered for more detailed analysis.

Clearly, the two lower doses of 3R4F have a similar network perturbation pattern, whereas the effect at the highest dose is more intense, not only in the number of perturbed subnetworks but also with respect to the intensity of the perturbation itself. By contrast, exposure to P1 doses even three times higher than the highest 3R4F dose showed only a moderate impact on the different subnetworks.

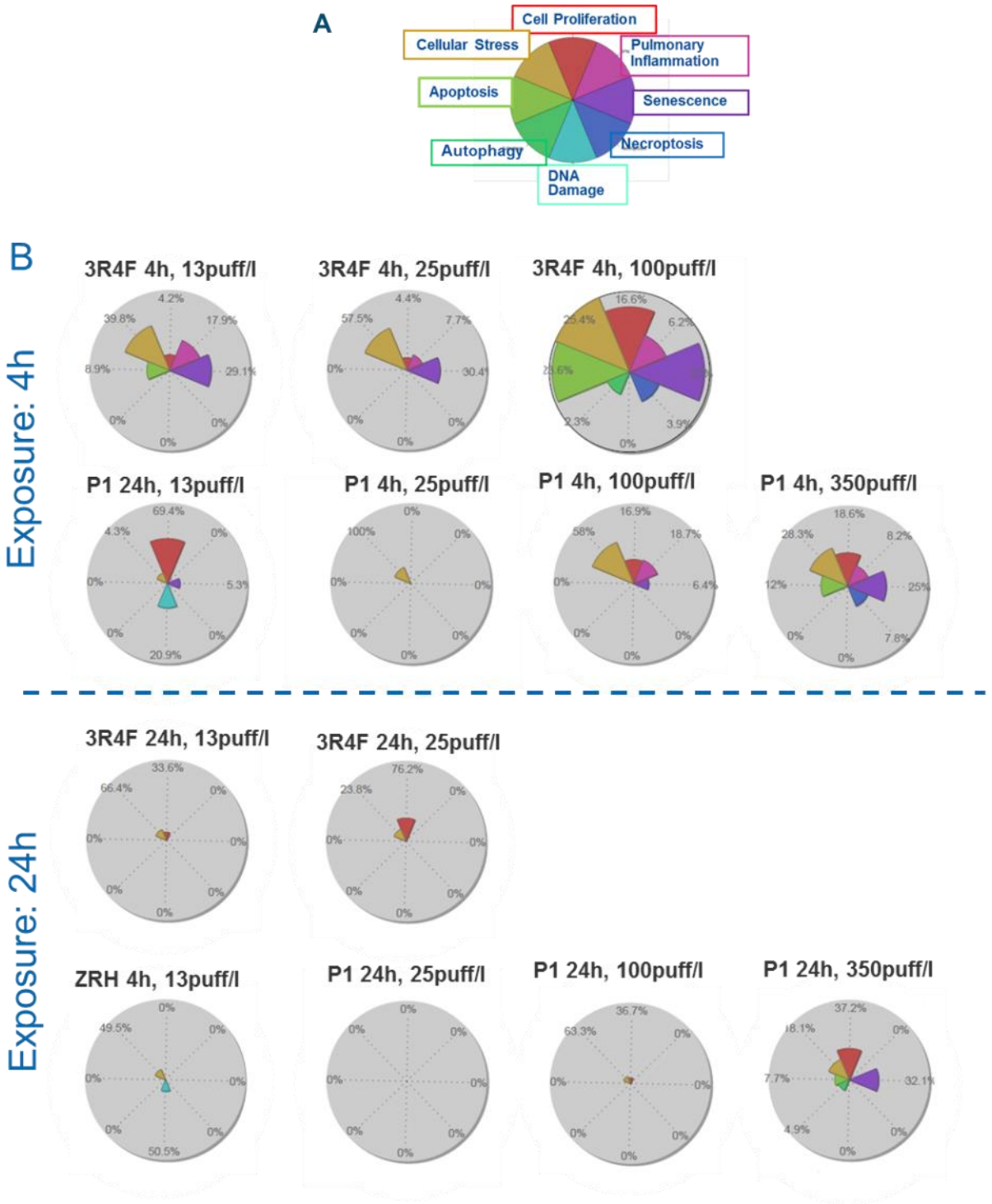

Figure 47: Individual contributions to overall BIF values. *(A) Color code of the BIF networks. (B) Starplots illustrating the decomposition of the overall relative BIF (RBIF) into its mechanistic components (from cell proliferation to inflammation, indicated by the colors of the segments) for each treatment group. The surface area of each segment is proportional to the contribution within a particular treatment of each network perturbation (shown as percent in the labels). It is further adjusted by the RBIF for the treatment compared with the reference, so that the sum of the segment areas for each treatment equals the RBIF for the treatment. The pie chart represents the distribution of the sum of contributions for each network across all treatment groups. They all sum to 100%.*

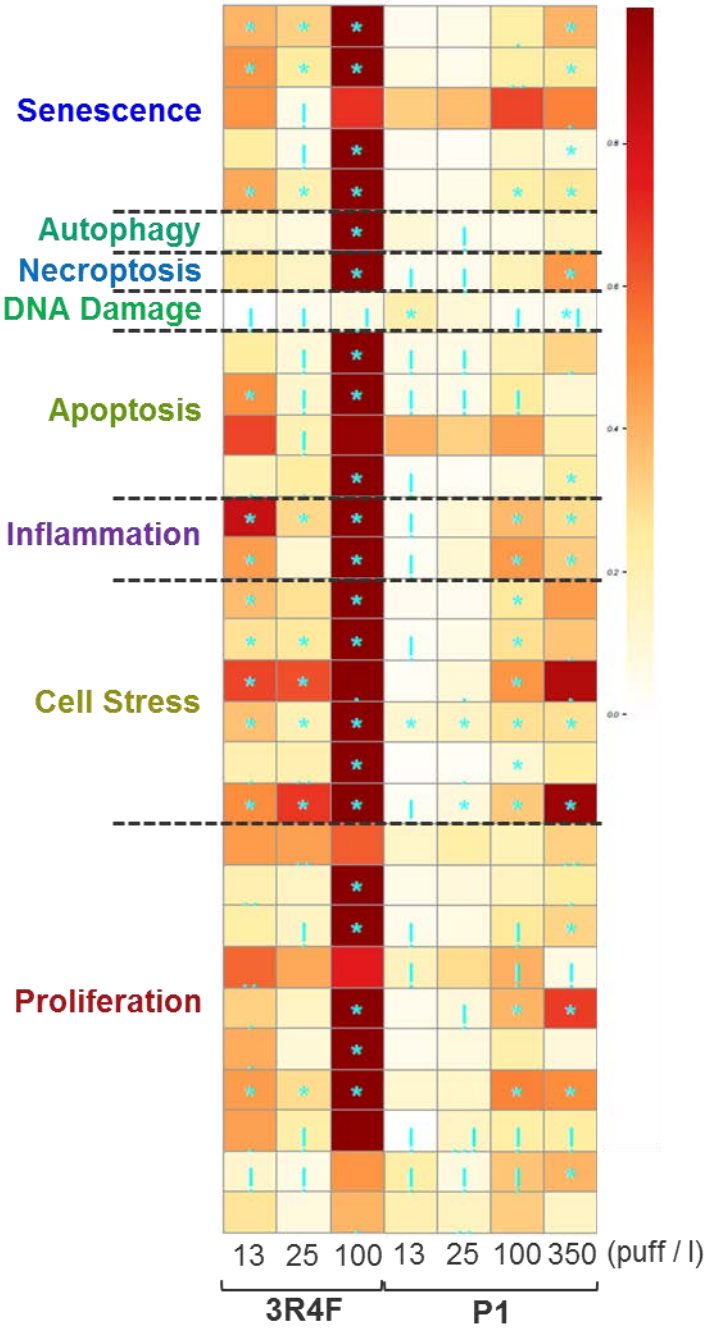

Figure 48: Heatmap with perturbed subnetwoks*. Heatmap summarizing subnetworks significantly perturbed in at least one treatment. A network is considered to be perturbed if, in addition to the significance of the NPA score with respect to the experimental variation, the two companion statistics (O and K) that inform on the specificity of the NPA score with respect to the biology described in the network, are also significant.*

10.2 TPM

10.2.1 Differentially expressed genes

Figure 49 shows the volcano plots for NHBE cells exposed to the TPM fraction from 3R4F and P1 after 4 h of exposure compared with a control exposure (ethanol). Cells were exposed to three doses of 3R4F (13, 25, and 32 puffs/L) and three doses of P1 (25, 32, and 380 puffs/L).

Exposure to 3R4F gradually increased the number of DEG, with the highest number observed at the 32 puffs/L dose (108 up-regulated and 27 down-regulated). By contrast, exposure to P1 TPM at comparable doses resulted in only two DEG (one up-regulated and one down-regulated). Even exposure to a P1 dose 10-fold higher than the highest 3R4F dose (380 puffs/L) resulted in only two DEG.

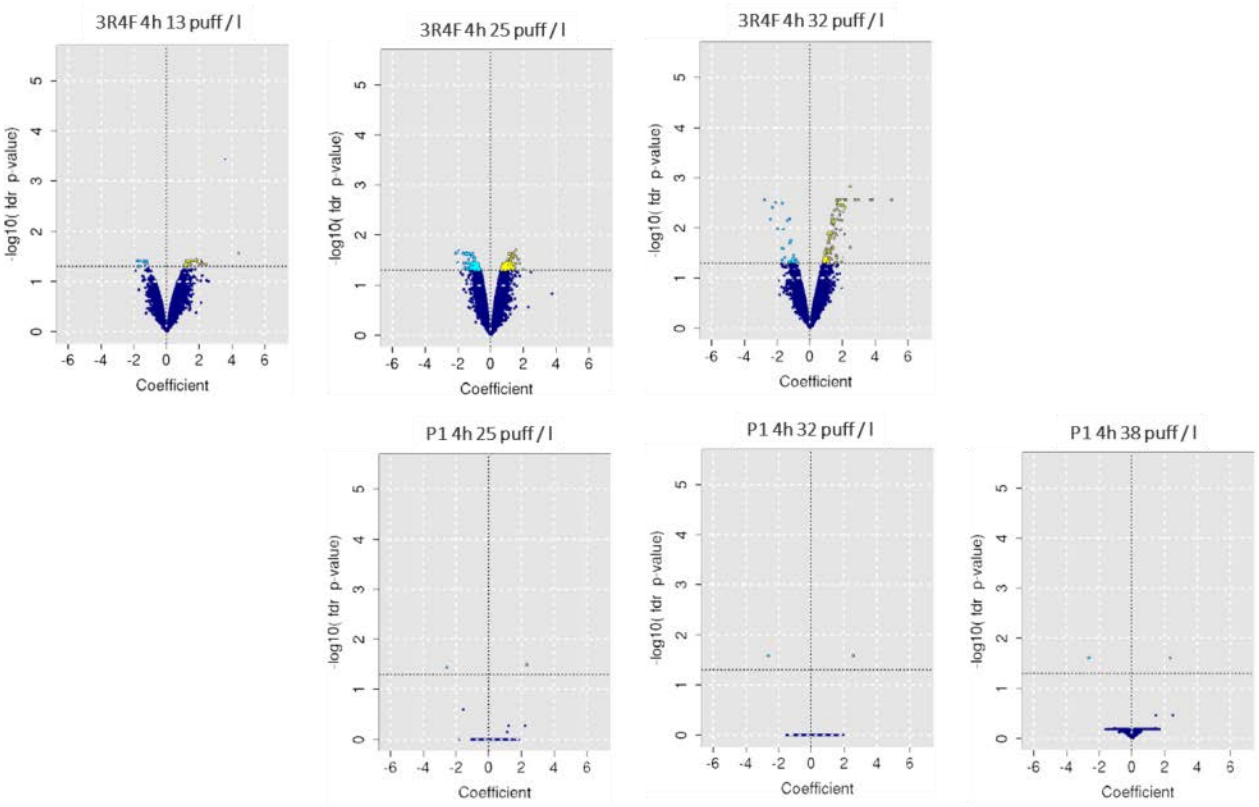

Figure 49. Volcano plots for NHBE cells exposed to the TPM from 3R4F or P1 at the 4-h timepoint. *The gene expression change, calculated as the log2 fold-change, is plotted on the x-axis and the statistical significance, proportional to the negative log10-adjusted p-value, is plotted on the y-axis. Yellow and cyan dots highlight genes that are significantly up- and down-regulated, respectively. Dark blue dots are not statistically significant.*

Figure 50 shows the volcano plots for NHBE cells exposed to the TPM fraction from 3R4F and P1 after 24 h of exposure compared with a control exposure (ethanol). The 32 puffs/L dose of 3R4F could not be analyzed at 24 h because of the high cell death rate. At lower 3R4F concentrations, the number of DEG gradually increased dose-dependently, with the highest number observed at the 25 puffs/L dose (2,259 up-regulated and 2,362 down-regulated). No DEG were found in P1-exposed cells.

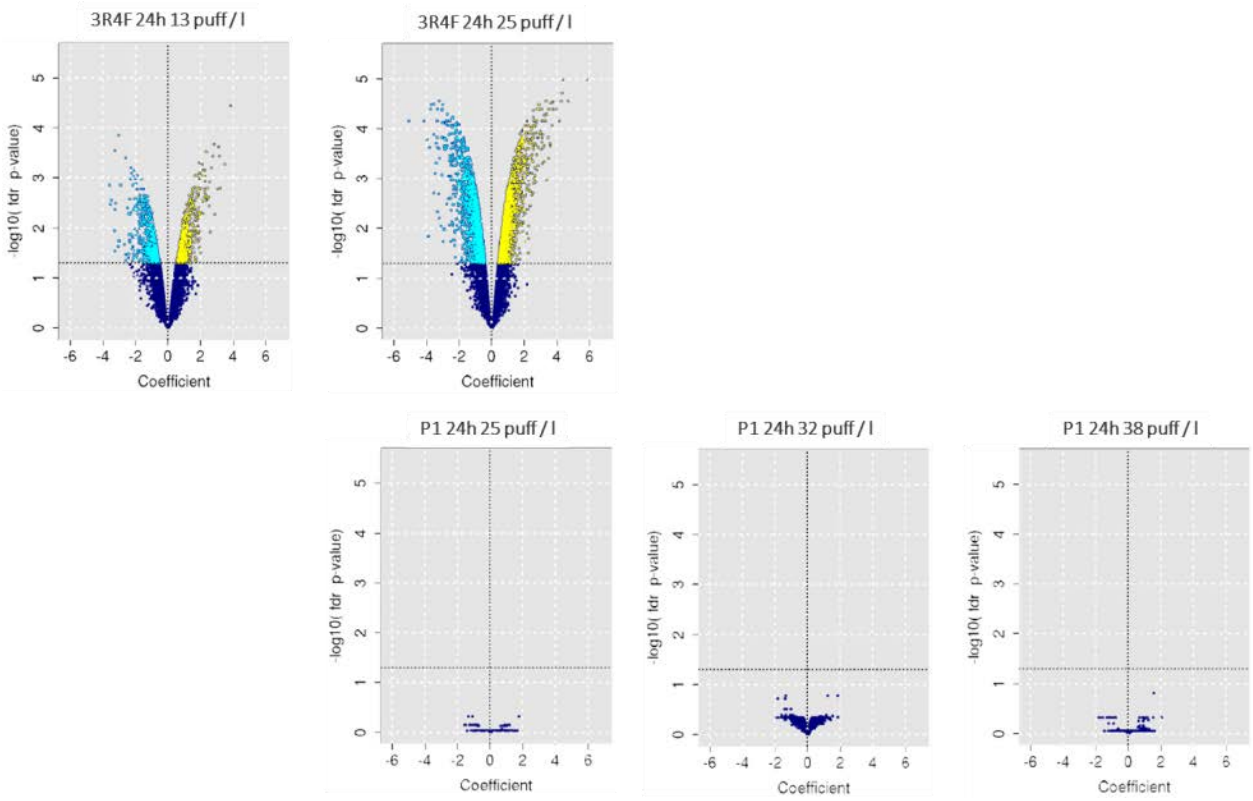

Figure 50. Volcano plots for NHBE cells exposed to the TPM from 3R4F or P1 at the 24-h timepoint. *The gene expression change, calculated as the log2 fold change, is plotted on the x-axis and the statistical significance, proportional to the negative log10-adjusted p-value, is plotted on the y-axis. Yellow and cyan dots highlight genes that are significantly up- and down-regulated, respectively. Dark blue dots are not statistically significant.*

10.2.2 Analysis of transcriptomic data using a network approach

10.2.2.1 Relative BIF

Figure 51 shows the relative BIF values for NHBE cells exposed to 3R4F and P1 TPM at each timepoint. The highest BIF value corresponded to 32 puffs/L 3R4F at 4 h and was used as a reference (100% response). The BIF values in the other groups are expressed as % of the maximum response.

At the 4 h timepoint, exposure to 3R4F caused an increase in relative BIF. By contrast, the biological impact of exposure to the tested doses of P1 TPM was minimal, as shown by the low BIF values. Even the highest P1 TPM dose (38 puffs/L) has a much lower BIF value than the highest 3R4F dose (32 puffs/L).

Similar results were observed at 24 h, with 3R4F-exposed cells showing higher BIF values than P1-exposed cells. However, the values at this timepoint were lower than those observed at 4 h.

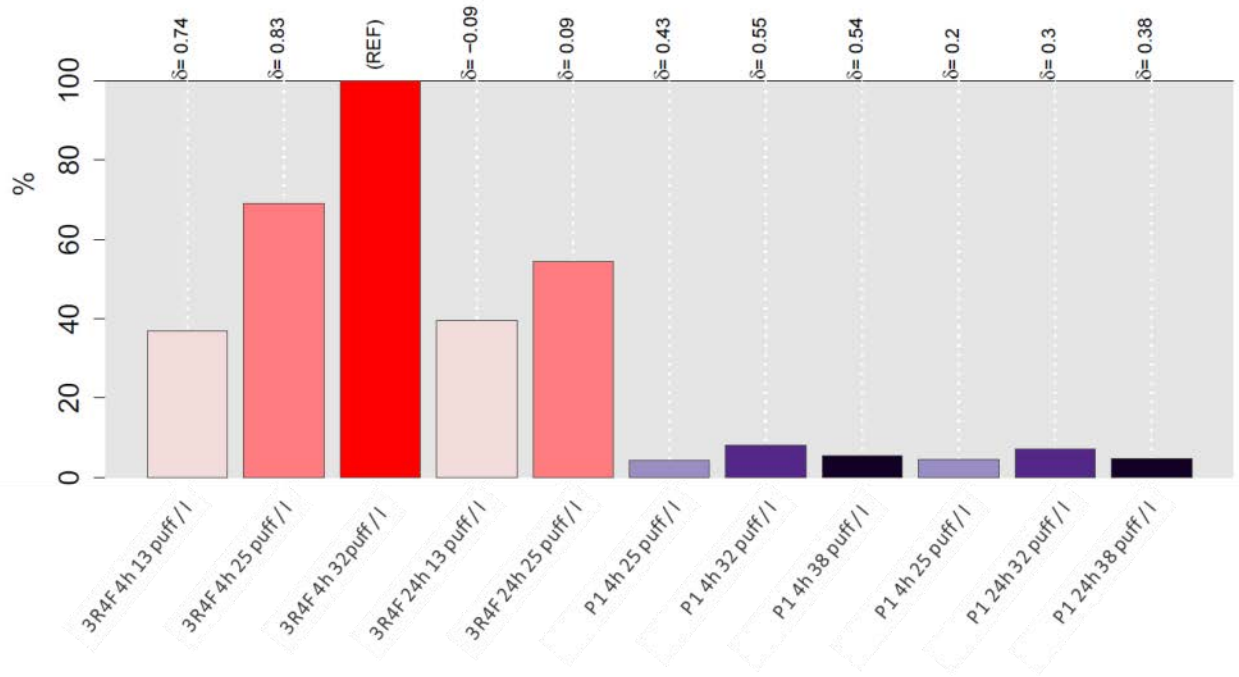

Figure 51: Overall BIF for NHBE cells exposed to the 3R4F or P1 TPM using the selected networks (see Table 5). *Biological Impact Factor (BIF) analysis. The percentages show the relative biological impact derived from the cumulated network perturbations caused by the treatment relative to the reference (defined as the treatment comparison showing the highest perturbation). For each treatment comparison, the value (–1 to 1) indicates how similar the underlying network perturbations are with respect to the reference (REF). A value of 1 indicates that all the networks are perturbed by the same mechanisms.*

10.2.2.2 Individual network contribution

The biological processes that contributed most to the overall BIF at each timepoint are detailed in the star plots in ***Figure 52***. After 4 h of exposure to 3R4F TPM, multiple networks were perturbed. At the lower 3R4F dose, all networks except necroptosis showed significant perturbation, with proliferation, inflammation, and cells stress the top contributors. In the case of P1, cell stress was the most perturbed network, although once again, the overall effects were much lower than 3R4F.

At 24 h, the biological impact of exposure to 3R4F was similar to that at 4 h, although the level of perturbation was lower. Proliferation, cell stress, and inflammation networks were the most significant, although all networks except necroptosis were perturbed. In the case of P1, the level of perturbation was again much lower than 3R4F.

The TPM fraction contains both insoluble material and volatile smoke constituents (e.g. carbonyls). After 24 h of exposure, volatile compounds are likely to have evaporated; however, the insoluble particulate would still be present in the culture medium. This could explain why the biological impact of 3R4F was observed both at 4 h and 24 h of exposure, in contrast to GVP.

Both the amount of P1 TPM per stick and its chemical complexity are much lower than in 3R4F. This may help explain why the biological impact of P1 was much lower than 3R4F even at very high doses (38 puffs/L).

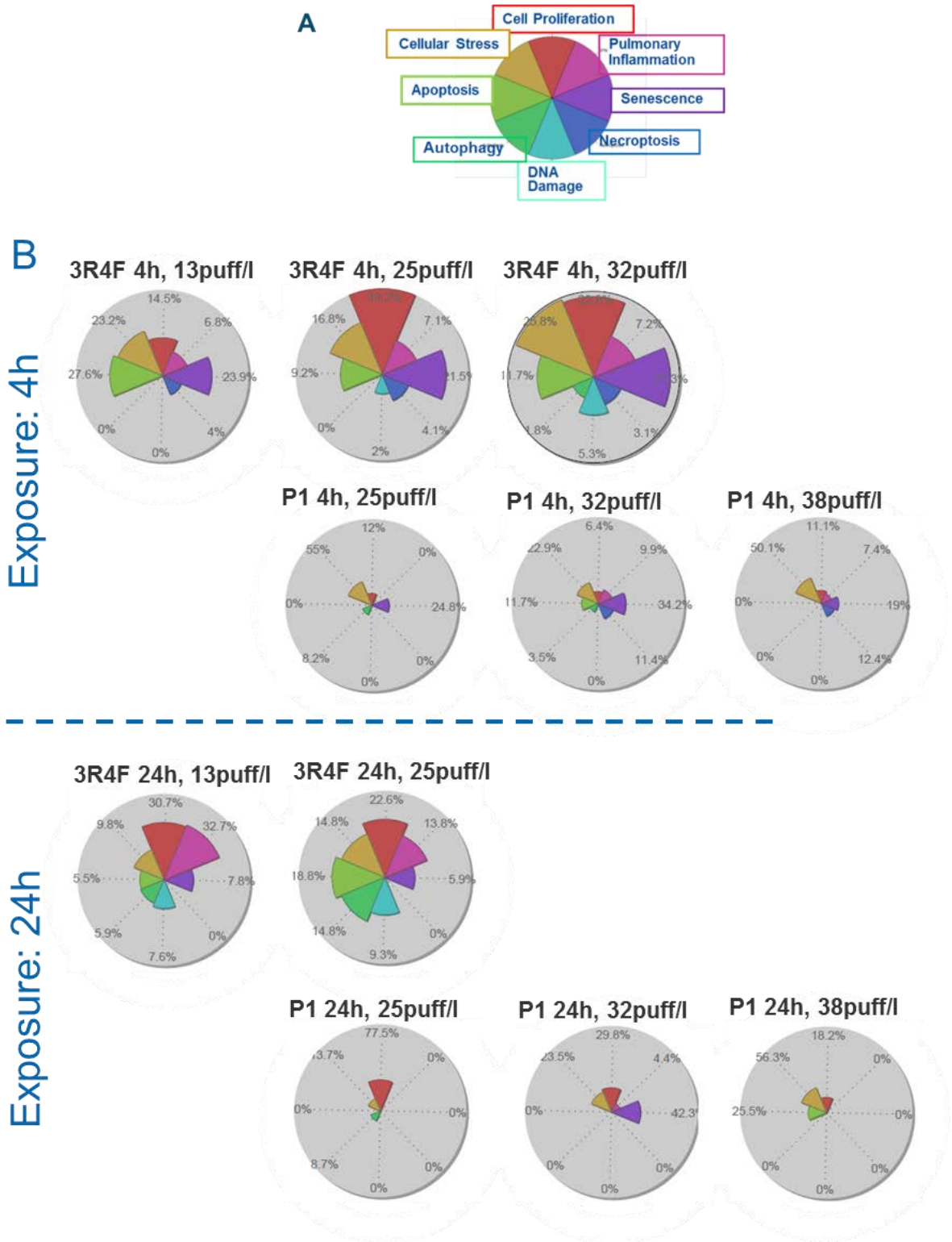

Figure 52: Individual contributions to overall BIF values. *(A) Color code of the BIF networks. (B) Starplots illustrating the decomposition of the overall relative BIF (RBIF) into its mechanistic components (from cell proliferation to inflammation, indicated by the colors of the segments) for each treatment group. The surface area of each slice is proportional to the contribution within a particular treatment of each network perturbation (shown as percent in the labels). It is further adjusted by the RBIF for the treatment compared with the reference, so that the sum of the segment areas for each treatment equals the*

RBIF for the treatment. The pie chart represents the distribution of the sum of contributions for each network across all treatment groups. They all sum to 100%.

Each network can be decomposed into several subnetworks representing one or more specific biological processes. Heat maps were generated to gain more insights into the similarities and differences of the perturbed subnetworks at the 4 h and 24 h timepoints (***Figure 53***).

A dose-dependent increase in network perturbation was observed for 3R4F at both 4 h and 24 h. This was observed across most subnetworks investigated, with the exception of autophagy. Clearly, the two lower doses of 3R4F have a similar network perturbation pattern, whereas the effect at the highest dose was more intense, not only in the number of perturbed subnetworks but also with respect to the intensity of the perturbation itself. By contrast, exposure to P1 doses even three times higher than the highest 3R4F dose showed only a moderate impact on the different subnetworks. In the case of P1, very little network perturbation was observed at either 4 h or 24 h, thus confirming the lower biological impact compared with 3R4F.

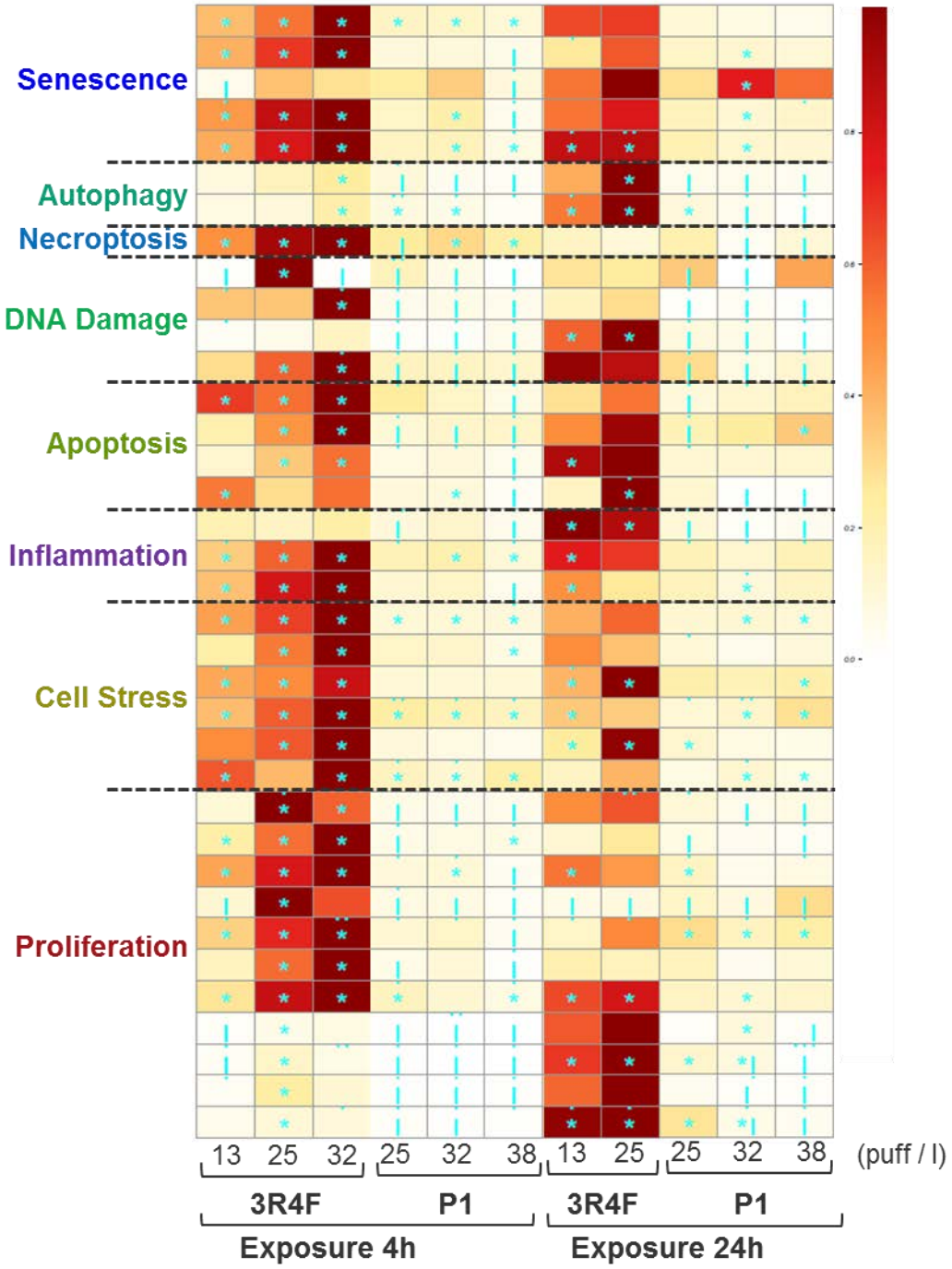

Figure 53: Heatmap with perturbed subnetworks*. Heatmap summarizing subnetworks significantly perturbed in at least one treatment. A network is considered to be perturbed if, in addition to the significance of the NPA score with respect to the experimental variation, the two companion statistics (O and K) that show the specificity of the NPA score with respect to the biology described in the network, are also significant.*

10.3 sbPBS

10.3.1 Differentially expressed genes

Figure 54 shows the volcano plots for NHBE cells exposed to the sbPBS from 3R4F and P1 after 4 h of exposure compared with a control exposure (PBS). Cells were exposed to three doses of 3R4F (13, 25, and 100 puffs/L) and three doses of P1 (25, 100, and 350 puffs/L).

Exposure to 3R4F gradually increased the number of DEG, with the highest number observed at the 100 puffs/L dose (790 up-regulated and 405 down-regulated). By contrast, exposure to P1 sbPBS at comparable doses resulted in no DEG and only 28 DEG (18 up-regulated and 10 down-regulated) at a dose 3.5-fold higher than the highest 3R4F dose (350 puffs/L).

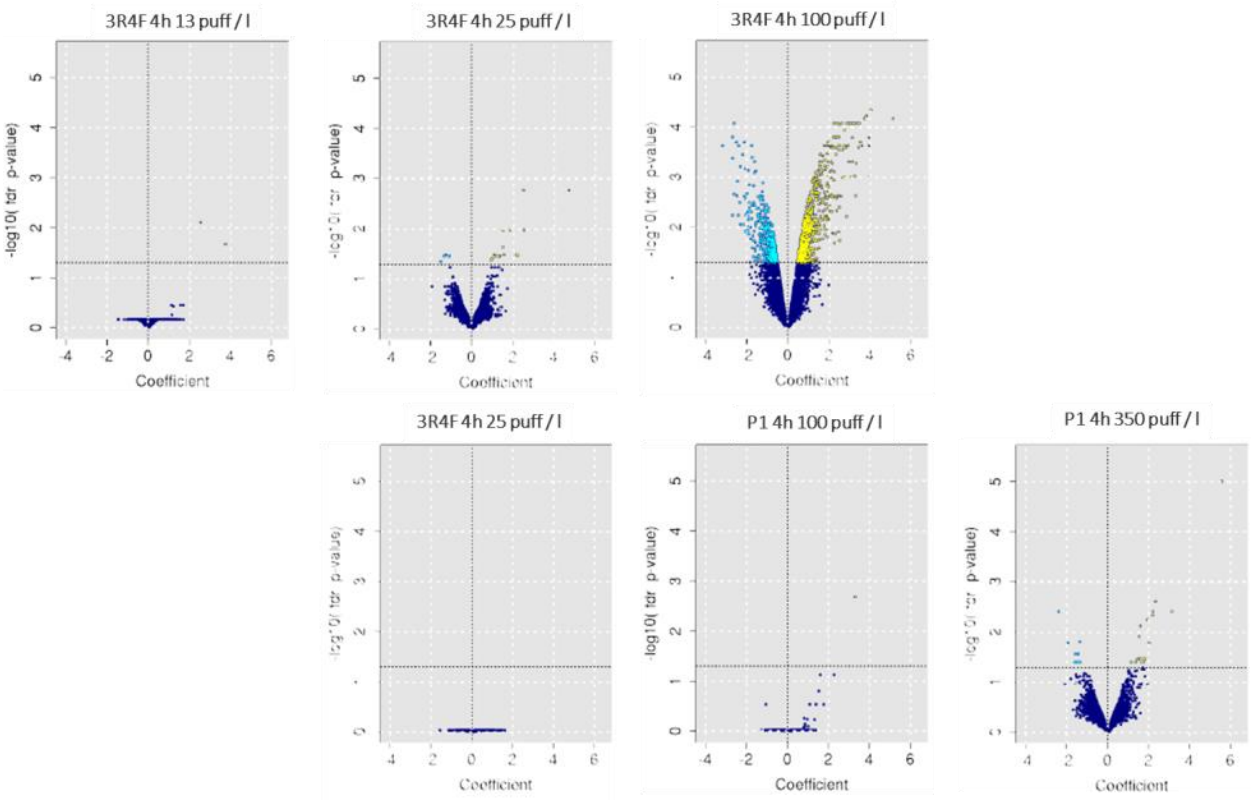

Figure 54. Volcano plots for NHBE cells exposed to the 3R4F and P1 sbPBS at the 24-h timepoint. *The gene expression change, calculated as the log2 fold change, is plotted on the x-axis and the statistical significance, proportional to the negative log10-adjusted p-value, is plotted on the y-axis. Yellow and cyan dots highlight genes that are significantly up- and down-regulated, respectively. Dark blue dots are not statistically significant.*

Figure 55 shows the volcano plots for NHBE cells exposed to the sbPBS from 3R4F and P1 after 24 h of exposure compared with a control exposure (PBS). The 100 puffs/L dose of 3R4F could not be analyzed at 24 h because of the high levels of cell death. No DEG were found in cells exposed to 3R4F. At comparable doses of P1, no DEG were found either, and only five DEG (one up-regulated and four down-regulated) were found at a dose 3.5-fold higher than the highest 3R4F dose (350 puffs/L).

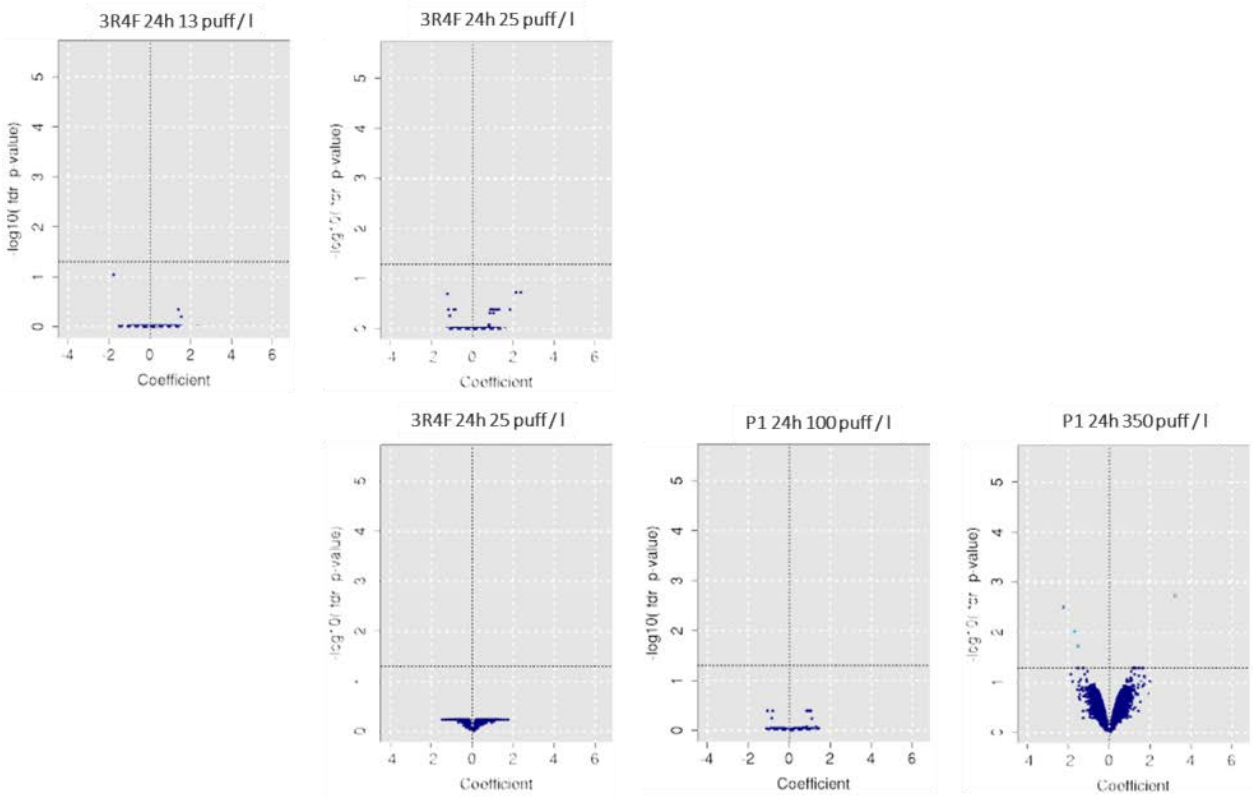

Figure 55. Volcano plots for NHBE cells exposed to the 3R4F or P1 sbPBS at the 4-h timepoint. *The gene expression change, calculated as the log2 fold change, is plotted on the x-axis and the statistical significance, proportional to the negative log10-adjusted p-value, is plotted on the y-axis. Yellow and cyan dots highlight genes that are significantly up- and down-regulated, respectively. Dark blue dots are not statistically significant.*

10.3.2 Analysis of transcriptomic data using a network approach

10.3.2.1 Relative BIF

Figure 56 shows the relative BIF values for NHBE cells exposed to the 3R4F and P1 sbPBS at each timepoint. The highest BIF value corresponded to 3R4F 100 puffs/L at 4h and was used as the reference (100% response). The BIF values in the other groups are expressed as % of the maximum response.

At the 4 h timepoint, exposure to increasing doses of either 3R4F or P1 caused an increase in relative BIF. However, the biological impact of P1 was much lower compared with 3R4F. Exposure to even the highest dose of P1 (350 puffs/L) resulted in a lower BIF value than a 3.5-fold lower dose of 3R4F (100 puffs/L).

At 24 h, relative BIF values for both test items were lower than at the 4 h timepoint. Nevertheless, the biological impact of exposure to P1 was lower than that of exposure to 3R4F.

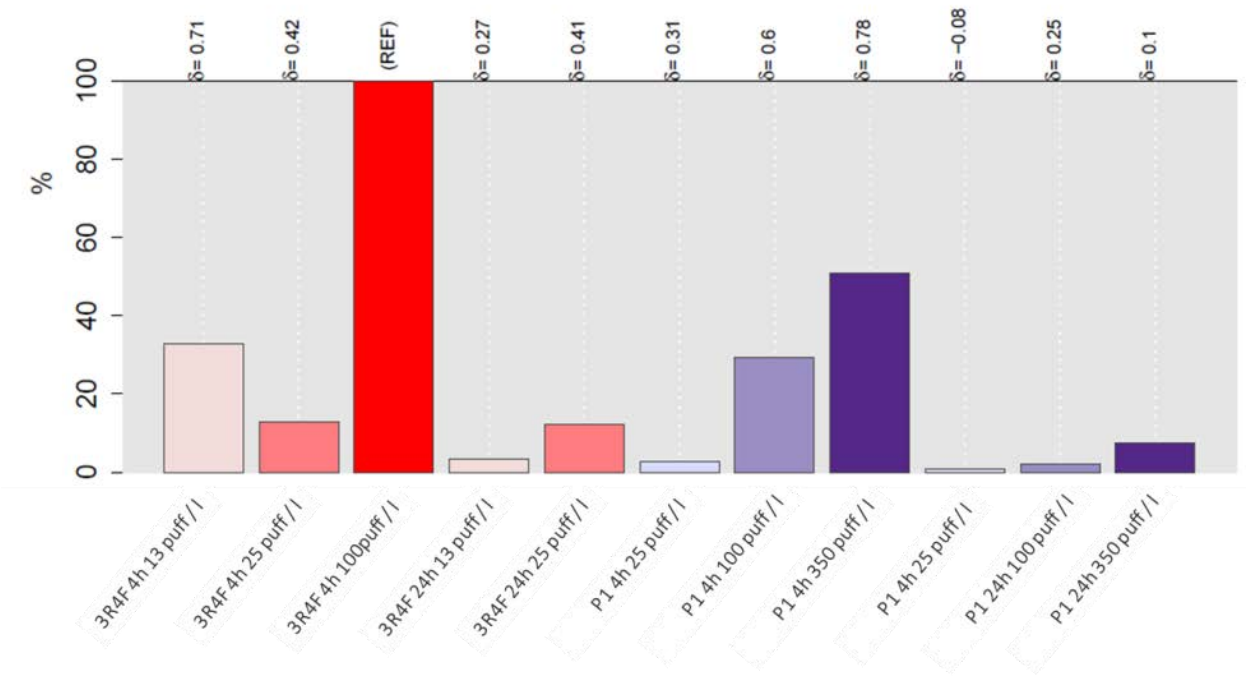

Figure 56: Overall BIF for NHBE cells exposed to sbPBS from 3R4F or P1 using the selected networks (see Table 5). *Biological Impact Factor (BIF) analysis. The percentages give the relative biological impact derived from the cumulated network perturbations caused by the treatment relative to the reference (defined as the treatment comparison showing the highest perturbation). For each treatment comparison, the value (–1 to 1) indicates how similar the underlying network perturbations are with respect to the reference (REF). A value of 1 indicates that all the networks are perturbed by the same mechanisms.*

10.3.2.2 Individual network contribution

The biological processes that contributed most to the overall BIF at each timepoint are detailed in the star plots in ***Figure 57.*** After 4 h exposure to 3R4F most networks were perturbed, with proliferation, cell stress, and senescence the most impacted. In the case of P1, a dose-dependent increase in network perturbation was observed, with proliferation, cell stress, and senescence the most perturbed networks. Nevertheless, at comparable doses, the biological impact of P1 was lower than that of 3R4F. Even at the highest P1 dose (350 puffs/L), the level of perturbation across all networks was lower than the highest 3R4F dose (100 puffs/L).

At 24 h, we observed a dramatic decrease in network perturbation in both test items. In the case of 3R4F, only the inflammation network was significantly perturbed at the lowest dose (13 puffs/L). At a higher dose (25 puffs/L), most networks were perturbed, particularly proliferation. In the case of P1, a dose-dependent increase in cell stress and proliferation network perturbation was observed. However, the effects were lower than those of 3R4F.

The differences in response between the two timepoints could again be related to the chemical composition of the fraction. Although sbPBS contains TPM, this only contributes a small percentage to the overall fraction composition. Most of the sbPBS fraction is formed by vapor phase constituents, many of which are highly volatile. Therefore, it is reasonable to assume that, similar to GVP, most phase constituents would be evaporated after 24 h in cell culture medium. Once again, this

observation also suggests the existence of a toxicity threshold for 3R4F sbPBS exposure. At doses of 13-25 puffs/L, the cells would tolerate the toxic effects of 3R4F. However, at a dose of 100 puffs/L, the acute effects of 3R4F exposure would likely overcome the cell's defense mechanisms, leading to the activation of cellular death programs. This hypothesis would explain the high cellular death observed after exposure to 100 puffs/L (***Figure 5***) 3R4F for 24 h, which prevented the use of this concentration for transcriptomic analysis.

Each network can be decomposed into several subnetworks representing one or more specific biological processes. Heat maps were generated to gain more insights into the similarities and differences of the perturbed subnetworks at the 4 h and 24 h timepoints (***Figure 57***).

At 4 h, the 13 puffs/L and 100 puffs/L doses of 3R4F showed a similar network perturbation pattern, although the latter at a much higher level. It is not clear why the 25 puffs/L 3R4F dose behaved differently, although it is possible that the higher experimental variation in this sample prevented the NPA values from overcoming the statistical cutoffs. In the case of P1, a dose-dependent increase in the number and intensity of network perturbation was observed, although the effect was lower than at comparable 3R4F doses.

Very few perturbed subnetworks were observed for both items at 24 h.

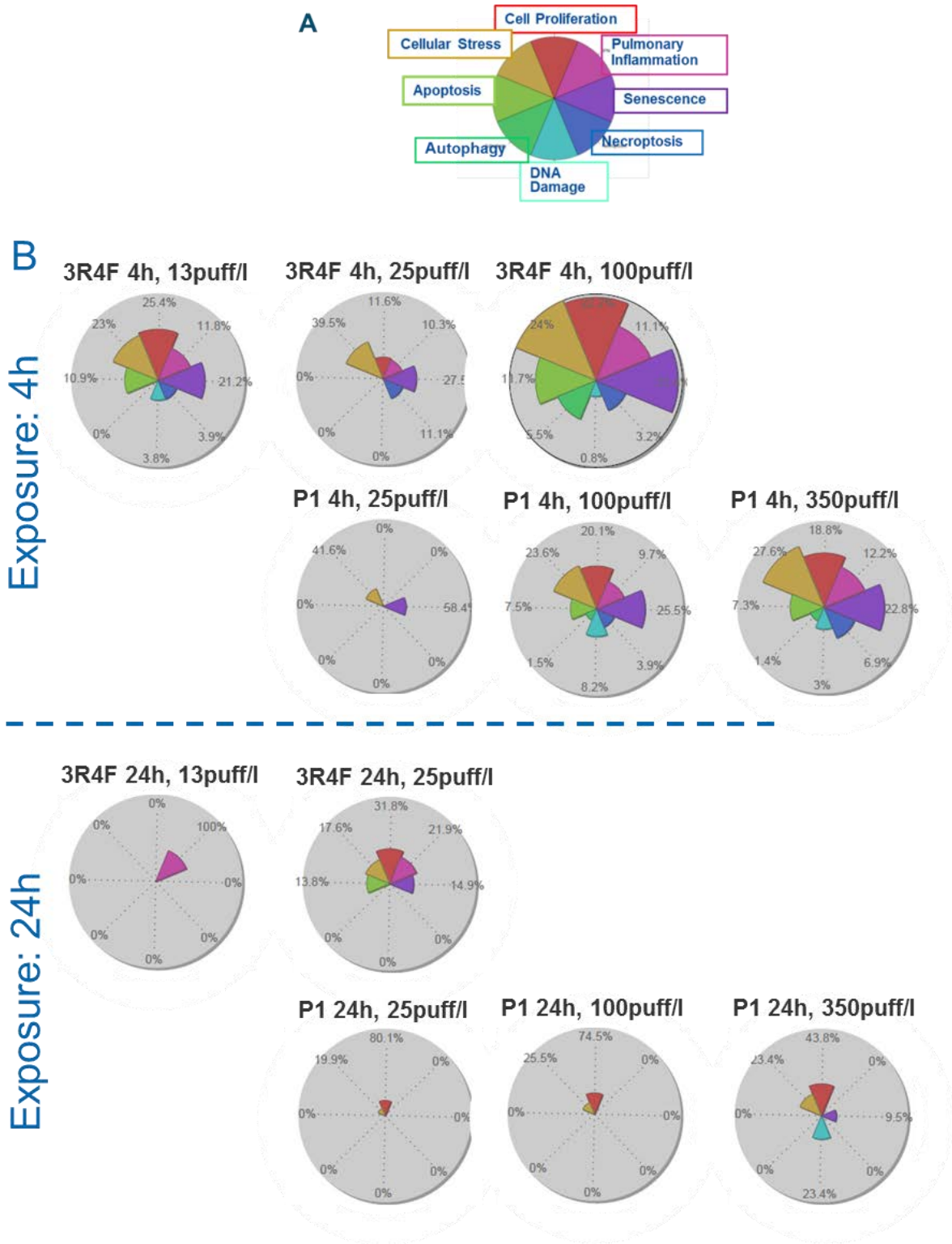

Figure 57: Individual contributions to overall BIF values. *(A) Color code of the BIF networks. (B) Starplots illustrating the decomposition of the overall relative BIF (RBIF) into its mechanistic components (from cell proliferation to inflammation, indicated by the colors of the segments) for each treatment group. The surface area of each segment is proportional to the contribution within a particular treatment of each network perturbation (shown as percent in the labels). It is further adjusted by the RBIF for the treatment compared with the reference so that the sum of the segment areas for each treatment equals the*

RBIF for the treatment. The pie chart represents the distribution of the sum of contributions for each network across all treatment groups. They all sum to 100%.

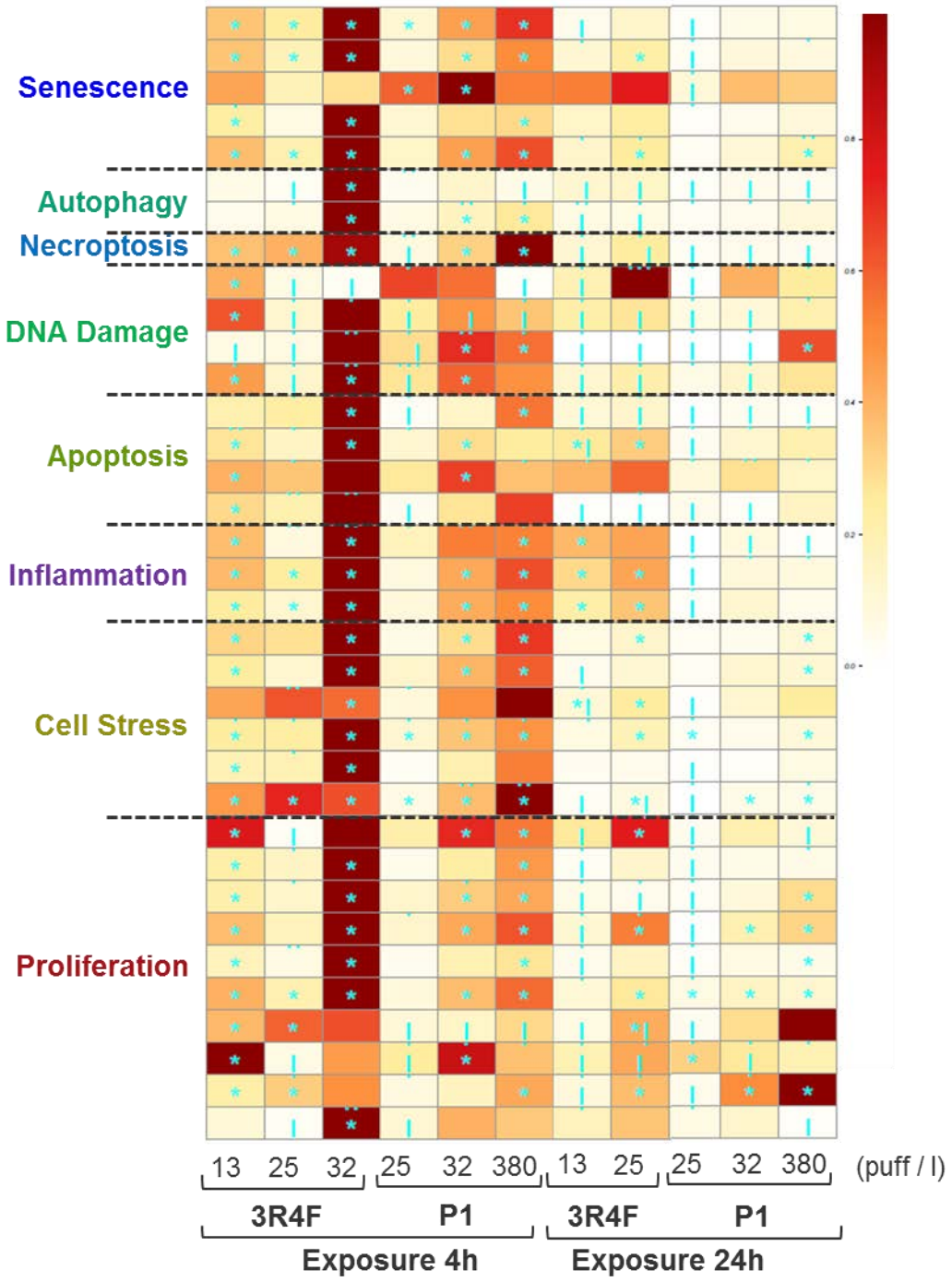

***Figure 58: Heatmap with perturbed subnetworks**. Heatmap summarizing subnetworks significantly perturbed in at least one treatment. A network is considered perturbed if, in addition to the significance of the NPA score with respect to the experimental variation, the two companion statistics (O and K) that show the specificity of the NPA score with respect to the biology described in the network, are also significant.*

11. COMPARISON ALL THREE 3R4F SMOKE FRACTIONS

11.1 HCS

Exposure to any of the 3R4F smoke fractions resulted in a dose-dependent increase in cell viability after 24 h of exposure (***Figure 59A***). When all data were fitted to a nonlinear dose-response inhibitory curve using GraphPad Prism (V. 5.00 for Windows, GraphPad Software), the most toxic effect was observed with TPM (EC50 30 puffs/L), followed by sbPBS (EC50: 42 puffs/L), and finally GVP (EC50: 61 puffs/L).

A similar result was observed with HCS via the cell count measurement (***Figure 59 B and C***). While no changes in cell count were observed at 4 h, a dose-dependent decrease in cell count was observed at 24 h. TPM was again the most toxic fraction, with GVP and sbPBS showing a similar response.

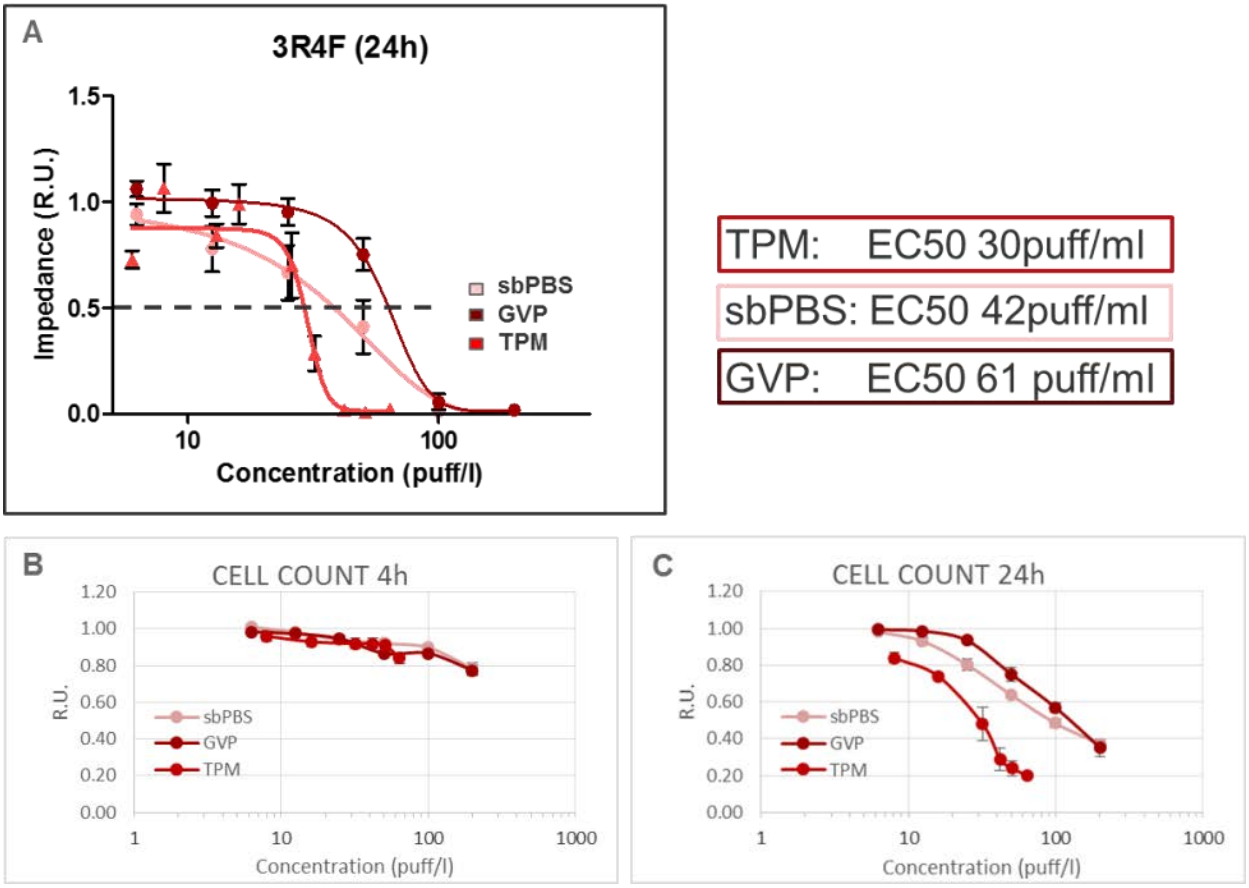

Figure 59. Cell viability in NHBE cells exposed to all three 3R4F smoke fractions. *(A) Cell viability at 24 h (xCELLigence. (B) Cell count (HCS) at 4 h and (C) 24 h. Values are normalized to each respective vehicle. Dotted line indicates 50% cell viability. Values represent mean ± SEM from all experiments.*

Exposure to all three 3R4F smoke fractions resulted in increased DNA damage in NHBE cells. The effect was observed at both 4 h and 24 h (***Figure 60 A and B***). TPM showed a more potent effect

than the other fractions (i.e. a lower TPM dose was required to observe the same increase in signal). The effect of GVP and sbPBS was very similar.

No effect on p-H3 levels was observed at 4 h (***Figure 60C***), but dose-dependent increases were observed for all fractions at 24 h (***Figure 60D)***. TPM showed an effect at doses above 16 puffs/L, whereas higher doses of sbPBS (50 puffs/L) and GVP (100 puffs/L) were necessary to observe a similar response.

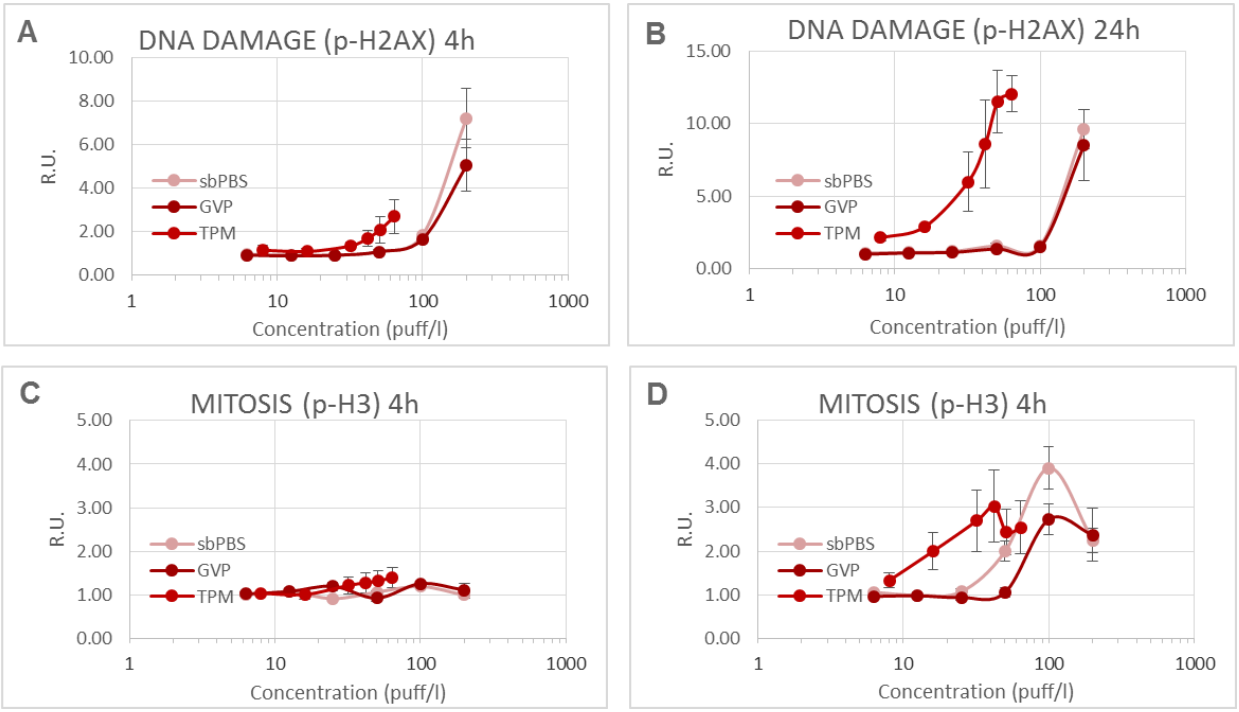

Figure 60. DNA damage (A and B) and changes in p-H3 levels (C and D) in NHBE cells exposed to all three 3R4F smoke fractions for 4 or 24 h. *DNA damage was measured as pH2AX. Values are normalized to the vehicle control and represent mean ± SEM.*

At 4 h, exposure to TPM, but not to sbPBS or GVP, resulted in a moderate increase in stress kinase pathway activation (increased p-cJun, ***Figure 61A***). At 24 h, all three 3R4F smoke fractions resulted in cellular stress, although TPM showed a more potent effect (***Figure 61B***).

All three fractions showed a similar ability to induce oxidative stress in exposed cells, which was observed as a decrease in GSH levels at 4 h and 24 h (***Figure 61 C and D***). Moreover, exposure to sbPBS and GVP resulted in the increased formation of ROS at 24 h, although no effect was detected at 4 h (***Figure 61 E and F***). Because of interference with the method, TPM could not be analyzed by this endpoint.

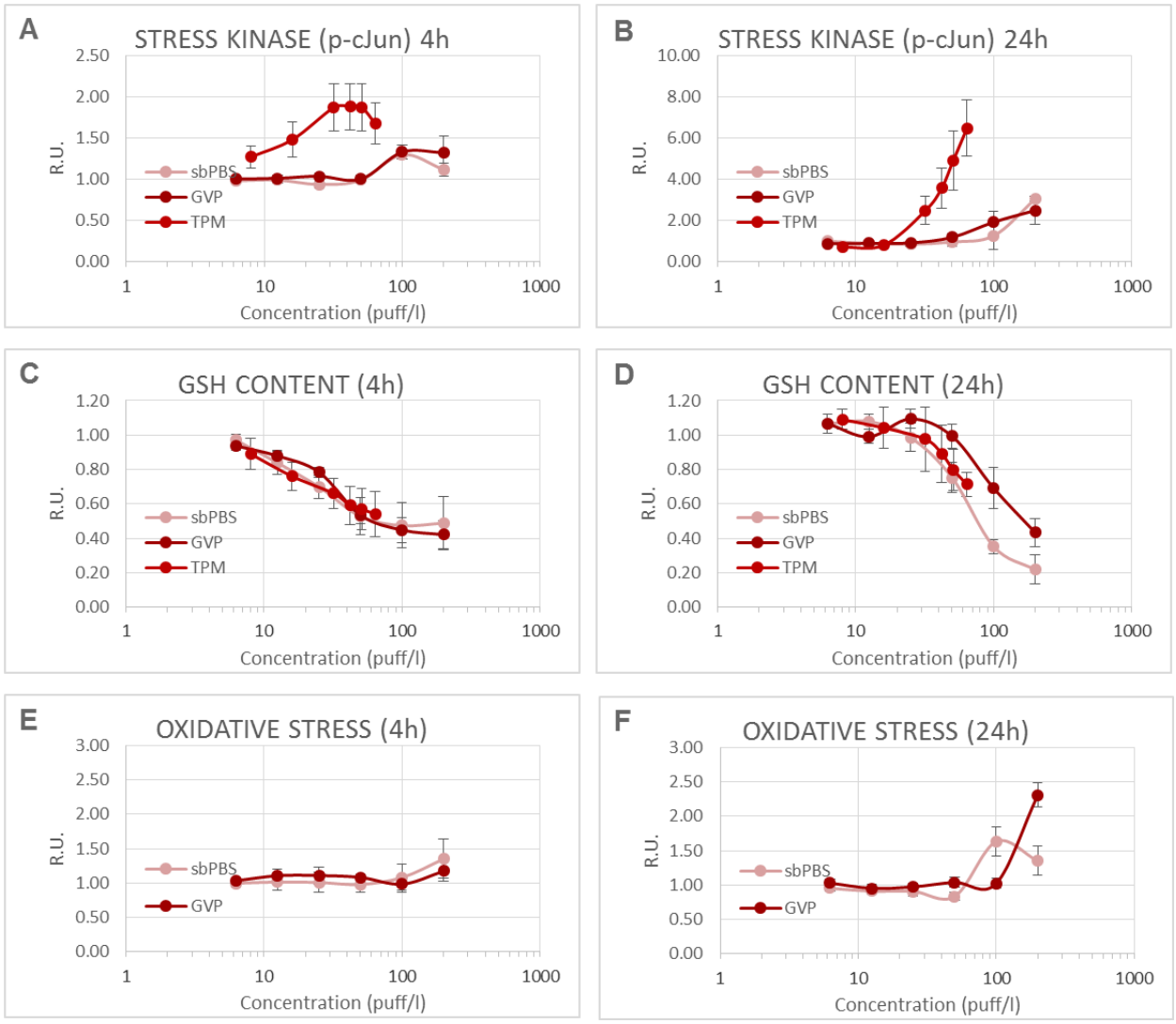

Figure 61. Effect of 3R4F smoke fractions on cellular and oxidative stress at 4 h and 24 h. *(A and B) Stress kinase. (C and D) GSH content. (E and F) Oxidative stress. Stress kinase activation was measured as p-cJun. Values are normalized to the vehicle control and represent mean ± SEM.*

No apoptosis was observed at 4 h in terms of cytochrome c release or caspase 3/7 activity (***Figure 62 A and C***). At 24 h, all smoke fractions caused a dose-dependent increase in cytochrome c release (***Figure 62B).*** The effect of TPM was more potent than that of sbPBS, and lower doses were required to achieve a similar response (42 puffs/L versus 100 puffs/L, respectively, for a 2-fold increase in signal compared with control). In the case of GVP, an increase in cytochrome c release was only observed at the highest dose (200 puffs/L). This was in the presence of >50% cell loss, suggesting that the effect was non-specific. With respect to caspase activity, only moderate increases were observed at high doses of GVP or sbPBS. Because of interference with the method, TPM could not be analyzed.

All fractions induced a dose-dependent increase in cell membrane permeability at 4 h and 24 h (***Figure 62 E and F***). Once again, the strongest effect was observed with TPM, with sbPBS and GVP showing a more similar level of toxicity.

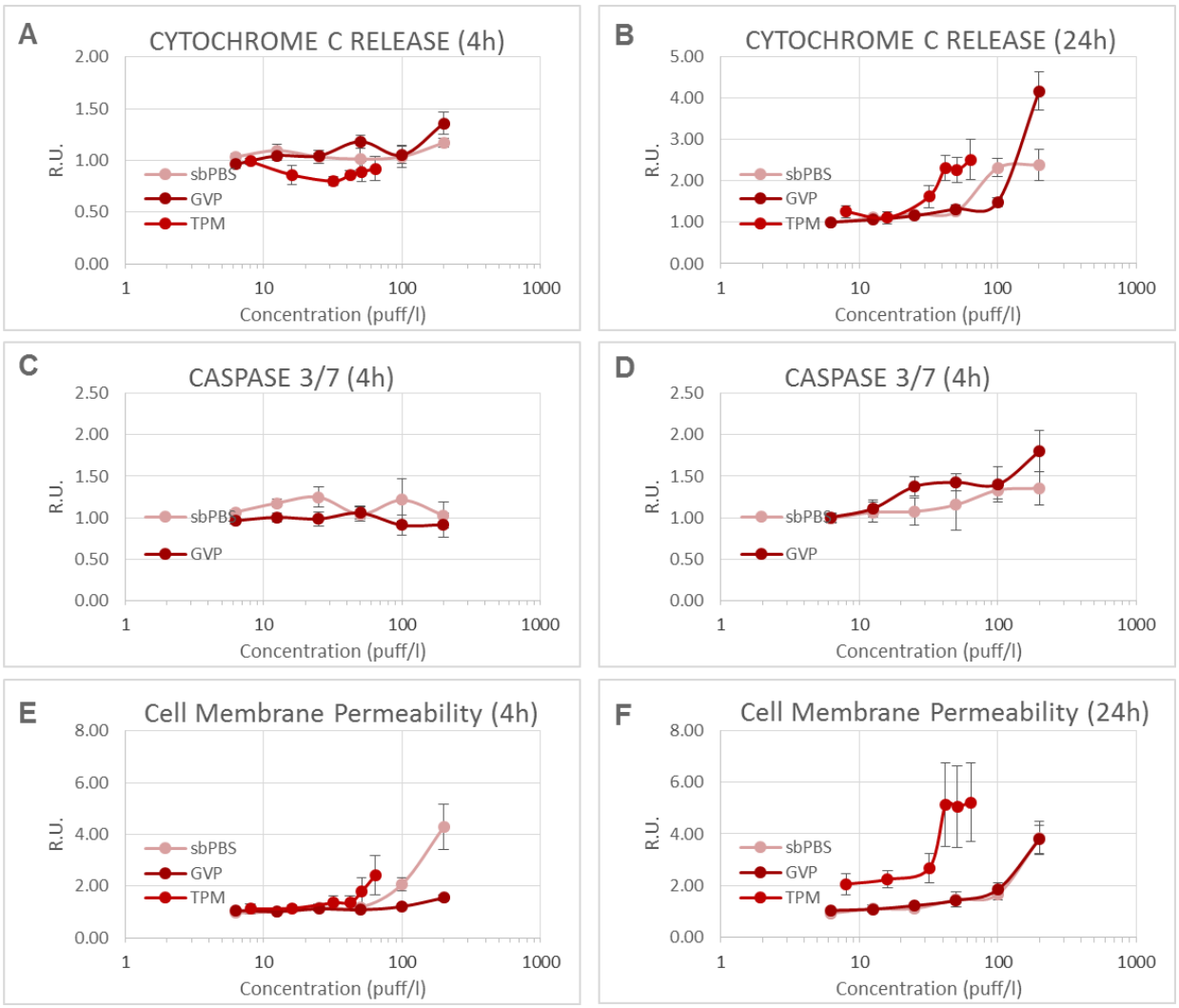

Figure 62. Apoptosis and necrosis in NHBE cells exposed to all 3R4F smoke fractions for 4 or 24 h*. (A and B) Cytochrome c release. (C and D) Caspase 3/7 activity. (D and E) Cell membrane permeability. Values are normalized to the vehicle control and represent mean ± SEM.*

3R4F TPM caused a dose-dependent decrease in the mitochondrial potential at 4 h and 24 h (***Figure 63 A and B).*** At 4 h, a similar trend was observed for GVP and sbPBS, although the effect was less intense. This effect was not observed at 24 h. The sudden increase in mitochondrial membrane potential observed at high doses of GVP and sbPBS occurred in the presence of significant cell loss, so could be a non-specific effect.

No major changes were observed in the mitochondrial mass upon exposure to TPM (***Figure 63 C and D***). By contrast, a dose-dependent decrease in mass was observed upon exposure to GVP and sbPBS.

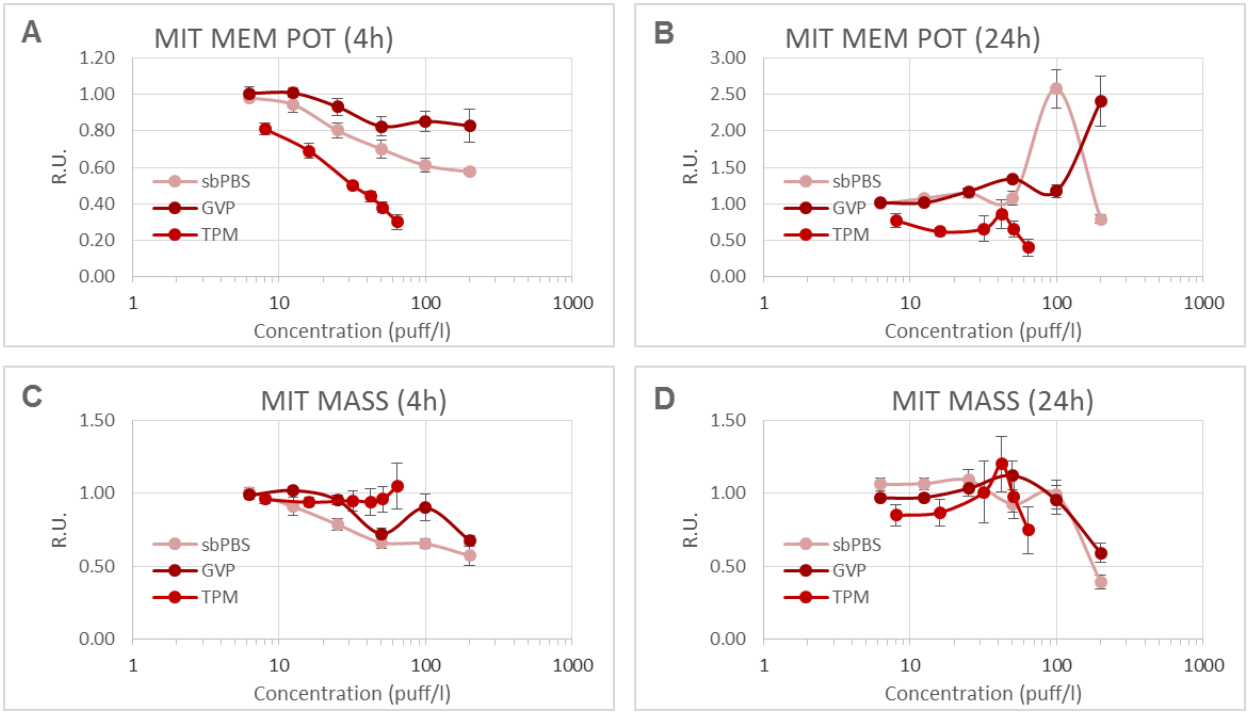

Figure 63. Mitochondrial membrane potential (A and B) and mitochondrial mass (C and D) in NHBE cells exposed to all three 3R4F fractions for 4 or 24 h*. Values are normalized to the vehicle control and represent mean ± SEM.*

Taken together, these results indicate that TPM is the most toxic fraction of 3R4F smoke, whereas sbPBS and GVP have similar and lower levels of toxicity.

11.2 Gene expression

Figure 64 shows the relative BIF values for NHBE cells exposed to all three 3R4F fractions at comparable doses in each timepoint. The highest BIF value corresponded to 25 puffs/L TPM at 4 h and was used as the reference (100% response). The BIF values in the other groups are expressed as % of the maximum response.

At the 4 h timepoint, exposure to increasing doses of TPM caused an increase in relative BIF. The impact of the other two fractions was lower, with sbPBS showing higher values than GVP.

At 24 h, BIF values for all fractions were lower than at 4 h, which could reflect the evaporation of volatile compounds from the culture media. This would explain why the GVP fraction (enriched in volatile compounds) has a very low BIF value, while sbPBS (also enriched in volatiles but containing some particulate) has a slightly higher BIF value, and TPM a much higher BIF value.

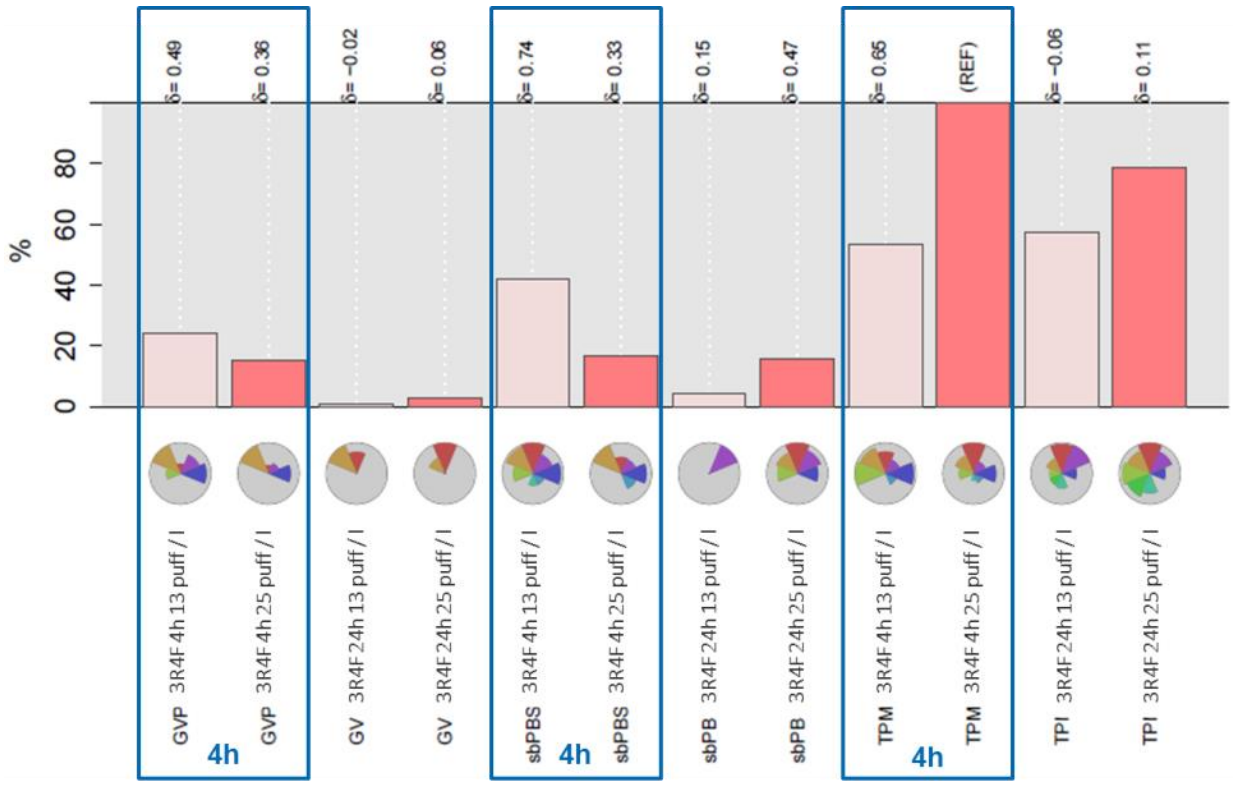

Figure 64: Overall BIF for NHBE cells exposed to all 3R4F fractions using the selected networks (see Table 5). *Biological Impact Factor (BIF) analysis. The percentages show the relative biological impact derived from the cumulated network perturbations caused by the treatment relative to the reference (defined as the treatment comparison showing the highest perturbation). For each treatment comparison, the value (–1 to 1) indicates how similar the underlying network perturbations are with respect to the reference (REF). A value of 1 indicates that all the networks are perturbed by the same mechanisms. BIF values at 4 h are boxed in blue.*

Each network can be decomposed into several subnetworks representing one or more specific biological processes. Heat maps were generated to gain more insights into the similarities and differences of the perturbed subnetworks at the 4 h and 24 h timepoints (Figure 65).

At 4 h, the GVP fraction had the least number of perturbed subnetworks (mostly within the senescence and cell stress networks). sbPBS and TPM were more similar, although the magnitude was consistently higher for TPM in most cases.

At 24 h, the number of perturbed subnetworks was lower in all three fractions, although a similar hierarchical pattern (GVP<sbPBS<TPM) could still be observed.

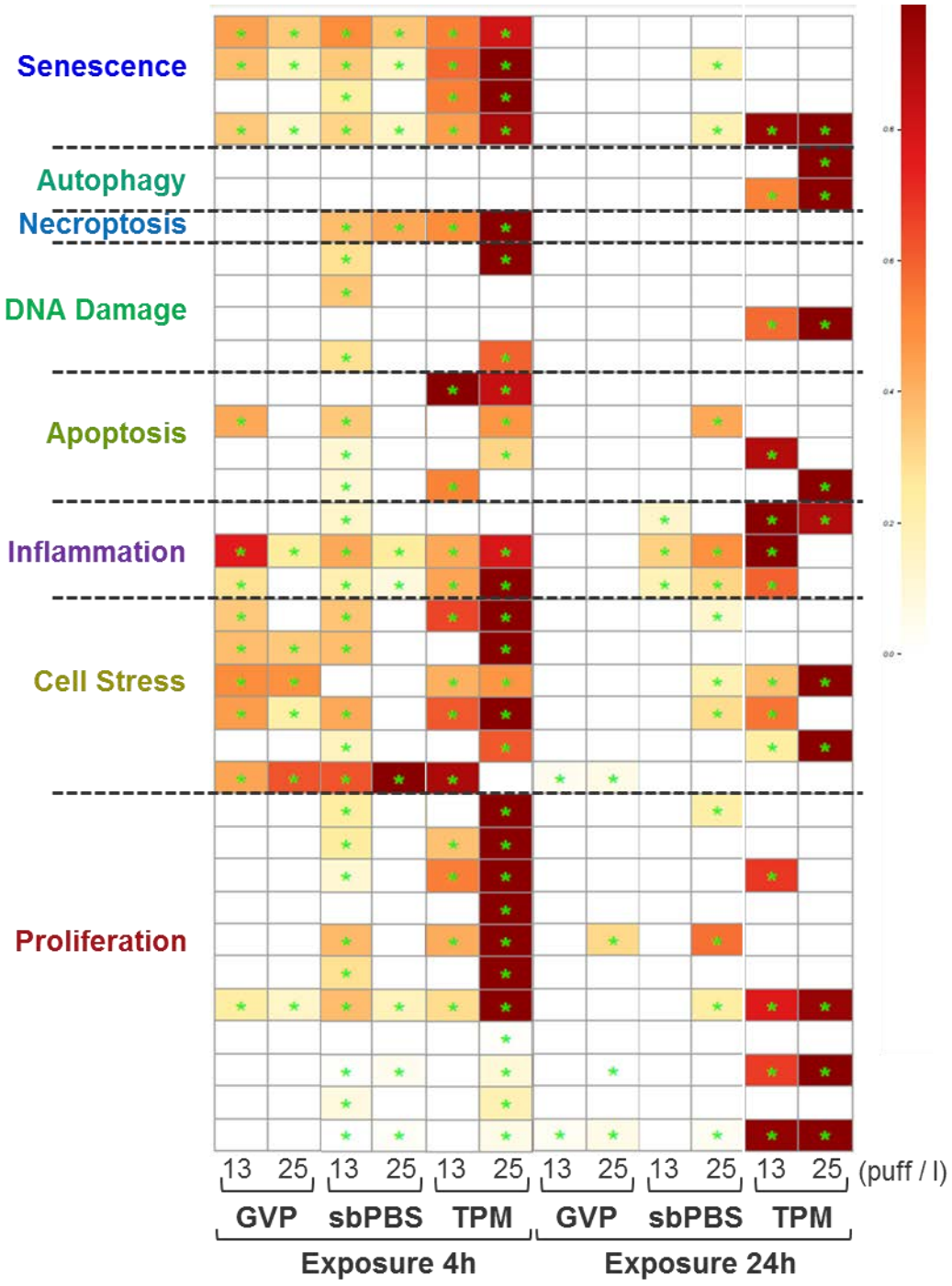

Figure 65: Heatmap with perturbed subnetworks*. Heatmap summarizing subnetworks significantly perturbed in at least one treatment. Only statistically significant perturbed networks are shown. A network is considered perturbed if, in addition to the significance of the NPA score with respect to the experimental variation, the two companion statistics (O and K) showing the specificity of the NPA score with respect to the biology described in the network, are also significant.*

Taken together, the results from cellular analysis, HCS, and gene expression analysis clearly indicated that the TPM fraction of 3R4F smoke has the highest biological impact both at 4 h and 24 h, and that GVP and sbPBS have a lower biological impact. HCS assays showed similar levels of response. However, gene expression analysis showed that exposure to sbPBS resulted in a higher number of perturbed networks than GVP. Indeed, this analysis revealed that sbPBS and TPM were more similar in terms of the number and type of networks perturbed. This suggests the existence of toxicity thresholds which determine whether the network perturbation predicted at the transcriptomics level will translate into phenotypic changes.

12. COMPARISON ALL THREE P1 AEROSOL FRACTIONS

12.1 HCS

No significant decrease in cell viability or cell count was observed upon exposure to P1 aerosol fractions for 4 h or 24 h (***Figure 66***). No differences between fractions were observed either.

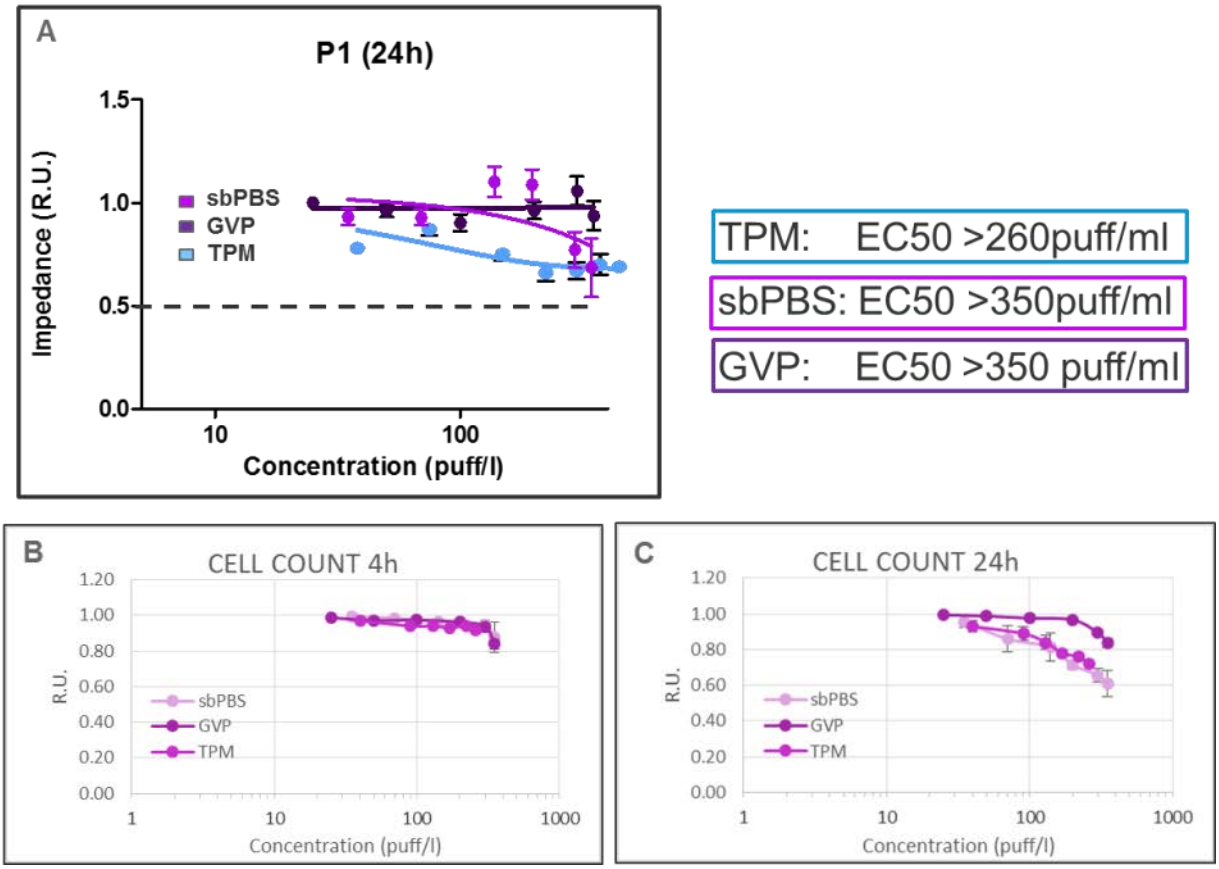

Figure 66. Cell viability in NHBE cells exposed to all three P1 aerosol fractions. (A) Cell viability at 24 h (xCELLigence. B) Cell count (HCS) at 4 h and (C) at 24 h. *Values are normalized to each respective vehicle. The dotted line indicates 50% cell viability. Values represent mean ± SEM from all experiments.*

Exposure to P1 GVP or sbPBS did not induce DNA damage, however a dose-dependent increase in p-H2AX was observed at high TPM doses (>130 puffs/L) at 4 h and 24 h (***Figure 67 A and B***). With respect to p-H3 levels, no effects were observed at 4 h (***Figure 67C***), but a response was observed for sbPBS at doses above 300 puffs/L (***Figure 67D***). No major changes were observed at 24 h for GVP or TPM.

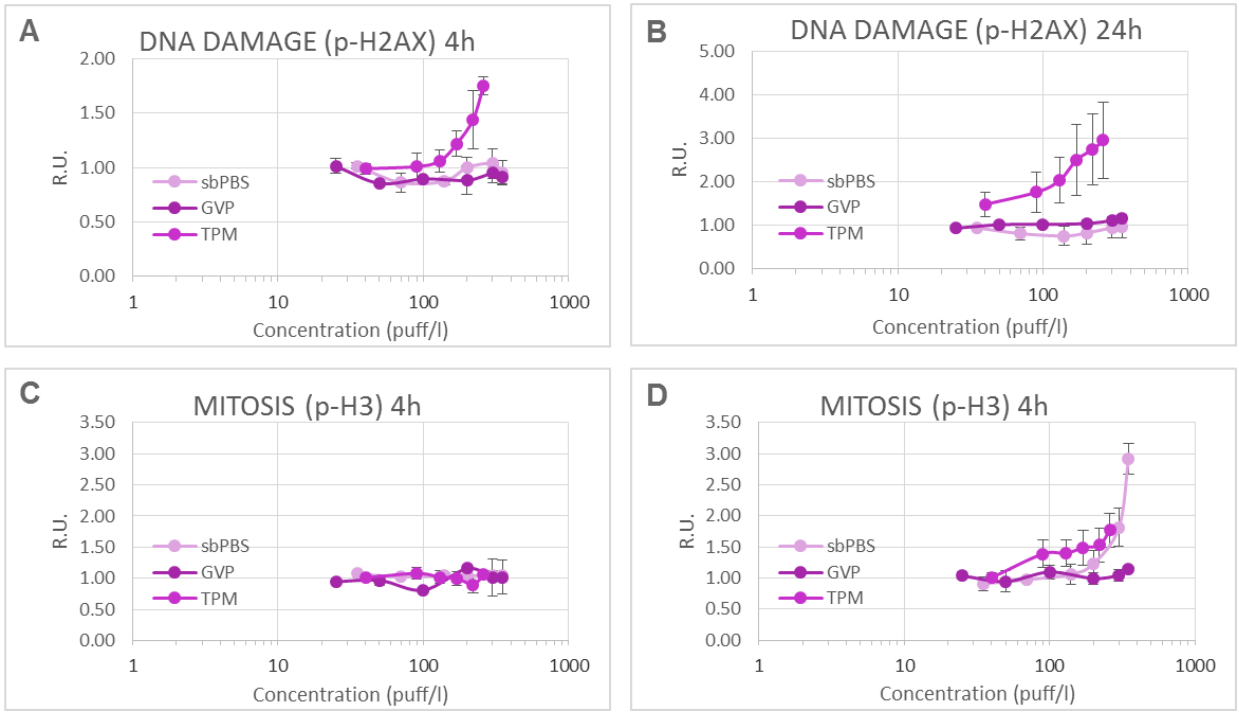

Figure 67. DNA damage (A and B) and changes in p-H3 levels (C and D) in NHBE cells exposed to all three P1 aerosol fractions for 4 or 24 h. *DNA damage was measured as pH2AX. Values are normalized to the vehicle control and represent mean ± SEM.*

No effect in p-cJun was observed for any aerosol fraction at 4 h. At 24 h, only a moderate increase was observed at high sbPBS doses (>300 puffs/L), although this resulted in a less than 2-fold increase in response compared with the vehicle control. No effects were observed for GVP and TPM at 24 h (***Figure 68 A and B)***.

All P1 fractions showed a trend towards a decreased GSH content after 4 h of exposure, although the effects of GVP and sbPBS were only moderate (20–25% GSH decrease at the highest dose, 350 puffs/L). The effect of TPM was stronger, and resulted in a 50% decrease in GSH compared with vehicle at 260 puffs/L. At 24 h, no effect was observed for GVP, and only a mild decrease in GSH (30%) was observed at the highest TPM and sbPBS doses (***Figure 68 C and D)***.

With respect to oxidative stress, no effects were observed for GVP and sbPBS, and only a moderate effect was observed at 24 h at the highest TPM doses (***Figure 68 E and F)***.

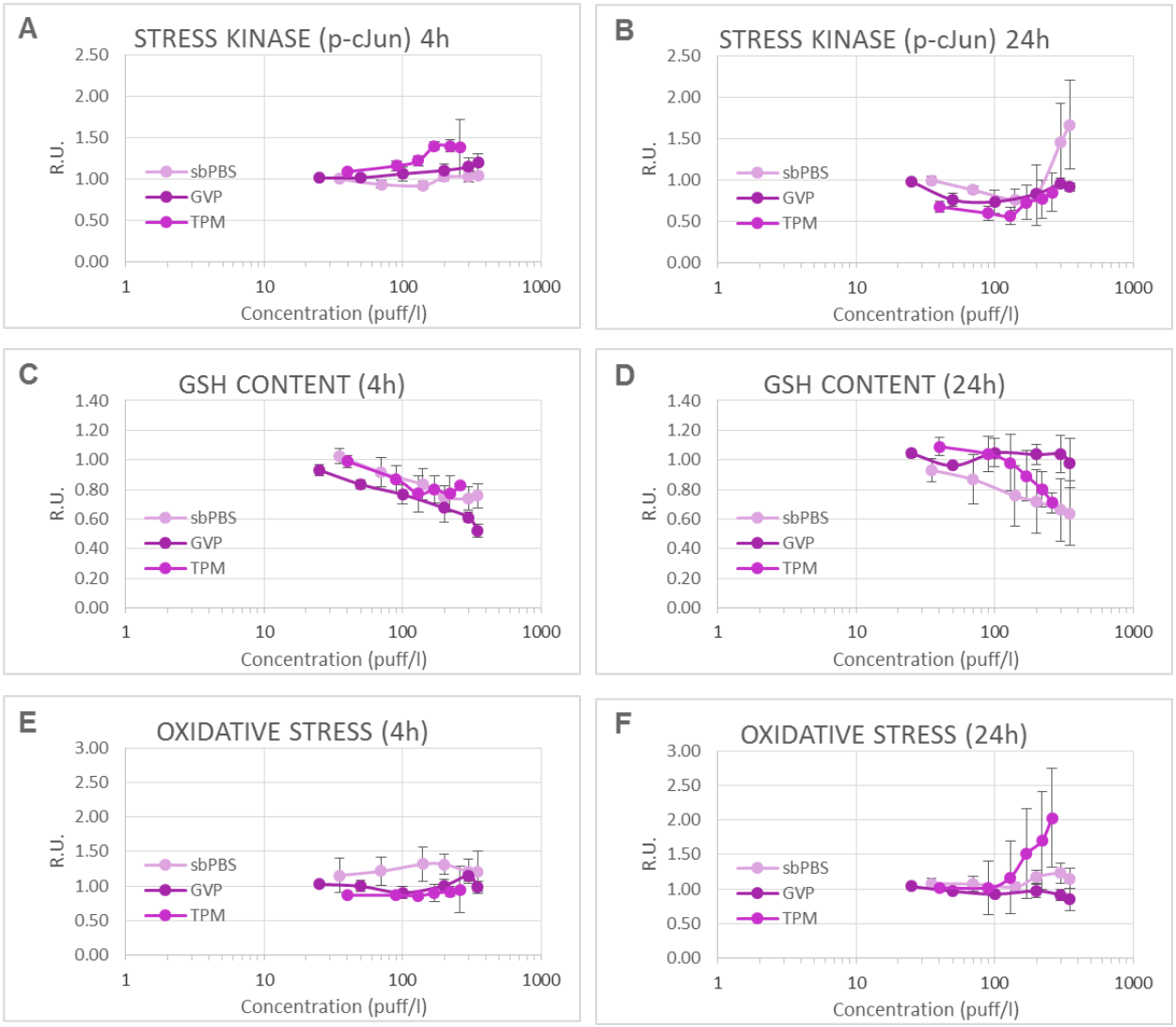

Figure 68. Effect of P1 aerosol fractions on cellular and oxidative stress at 4 h and 24 h. (A and B) Stress kinase. (C and D) GSH content. (E and F) Oxidative stress. *Stress kinase activation was measured as p-cJun. Values are normalized to the vehicle control and represent mean ± SEM.*

No major changes in cytochrome c release were observed for any P1 aerosol fraction at 4 h or 24 h (***Figure 69 A and B).*** With respect to caspase 3/7 activity, no major changes were observed at 4 h, but a dose-dependent increase was observed for TPM. A moderate increase in caspase 3/7 was also observed at high doses of P1 sbPBS (***Figure 69 C and D).***

TPM caused an increase in cell membrane permeability at 24 h, but only at doses above 130 puffs/L. No effects were observed for GVP or sbPBS (***Figure 69 E and F).***

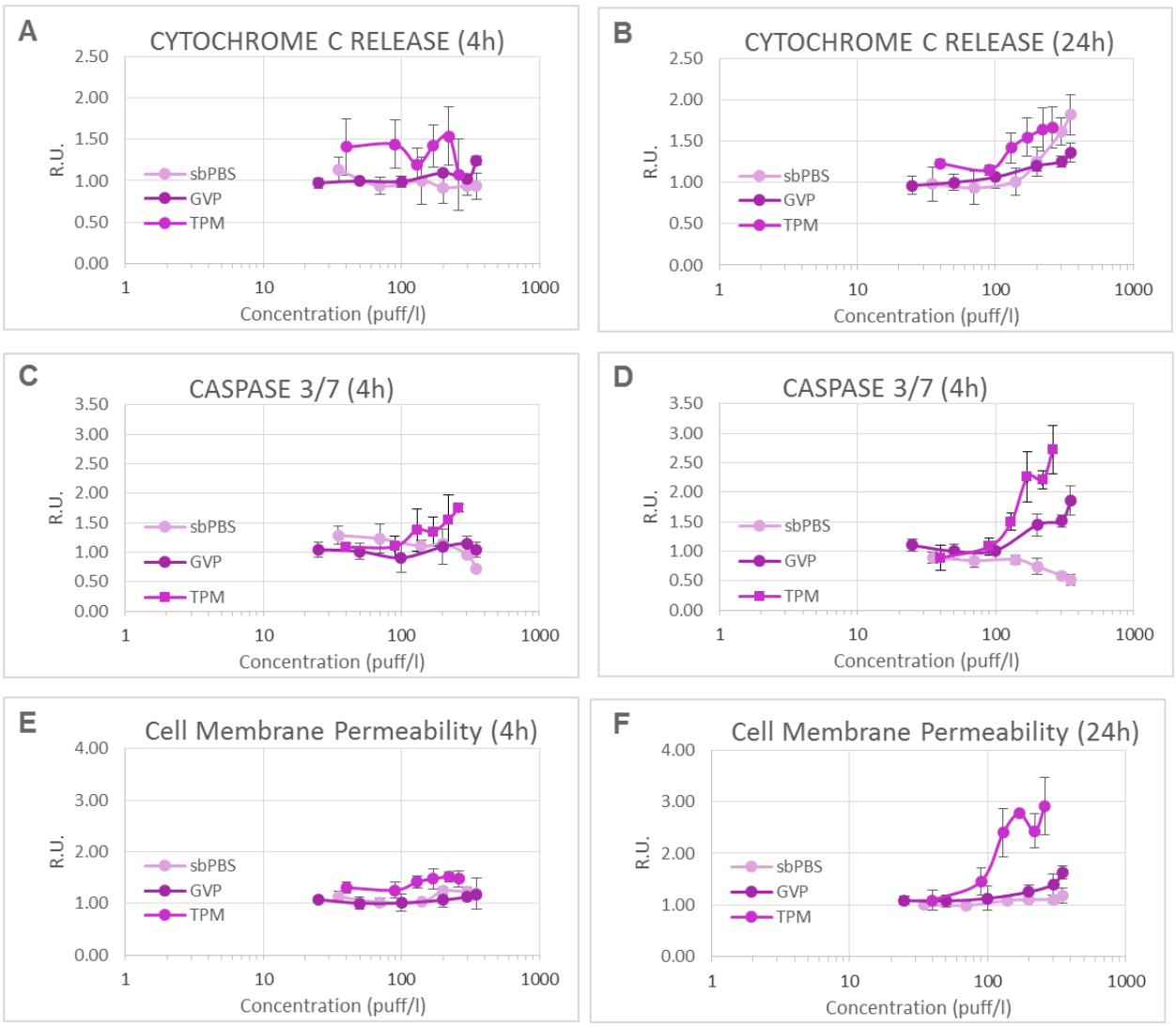

Figure 69. Apoptosis and necrosis in NHBE cells exposed to all P1 aerosol fractions for 4 or 24 h*. (A and B) Cytochrome c release. (C and D) Caspase 3/7 activity. (D and E) Cell membrane permeability. Values are normalized to the vehicle control and represent mean ± SEM.*

No effects in mitochondrial membrane potential or mitochondrial mass were observed at 4 h (***Figure 70 A and C)***. At 24 h, TPM caused a dose-dependent decrease in both parameters. sbPBS showed a bimodal response, with decreases in mitochondrial potential and mass at doses below 140 puffs/L, and increases in mitochondrial potential and mass at higher doses. No major changes were observed upon exposure to GVP (***Figure 69 B and D)***.

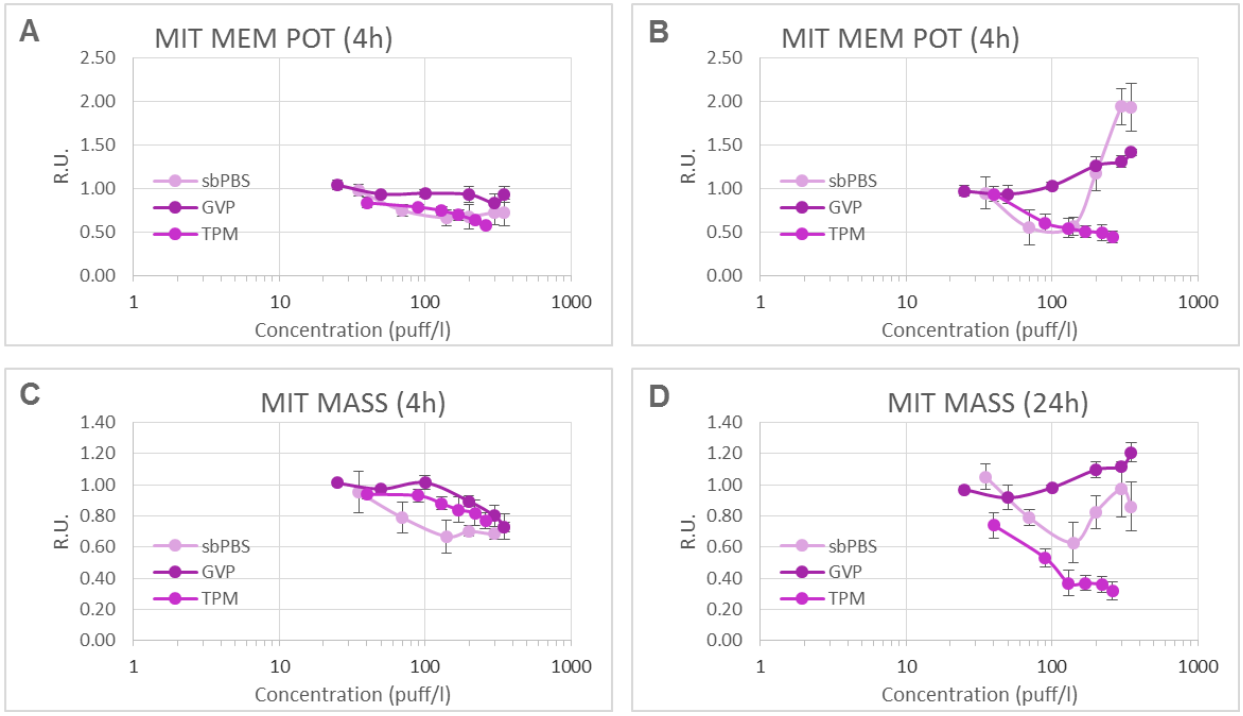

Figure 70. Mitochondrial membrane potential (A and B) and mitochondrial mass (C and D) in NHBE cells exposed to all three P1 aerosol fractions for 4 or 24 h*. Values are normalized to the vehicle control and represent mean ± SEM.*

Taken together, these results indicate that TPM is the most toxic fraction of the P1 aerosol, followed by sbPBS. Nevertheless, most of the toxic effects were observed at high doses and following prolonged exposure times.

12.2 Gene expression

Figure 71 shows the relative BIF values for NHBE cells exposed to all three P1 aerosol fractions at comparable doses in each timepoint. The highest BIF value corresponded to 25 puffs/L TPM at 24 h and was used as a reference (100% response). The BIF values in the other groups are expressed as % of the maximum response.

At the 4 h timepoint, TPM showed the highest biological impact, followed by sbPBS. GVP showed the lowest BIF value. The same trend was observed at 24 h. Interestingly, the BIF value of the TPM fraction was similar at both timepoints, whereas the 24 h values for sbPBS and GVP were much lower than at 4 h. As previously discussed, the different results observed at 4 h and 24 h could be explained, at least in part, by the presence of volatile compounds, which would likely be evaporated after 24 h of exposure.

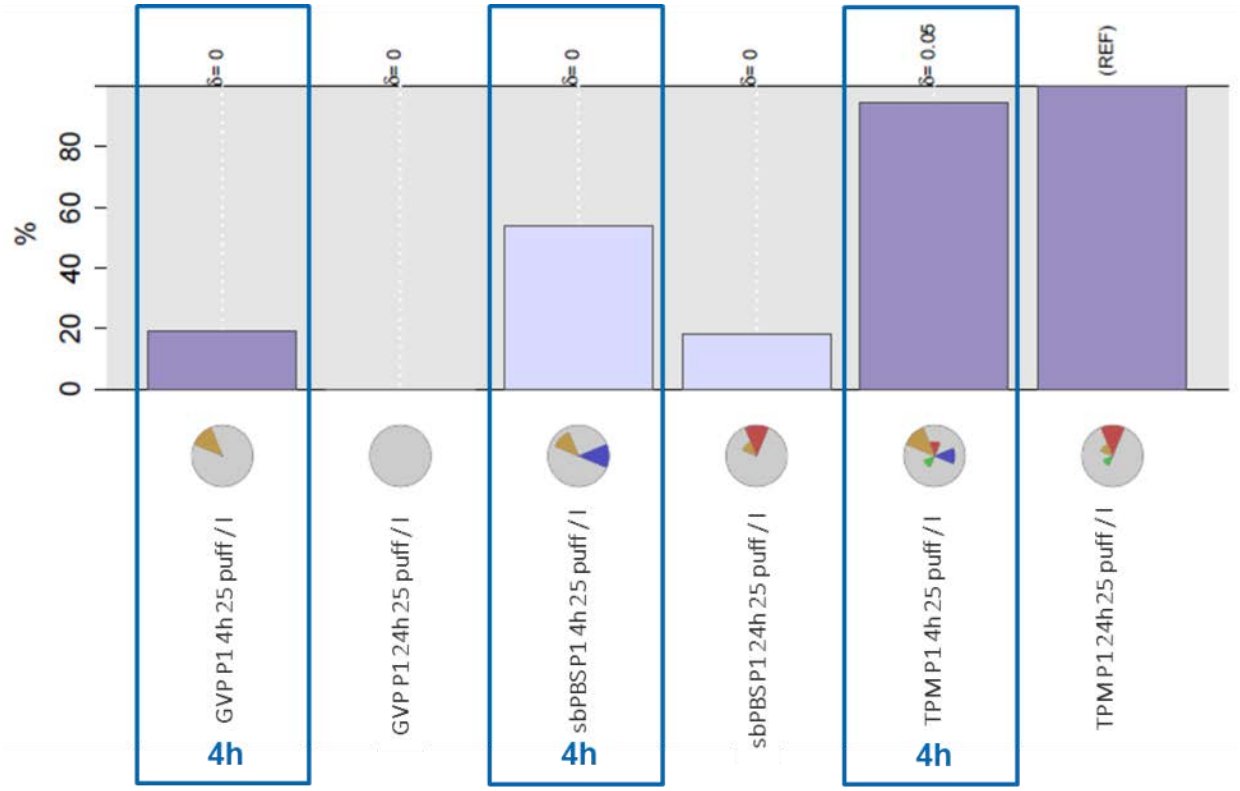

Figure 71: Overall BIF for NHBE cells exposed to all P1 aerosol fractions using the selected networks (see Table 5). *Biological Impact Factor (BIF) analysis. The percentages show the relative biological impact derived from the cumulated network perturbations caused by the treatment relative to the reference (defined as the treatment comparison showing the highest perturbation). For each treatment comparison, the value (–1 to 1) indicates how similar the underlying network perturbations are with respect to the reference (REF). A value of 1 indicates that all the networks are perturbed by the same mechanisms. BIF values at 4 h are boxed in blue.*

Each network can be decomposed into several subnetworks representing one or more specific biological processes. Heat maps were generated to gain more insights into the similarities

and differences of the perturbed subnetworks at the 4 h and 24 h timepoints (Figure 72).

The number of subnetworks significantly perturbed was much lower than in the case of 3R4F, which is indicative of the reduced toxicity of P1. The GVP fraction had the smallest number of perturbed subnetworks, with only two cell stress subnetworks perturbed at 4 h and no significant perturbations observed at 24 h. Exposure to sbPBS for 4 h increased the number of significantly perturbed subnetworks compared with GVP, including cell stress and senescence. The effect at 24 h was lower than at 4 h. Finally, TPM showed the highest number of significantly perturbed subnetworks at both timepoints. Interestingly, most of the subnetworks related to cell stress and senescence at 4 h (similar to sbPBS), but mainly involved the cell proliferation network at 24 h.

Taken together, the results from cellular analysis, HCS, and gene expression analysis clearly indicated that the TPM fraction of the P1 aerosol had the highest biological impact both at 4 h and 24 h, and that GVP and sbPBS had lower biological impacts.

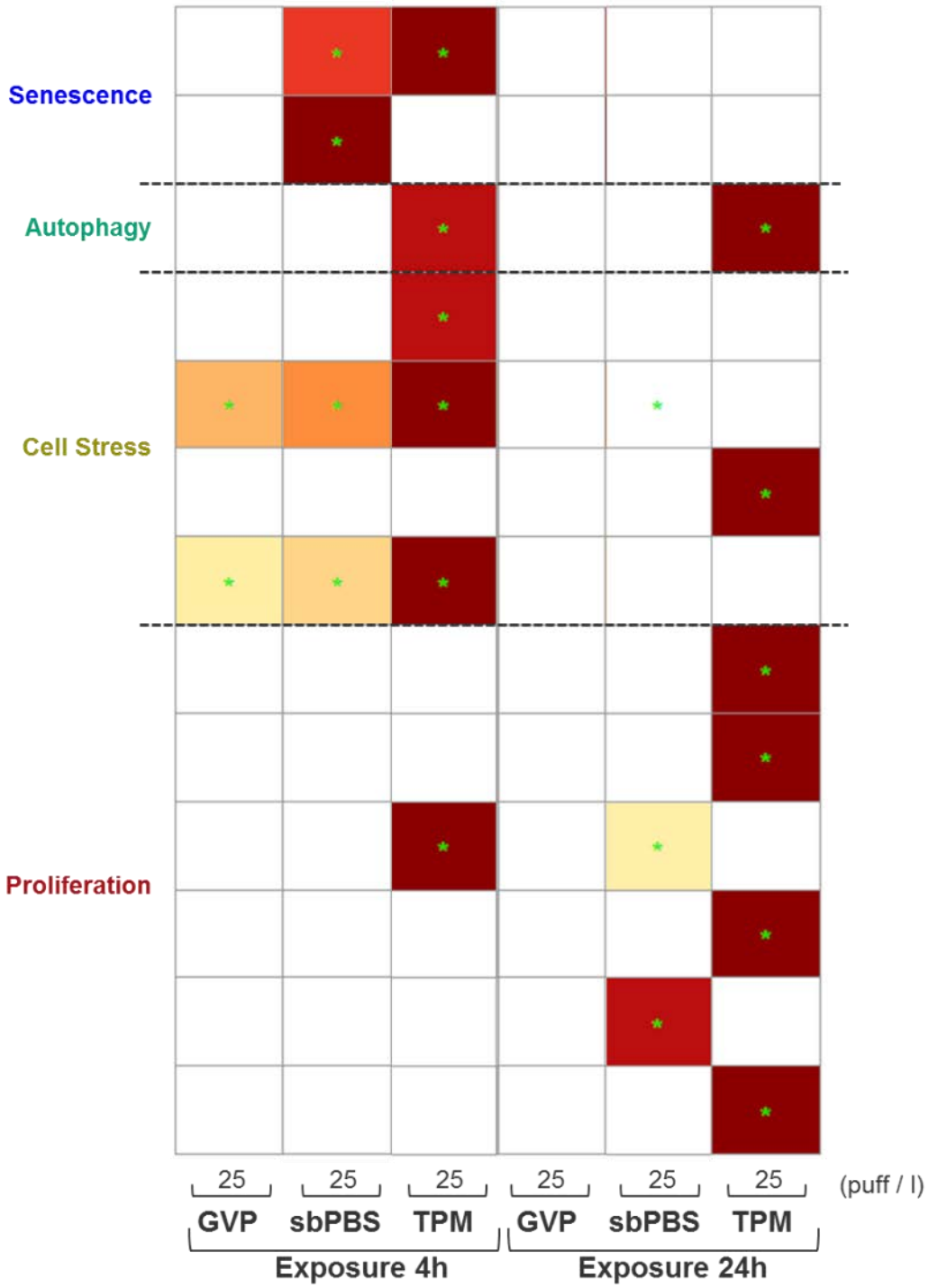

Figure 72: Heatmap with perturbed subnetworks*. Heatmap summarizing subnetworks significantly perturbed in at least one treatment. Only significant perturbed networks are shown. A network is considered perturbed if, in addition to the significance of the NPA score with respect to the experimental variation, the two companion statistics (O and K) showing the specificity of the NPA score with respect to the biology described in the network, are also significant.*

13. Conclusions

- Cell viability assays revealed that the cytotoxicity of each 3R4F smoke fraction was between six and nine times higher than the respective P1 aerosol fraction.
- HCS assays showed that 3R4F smoke fractions have a greater potential to induce genotoxicity, cellular and oxidative stress, apoptosis, necrosis, and mitochondrial damage compared with the respective P1 aerosol fractions.
- Transcriptomic analysis found that, overall, exposure to 3R4F smoke fractions had a higher biological impact on NHBE cells than exposure to similar doses of the respective P1 fractions.
- The biological impact of GVP and sbPBS was higher at 4 h than at 24 h, whereas similar effects at both timepoints were observed for TPM. These differences may reflect the higher presence of volatile smoke constituents in GVP and sbPBS, which would have evaporated after 24 h of exposure.
- In general, a very good correlation was observed between the biological networks predicted to be perturbed by transcriptomics analysis and the phenotypic changes seen in HCS assays.
- A comparison of all three 3R4F smoke fractions showed that TPM was associated with the highest level of toxicity by cell viability assays, HCS endpoints, and transcriptomics analysis. GVP and sbPBS showed a more similar and lower effect on NHBE cells.
- Despite the generally low level of toxicity, a comparison of all three P1 aerosol fractions revealed that TPM also had a higher toxicity than GVP and sbPBS.
- Taken together, these results clearly demonstrate that the P1 aerosol has a much lower toxicity than 3R4F smoke.

14. REFERENCES

Armstrong JS, Steinauer KK, Hornung B, Irish JM, Lecane P, Birrell GW, Peehl DM, Knox SJ (2002) Role of glutathione depletion and reactive oxygen species generation in apoptotic signaling in a human B lymphoma cell line. Cell Death Differ 9: 252-263

Bolstad BM, Irizarry RA, Astrand M, Speed TP (2003) A comparison of normalization methods for high density oligonucleotide array data based on variance and bias. Bioinformatics 19: 185-193

Brettschneider J, Collins F, Bolstad BM (2008) Quality Assessment for Short Oligonucleotide Microarray Data. Technometrics 50: 241-264

Edinger AL, Thompson CB (2004) Death by design: apoptosis, necrosis and autophagy. Curr Opin Cell Biol 16: 663-669

Gautier L, Cope L, Bolstad BM, Irizarry RA (2004) affy---analysis of Affymetrix GeneChip data at the probe level. Bioinformatics 20: 307-315

Gebel S, Lichtner RB, Frushour B, Schlage WK, Hoang V, Talikka M, Hengstermann A, Mathis C, Veljkovic E, Peck M, Peitsch MC, Deehan R, Hoeng J, Westra JW (2013) Construction of a Computable Network Model for DNA Damage, Autophagy, Cell Death, and Senescence Bioinformatics and Biology Insights 7: 97-117

Gentleman RC, Carey VJ, Bates DM, Bolstad B, Dettling M, Dudoit S, Ellis B, Gautier L, Ge Y, Gentry J, Hornik K, Hothorn T, Huber W, Iacus S, Irizarry R, Leisch F, Li C, Maechler M, Rossini AJ, Sawitzki G, Smith C, Smyth G, Tierney L, Yang JY, Zhang J (2004) Bioconductor: open software development for computational biology and bioinformatics. Genome Biol 5: R80

Hoeng J, Deehan R, Pratt D, Martin F, Sewer A, Thomson TM, Drubin DA, Waters CA, de Graaf D, Peitsch MC (2012) A network-based approach to quantifying the impact of biologically active substances. Drug Discov Today 17: 413-418

Krewski D, Westphal M, Al-Zoughool M, Croteau MC, Andersen ME (2011) New directions in toxicity testing. Annu Rev Public Health 32: 161-178

Lowndes NF, Toh GW (2005) DNA repair: the importance of phosphorylating histone H2AX. Curr Biol 15: R99-R102

Martin F, Sewer A, Talikka M, Xiang Y, Hoeng J, Peitsch MC (2014) Quantification of biological network perturbations for mechanistic insight and diagnostics using two-layer causal models. BMC Bioinformatics 15: [Epub ahead of print]

Martin F, Thomson TM, Sewer A, Drubin DA, Mathis C, Weisensee D, Pratt D, Hoeng J, Peitsch MC (2012) Assessment of network perturbation amplitude by applying high-throughput data to causal biological networks. BMC Syst Biol 6: 54

Nielsen HB, Gautier L, Knudsen S (2005) Implementation of a gene expression index calculation method based on the PDNN model. Bioinformatics 21: 687-688

Ott M, Robertson JD, Gogvadze V, Zhivotovsky B, Orrenius S (2002) Cytochrome c release from mitochondria proceeds by a two-step process. Proc Natl Acad Sci U S A 99: 1259-1263

R Development Core Team. (2007) R: A Language and Environment for Statistical Computing.

Schlage WK, Westra JW, Gebel S, Catlett NL, Mathis C, Frushour BP, Hengstermann A, Van Hooser A, Poussin C, Wong B, Lietz M, Park J, Drubin D, Veljkovic E, Peitsch MC, Hoeng J, Deehan R (2011) A computable cellular stress network model for non-diseased pulmonary and cardiovascular tissue. BMC Syst Biol 5: 168

Smyth GK (2005) limma: linear models for microarray data. In Bioinformatics and Computational Biology Solutions using R and Bioconductor, Gentleman RC, Carey V, Dudoit S, Irizarry R, Huber W (eds), pp 397-420. New York: Springer

Thermo_Scientific. (2012) Thermo Scientific CellInsight NXT High COntent Screening Platform Brochure. https://static.thermoscientific.com/images/D21328~.pdf.

Westra JW, Schlage WK, Frushour BP, Gebel S, Catlett NL, Han W, Eddy SF, Hengstermann A, Matthews AL, Mathis C, Lichtner RB, Poussin C, Talikka M, Veljkovic E, Van Hooser AA, Wong B, Maria MJ, Peitsch MC, Deehan R, Hoeng J (2011) Construction of a computable cell proliferation network focused on non-diseased lung cells. BMC Syst Biol 5: 105

Wisdom R, Johnson RS, Moore C (1999) c-Jun regulates cell cycle progression and apoptosis by distinct mechanisms. EMBO J 18: 188-197